DOE/ER/03023--27

DE82 005515

Investigation of the Validity of the OZI Rule and Study of Production Properties of the $\bar{K}^{*0}$ Resonance in $\pi^+ p$ Interactions at 16 GeV/c.

A Dissertation

submitted by

Abolhassan Jawahery

In partial fulfillment of the requirements

for the degree of

Doctor of Philosophy

Report of Work Conducted under
Department of Energy Contract DE-AC02-76ER03023
with Tufts University

TUFTS UNIVERSITY

September 1981

DISCLAIMER

ABSTRACT

Results are reported from a streamer chamber experiment performed at Stanford Linear Accelerator Center (SLAC) to study the production of the $\Phi(1020)$ in OZI-allowed and forbidden processes in π^+P interactions at 16 GeV/c. Production properties of the $\bar{K}^*(896)$ are also studied and discussed. The data consisted of 300,000 streamer chamber photographs of π^+P interactions and information from Cerenkov and scintillation counters recorded on magnetic tapes.

The $\Phi(1020)$ resonances are observed in the semi-inclusive reactions

$$\pi^+ + P \longrightarrow \Phi \Lambda^\circ + X$$

$$\pi^+ + P \longrightarrow \Phi K_s^\circ + X$$

No clear $\Phi(1020)$ resonance is seen in the inclusive reaction

$$\pi^+ + P \longrightarrow \Phi + X$$

It is estimated that at least 35% of Φ,s are produced in association with a pair of strange particles. The longitudinal momentum distribution of $\bar{K}^*(896)$, expressed in terms of Feynman variable Xf, is compared with the predictions of the quark fusion model; it is observed that the model reproduces well the experimentally observed spectrum.

ACKNOWLEDGEMENTS

In the course of this experiment a great many people have contributed. I would like to take this opportunity to express my gratitude to all of them.

I am particularly indebted to my advisor Professor Richard H. Milburn for his guidance, assistance and encouragement through my entire graduate studies and the performance of this experiment.

I enjoyed working with other members of the group and I wish to express my thanks to Dr. Takashi Maruyama with whom I worked directly during the installation stage of this experiment, and Professors Anthony Mann, Jack Schneps, Ronald Thornton, William Oliver and Gary Goldstein for their guidance and advice in various stages of this experiment and their continuing interest in my graduate career.

I am also indebted to Professor Z. Ming Ma and Mr. Jim Hylen with whom I worked directly during the entire course of this experiment. I learned much from them and enjoyed their friendship as well.

I wish to thank E131 scanning staff Evelyn Engelstad, Paula Ward, Jacquelyn Beley, Laura Taylor, John Larson, Rene MacDonald, Joe Kwiatkowski, Nancy Helfrich, Hong Hong Li Fred Folch Pi and Peter Karen for their conscientious scanning and measuring of the events.

Thanks are also due to Mr. Lawrence McMaster, Ms. Celia Mees, Ms. Audrey Beaumonte and Ms.Cynthia Cole for their assistance in the course of this experiment.

Finally I wish to thank my brothers and sisters which with their encouragement and affection helped me to finish this work. At this point I would like to thank my wife Malihe for her love, constant encouragement and her assistance in completing this thesis.

I am also grateful to members of the SLAC group D under Professor Robert Mozley, and technical staff led by Mr. Bill Wadley for their advice and cooperation during the installation stage of this experiment.

TABLE OF CONTENTS

LIST OF TABLES

LIST OF ILLUSTRATIONS

V-12 Proper Life time Distribution for kOs

V-13 Proper Life Time Distribution for Λ°

V-14 Distribution of Measured Invariant Mass of KOs

V-15 Distribution of Measured Invariant Mass of Λ°

V-16 Distribution of (Xbm=Xv-Xbeam) for VO Decay Vertices

VI-1 Invariant Mass Distribution of (K-K+) Combinations

VI-2 Invariant Mass Distribution of (K-K+) Pairs for KOs and Λ° Associated Events

VI-3 (K-K+) Combinatorial Background

VI-4 Dependence of Φ (1020) Acceptance on Xf

VI-5 (K-K+) Invariant Mass Distribution for Inclusive events

VI-6 ($K-\pi^{+}$) Mass Distribution

VI-7 Invariant Mass Distribution of ($K-\pi^{+}$) Combinations For Both Particles Passing Through Ck-

VI-8 $\hat{P}t$ Distribution for $\bar{K}^{*\circ}$

VI-9 Xf Distribution for $\bar{K}^{*\circ}$

VI-10 Xf Dependence of Geometrical Acceptance of $\bar{K}^{*\circ}$(896)

VI-11 $\hat{P}t$ Dependence of Geometrical Acceptance of $\bar{K}^{*\circ}$(896)

VI-12 Distribution of $d\sigma/dXf$ for $\bar{K}^{*\circ}$ Production

VII-1 $d\sigma/dXf$ Distribution for $\bar{K}^{*\circ}$ Compared with Predictions of Quark Fusion Models

VII-2 Gluon Fusion ,Light Quark Annihilation and Strange Quark Fusion

C-1 Distribution of APACHE χ^{2} for Four Ranges of Average FRMS

C-2 Distribution of APACHE χ^{2} for Four Ranges of

Average FRMS After Scaling

C-3 Scatter Plot of χ^2 Versus $\langle(\text{FRMS})^2\rangle$

(blank page)

CHAPTER I- INTRODUCTION

We have investigated the validity of the OZI rule by studying reactions,

$$\pi^+ + P \longrightarrow \Phi K_s^\circ + X \qquad I\text{-}1$$

$$\pi^+ + P \longrightarrow \Phi \Lambda^\circ + X \qquad I\text{-}2$$

$$\pi^+ + P \longrightarrow \Phi + X \qquad I\text{-}3$$

and the production properties of the $\bar{K}^{*\circ}(896)$ resonance in the inclusive reaction

$$\pi^+ + P \longrightarrow \bar{K}^{*\circ} + X \qquad I\text{-}4$$

both at 16 GeV/c, using streamer chamber photographs of the interactions and information from Cerenkov and scintillation counters.

The origin of the OZI rule, its present status and a brief description of a generalized Drell-Yan process called the quark fusion model is summarized in Chapter II. Description of the apparatus and experimental set up is given in Chapter III. In Chapter IV, the general procedures in conducting the experiment, including data collection, scanning and measurement are discussed. Chapter V covers the reconstruction of the events from measured data and description of the processes in which charged and neutral strange particles were identified. Analysis of the particular reactions (I-1, 2, 3, 4) and the cross-section calculations are presented in detail in Chapter VI. In Chapter VII is presented a comparison of experimental

results from this work with the predictions of theoretical models.

CHAPTER II-THEORETICAL BACKGROUND

SUMMARY

In quark-parton models the $\Phi(1020)$ along with heavier vector mesons $J/\Psi(3100)$, $\Psi'(3600)$ and $\Upsilon(9460)$ are considered to be $(Q\bar{Q})$ states. The OZI rule suppression of disconnected quark lines in strong interactions has been used to interpret some of the production and decay properties of these states. Attempts have also been made to apply the Drell-Yan (quark-fusion) mechanism to vector meson production in hadron collisions. In this chapter, the origin of the OZI rule and its applicability to the associated production of $\Phi(1020)$ in $\pi^+ P$ interactions is described. The application of generalized Drell-Yan mechanisms to $\bar{K}^{*\circ}$ production in $\pi^+ P$ is also discussed.

A- The Okubo-Zweig-Iizuka (OZI) Rule[1,2,3,4]

1-Origin of the Rule

The OZI rule is also called the quark line rule and was originally proposed to explain the strong suppression of Φ-meson decays into three pions. There is no other conservation law or selection rule which would forbid such a reaction (Fig. II-1a) while allowing ω-decay(Fig. II-1b) to occur. The ratio of the relevant coupling constants is experimentally measured to be[1],

$$\frac{g^2_{\phi\rho\pi}}{g^2_{\omega\rho\pi}} = .007 \qquad \text{II-1}$$

This ratio would be expected to be nearly unity, were the (ω _ Φ) mixing model to hold. Thus Okubo[1], Zweig[4] and Iizuka postulated a rule to characterize the suppression of the reaction of Fig. II-1a. The OZI rule is: all processes involving a disconnected quark-antiquark line (a " hairpin " diagram) are suppressed in hadronic interactions. In other words, all processes in which a quark-antiquark pair belongs to one particle are forbidden. This rule evidently forbids the reaction of Fig. II-1a while allowing that of Fig. II-1b. At the same time the predominant decay of Φ into K-K+ is an OZI allowed process(Fig. II-1c).

2- Application to J/Ψ Decay[5]

The $J/\Psi(3100)$ is observed to be a very narrow resonance, in spite of decaying mostly into hadrons(Γ=100 Kev). A new selection rule was needed to explain this phenomenon because, despite the electromagnetic production of J/Ψ, it has neither a typically narrow electromagnetic width nor a typically large strong interaction width. The OZI rule applied to Φ-meson decay forbids, at least to first order, transitions in which a ($S\bar{S}$) quark pair is annihilated and only non-strange hadrons are produced. This was generalized to J/Ψ meson by considering it to be a charmed quark ($C\bar{C}$) pair so that it similarly would be forbidden, to first order, to decay into ordinary (non-charmed) hadrons. The OZI rule thus suppressed most of

the available decay channels for J/ψ which consequently is seen as a very narrow resonance.

The OZI rule is a qualitative prescription and a measurement of its strength is needed before it can be quantitatively applied to any particular phenomenon. The procedure to quantify the OZI rule has generaly been to measure the ratio of cross-sections of forbidden to allowed processes in particular reactions,

$$R = \frac{\sum \sigma(\text{hadron} + \text{hadron} \rightarrow \text{forbidden processes})}{\sum \sigma(\text{hadron} + \text{hadron} \rightarrow \text{Allowed Processes})}$$

Thus Okubo[1] has compared Φ to ω production in exclusive channels and concluded that R can not be larger than .02.

3- Conjoint Production of Φ or J/ψ

The OZI rule, as described in previous sections would require that a pair of strange particles be produced in association with a Φ meson whenever the latter is created in a collision between non-strange hadrons. The rule would require similarly the production of pairs of charmed particles in association with a J/ψ, ψ', ψ'' etc. Thus a quantitative test of the OZI rule in either case can be achieved by measuring the forbidden to allowed ratio.

$$R = \frac{\sigma(\text{hadron} + \text{hadron} \rightarrow \Phi(\text{or } J/\psi) + \text{non-Strange(Charm)})}{\sigma(\text{hadron} + \text{hadron} \rightarrow \Phi(\text{or } J/\psi) + \text{a pair of Strange(charm)})}$$

Lipkin[5] has argued however that in the case of Φ -production a measurement of this R would not be a good test of the OZI rule because other dynamical considerations reduce the probability of production of an extra pair of strange particles. This might lead to an apparent suppression of conjoint processes in favor of forbidden processes, which would not necessarily imply the failure of the OZI rule itself. Thus R is at least an upperbound to the violation of the rule.

Recently, the ACCMOR[7] collaboration observed an increase in the rate of KO production in conjunction with Φ -mesons,

$$(\pi/P)\,P \longrightarrow \Phi + X + K_s^\circ \qquad \text{II-2}$$

They also saw some indication of the same effect for Λ° production in association with Φ-mesons.

In the present experiment we shall study in particular the semi-inclusive reactions,

$$\pi^+ + P \longrightarrow \Phi + \Lambda^\circ + X \qquad \text{II-3}$$

$$\pi^+ + P \longrightarrow \Phi + K_s^\circ + X$$

The cross-section for these reactions at 16 GeV/c will be given and compared with that for inclusive production of Φ at the same incident momentum. In Fig. II-2, are shown examples of Φ production in the OZI-allowed and OZI forbidden processes.

B- Present Status of the OZI Rule

Experimental data on the OZI rule as it applies to production processes are very scarce and conclusions are often contradictory. However, most of the existing eveidence is in favor of the validity of the rule. The present status can be summarized as follows;

1-R. A. Donald[15] from the Liverpool group studied the reactions,

$$\bar{P}P \longrightarrow \Phi K^- K^+ \qquad \text{II-4a}$$

$$\bar{P}P \longrightarrow \Phi \pi\pi \qquad \text{II-4b}$$

at 3.6 Gev/c. They observed the suppression of the OZI forbidden reaction(II-4b) as compared with the reaction (II-4a). However, their result is based on a small number of events, identified by kinematic fits. They have not studied the phase space suppression of the reaction II-4a; consequently their result remains only a qualitative test of the rule.

2-Blobel[16], et al studied Φ production in PP collisons at 24 Gev/c. They examined the OZI rule, by searching for reactions in which a strange particle was produced accompanying Φ . In particular, they compared,

$$p\,p \longrightarrow \Phi + X\,(\text{non-strange}) \qquad \text{II-5a}$$

with

$$p\,p \longrightarrow \Phi + K^{\circ}_{s} + X \qquad \text{II-5b}$$

No tendency was observed for the OZI allowed conjoint reaction (II-5b) to dominate Φ production.

3-A.Etkin[17], et al studied the reaction,

$$\pi^- + p \longrightarrow K^- K^+ K^- K^+ n$$

at 22.6 Gev/c and selected 1 Φ and 2 Φ processes. A study of the OZI forbidden reaction(II-6a), gave an order of magnitude smaller cross-section for it than for the OZI-favored process (II-6b).

$$\pi^- + p \longrightarrow \Phi\,\Phi\,n \qquad \text{II-6a}$$

$$\pi^- + p \longrightarrow \Phi\,K^-\,K^+\,n \qquad \text{II-6b}$$

4. A report from the ACCMOR[7] collaboration shows evidence for an increase in the rate of K°_{s} production in reactions,

$$(\pi/p) + p \longrightarrow K^- K^+ + X$$

when M(K-K+) is in the Φ-meson region.

Given these experimental observations and their somewhat contradictory conclusions about the OZI rule, the need for further investigation of the rule is clear. So far, most experiments have studied Φ-meson production by first detecting a (K-K+) pair. In bubble chambers however, the low rate of visible $K^{\pm}$ decay and inefficiency of $K^{\pm}$ identification through kinematical fits have made it difficult to obtain a good sample of events in which the large geometrical acceptance could be exploited to study particles accompanying the Φ . Electronic spectrometers also have acceptance limitations.

C- Quark Fusion Models

1-General Description

The picture of nucleons obtained from analysis of deep inelastic scattering of electrons[8] and neutrinos is that they consist of three "valence" quarks and a "sea" of quark-antiquark pairs. Parton models provide information, based on these data about the momentum distributions of the quark and gluon constituents of the nucleon, and theorists have generalized these results and have parametrized the quark distribution functions for pions and kaons as well as for nucleons.[8,9] They have made use of this information and applied parton models to large transverse momentum (high Pt) reactions in hadron collisions.

In principle, an acceptable model must also describe low-P_t reactions quantitatively. One attempt to provide some information about low-pt phenomena is the quark fusion model, which is a generalization of the Drell-Yan mechanism. Gunion and Landshoff have generalized the Drell-Yan mechanism and formulated a model for J/ψ production in hadron-hadron collisions. According to this model, the J/ψ is created as a result of fusion of a quark Q emitted by one of the incident hadrons and the corresponding antiquark $\bar{Q}$ from the other. It is argued that fusion of a pair of charmed quarks, $(C\bar{C})$, from the "sea" dominates in J/ψ production over the fusion of ordinary non-charmed quarks.

Nandi[21] has argued that quark fusion model can also be applied to processes which involve production of ordinary(non-charmed) pseudo-scalar mesons and vector mesons in hadronic collisions. Thus, according to the model, a hadron of quark content $Q1\bar{Q}2$ is produced from fusion of a quark Q1 and an anti-quark $\bar{Q}2$ from incident hadrons.

2-Inclusive Cross-Sections

To obtain the inclusive cross-section for a quark fusion process a generalized form of the Drell-Yan[10] relation is used. This contains the quark distribution functions in the initial hadrons as the only ingredients. Thus the inclusive differential cross-section is given by

$$X_R \frac{d\sigma}{dx} = (1/3)(g^2/4\pi)(4\pi^2/m_T^2) x_1 x_2 \left(f_{q_1}^A(x_1) f_{\bar{q}_2}^B(x_2) + f_{\bar{q}_2}^A(x_2) f_{q_1}^B(x_1) \right)$$

where 1/3 is the color factor, m is the mass of the produced vector meson and $m_T = (m^2 + \langle P_T^2 \rangle)^{1/2}$. For directly produced mesons it is assumed that $\langle P_T^2 \rangle = .25\,(\text{Gev/c})^2$. From the Drell-Yan relations, we have:

$$X_R = x_1 + x_2$$

$$X = x_1 - x_2 \quad , \quad x_1 x_2 = m_T^2 / S$$

which result in,

$$X_R = (X^2 + 4m_T^2/S)^{1/2}$$

and

$$x_{1,2} = 1/2\,(\pm X + X_R)$$

$F_q^A(x)$ is the probability of finding a quark q with a momentum fraction x in the hadron A.

Recently R.Kinnunon[18] has compared experimental results on vector meson production in hadronic interactions with predictions of the quark fusion model. In this work the quark distribution functions given by the Kuti-Weisskopf model[19] and quark counting rules are used where,

$$V_u^P(x) = 1.7\,(1 + 2.3x)(1-x)^3/\sqrt{x} \quad ,$$

$$V_d^P(x) = 1.1\,(1-x)^{3.1}/\sqrt{x} \quad ,$$

$$S_{u,\bar{u}}^P(x) = S_{d,\bar{d}}^P(x) = S_{s,\bar{s}}^P(x)/\lambda_S = 0.36\,(1-x)^7/x$$

and where λ_s is the strange quark suppression factor in the proton sea. For mesons the parametrization of the Kuti-Weisskopf model based on several phenomenolgical arguments[18] were used. Then for pions,

$$V^{\pi}_{u,d}(x) = 0.75(1-x)/\sqrt{x}$$

for kaons

$$V^{K}_{s,\bar{s}}(x) = 2(1-x)$$

$$V^{K}_{u,\bar{u}}(x) = 0.85(1-x)^{1.5}/\sqrt{x}$$

and for the "sea" quark contributions from mesons,

$$S^{\pi,K}_{u,\bar{u}}(x) = S^{\pi,K}_{d,\bar{d}}(x) = S^{\pi,K}_{s,\bar{s}}(x)/\lambda_s = 0.3(1-x)^{5}/\sqrt{x}$$

The model has reproduced well the experimental results for ρ° and K* productions in PP and $\bar{P}P$ interactions.

The predictions of the model for K* and $\bar{K}$* production in $\pi^{+}P$ interactions at 16 Gev/c were also compared with the existing experimental data. Contributions of various subprocesses to the production of K* and $\bar{K}$* states are given in Table II-1. Predictions of the model for differential cross-sections are presented in Fig. II-4, and compared with the experimental data.

It can be seen that the predictions of the model are not in perfect agreement with the experimental results. This inconsistency for K* production in $\pi^{+}P$ interactions and the model's success in describing the experimental results

for PP interactions suggest that the quark distribution functions in mesons are not correctly parametrized. However some of the difficulties encountered by the model in describing the experimentally observed spectra for K^{*+} and K^{*-} production can be attributed to the fact that in former case several subprocesses contribute to K^{*} production and in the latter the contribution is only from "sea" quarks. However, a simpler and more direct test of the model is possible by comparing the experimental results for $\bar{K}^{*0}(s\bar{d})$ production in the forward region($x_F > 0.4$), where only the fusion of pion valence $\bar{d}$ and the proton sea quarks($V^{\pi} S^{p}$) is present.

The results from the present experiment on $\bar{K}^{*0}$ production in $\pi^{+}P$ interactions are presented in Chapter VI and a comparison of the results with the quark fusion model prediction is discussed in Chapter VII.

D- Motivation for the Experimental Methods

To overcome some of the difficulties encountered in previous attempts to study the OZI rule in ϕ production described in Section II-B, the present experiment was designed to combine features of bubble chamber and counter techniques in a single experiment.The procedure in selection was to detect ϕ-mesons by primarily triggering on forward K- from $\pi^{+}P$ collisions. The accurate measurement of the angles and momenta of interactions as well as the detection of secondary particles accompanying the ϕ-meson was

possible using streamer chamber photographs of the interactions occuring in a hydrogen target near the center of the chamber.

The choice of K- versus K+ for a trigger particle, was made to avoid triggers from associated production of $(K^{+} Y^{*})$ which are a large source of K+ production. A streamer chamber was selected as opposed to a bubble chamber because of the relatively high beam and trigger rate that were possible.

REFERENCES

1- S.Okubo, Phys. Rev. D16, 2336(1977)

2-D.Cohen et al, Phys. Rev. Lett. 38, 269(1977)

3- J.J.Sakurai, Phys. Rev. Lett. 9, 472(1962)

4-G.Zweig, CERN Report No. TH-401 and TH-412(1964) unpublished

5- H.J.Lipkin, Proceeding of Eleventh Recontre De Moriond Conference 169(1976)

6-D.R.O.Morrison, CERN-EP/79-102(1979)

7-C.Daum, et al, Phys. Lett 98B, 313(1980)

8-R.D.Field, R.P.Feynman, Phys. Rev. D15, 2590(1977)

9-V.Barger, R.J.N.Phillips, Nuclear Phys.B73, 269(1974)

10-S.D.Drell, T.M.Yan, Phys. Rev., Lett.25, 316(1970)

12-J.F.Gunion, Phys. Rev. D12, 1345(1975)

13-M.B.Green, et al, Nuovo Cimento, 29A, 128(1975)

14-A.Donnachie, P.V.Landshoff, Nucl. Phys. B112, 233(1976)

15-R.A.Donald, et al., Phys. Lett. 61B, 210(1976)

16-V.Blobel, et al., Phys. Lett. 59B, 87(1975)

17-A.Etkin, Phys. Rev. Lett. 40, 422(1978)

18-R.Kinnunen, HU-P-178(1980)

19-J.Kuti, P.V.Weisskopf, Phys. Rev. D4., 3418(1971)

20-R.Mcchaney and S.F.Tuan, Phys. Rev. Lett. 31(1973)

21-S.Nandi, Phys. Rev. D17, 1336(1978)

V	$V^{\pi+}V^{P}$	$V^{\pi+}S^{P}$	$V^{P}S^{\pi+}$	$S^{\pi+}S^{P}$
K^{*+}	—	$\lambda s V_u^{\pi} S_{\bar{s}}^{P}$	$\lambda s V_u^{P} S_{\bar{s}}^{\pi}$	$\lambda s(S_u^{\pi}S_{\bar{s}}^{P} + S_{\bar{s}}^{\pi}S_u^{P})$
K^{*-}	—		—	$\lambda s(S_{\bar{u}}^{\pi}S_s^{P} + S_s^{\pi}S_{\bar{u}}^{P})$
K^{o*}	—		$\lambda s V_d^{P} S_{\bar{s}}^{\pi}$	$\lambda s(S_d^{\pi}S_{\bar{s}}^{P} + S_{\bar{s}}^{\pi}S_d^{P})$
$\bar{K}^{*o}$		$\lambda s V_{\bar{d}}^{\pi} S_s^{P}$	—	$\lambda s(S_{\bar{d}}^{\pi}S_s^{P} + S_s^{\pi}S_{\bar{d}}^{P})$

Table II-1 - K^{*} and $\bar{K}^{*}$ Production in Quark fusion Processes

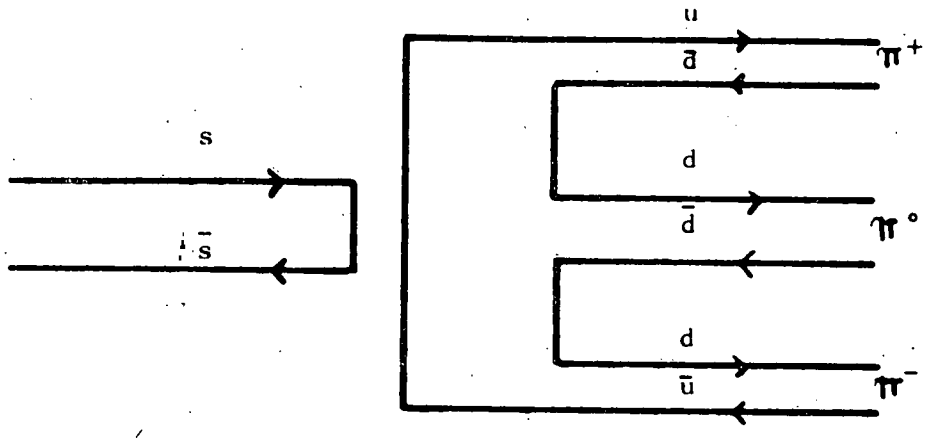

Fig. II-1a
$\phi \to \pi^+ \pi^- \pi^\circ$ (OZI Forbidden) Process

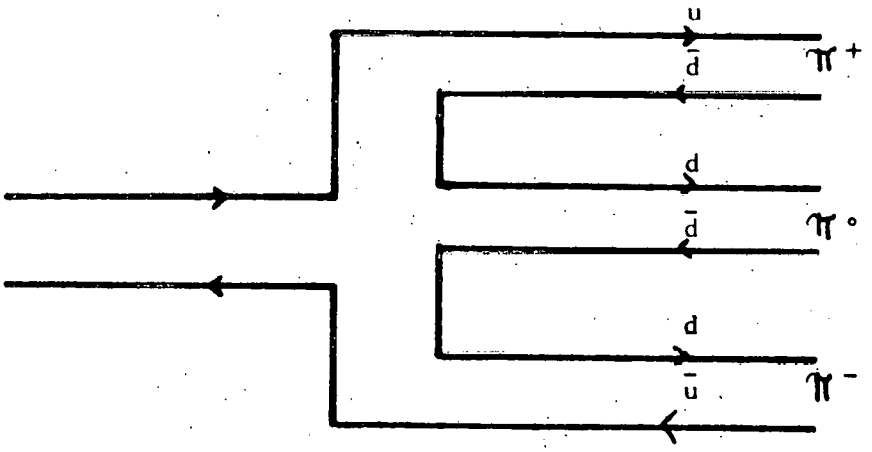

Fig. II-1b
$\omega \to \pi^+ \pi^- \pi$ (OZI Allowed) Process

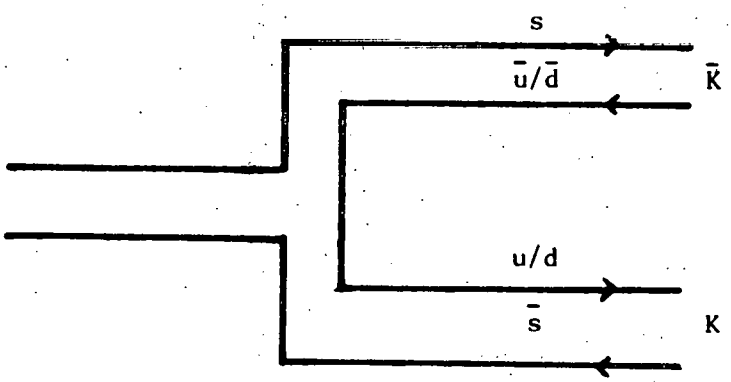

Fig. II-1c
$\phi \to K\bar{K}$ (OZI Allowed) Process

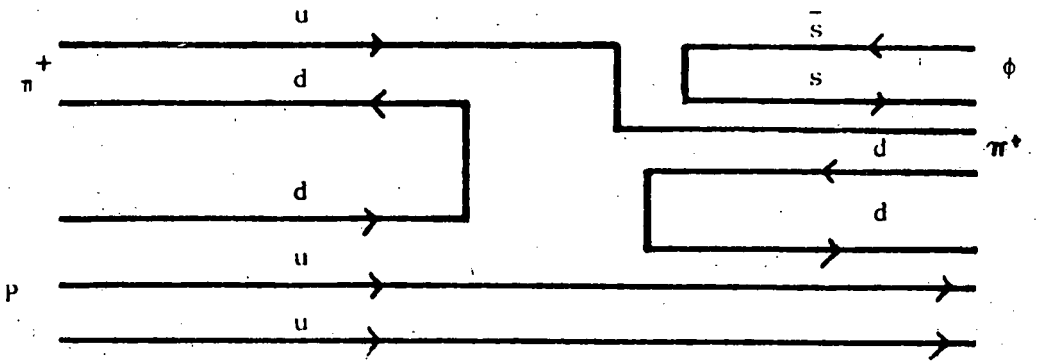

Fig. II-2a - An OZI - Forbidden Process for Production of ϕ-mesons: ($\pi^+ + P \rightarrow \phi +$ (non-strange))

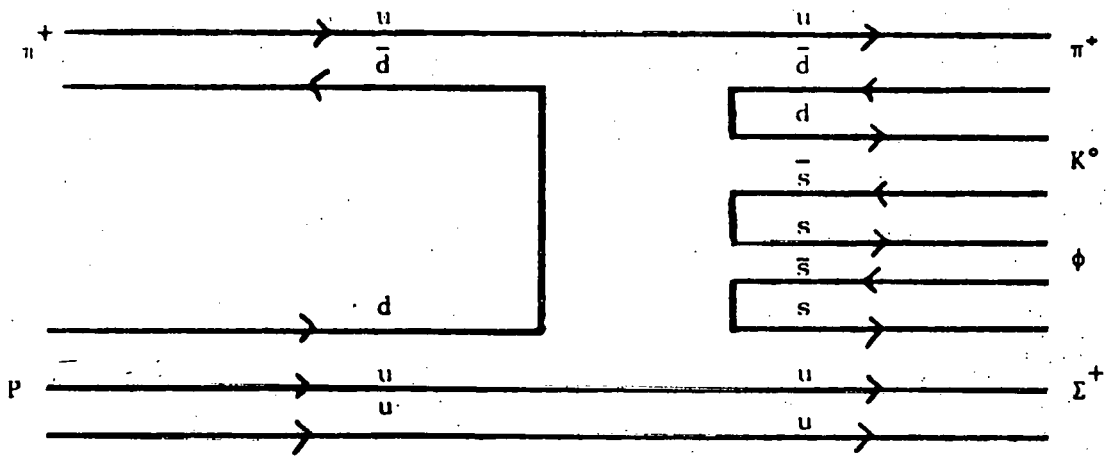

Fig. II-2b - An OZI Allowed conjoint Process ($\pi^+ + P \rightarrow \phi + K^\circ_s + X$)

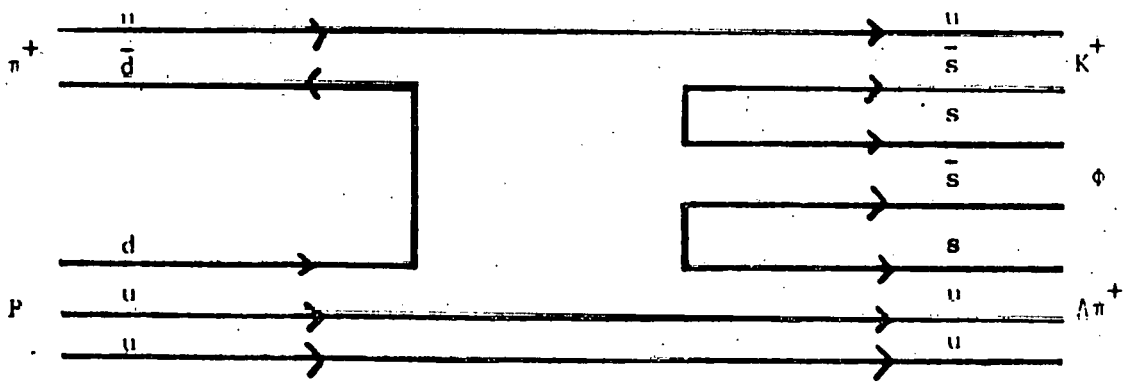

Fig. II-2c - An OZI Allowed conjoint Process ($\pi^+ + P \rightarrow \phi + \Lambda^\circ + X$)

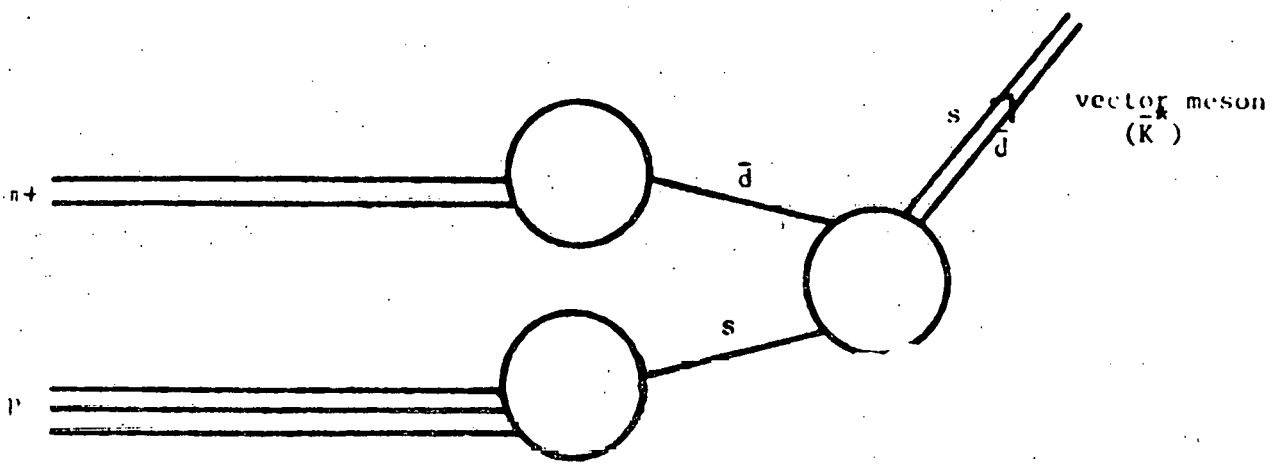

Fig. II-3 Quark fusion Process
$(\pi^{\pm}+P \rightarrow \bar{K}^{*}+X)$

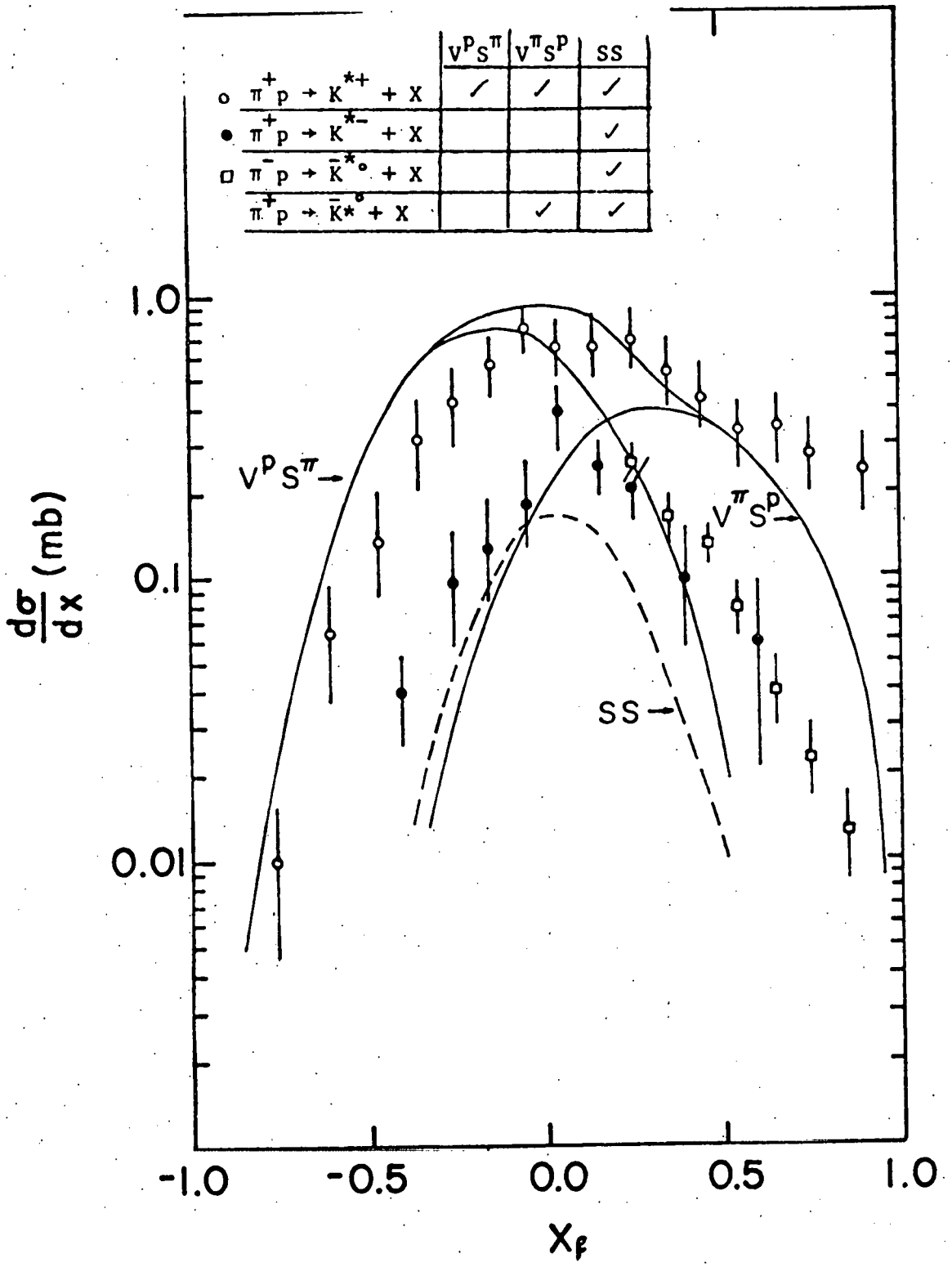

Fig II-4-Predictions of Quark Fusion Model for $d\sigma/dX_f$ of K* and $\bar{K}$* in π^+P interactions at 16 GeV/c.

CHAPTER III-EXPERIMENTAL APPARATUS

A-General Description of the Experimental Setup

This experiment was designed to search for mesons containing strange quarks as may be produced in $\pi^+ P$ interactions. The π^+ beam had a momentum of 16 GeV/C and was incident on a liquid hydrogen target 60 cm long. The apparatus was designed to select reactions of the class,

$$\pi^+ + P \longrightarrow K^- + X \qquad \text{III -1}$$

with K- momenta in the range $2.5 < P < 16$ (GeV/C).

A schematic diagram of the experimental setup is shown in Fig. III-1. The major element was the SLAC two meter streamer chamber with the hydrogen target located near its center. A set of scintillation counters including counter S3 and anti-counters An and As, shown in the Fig. III-1, and an upstream differential Cerenkov counter defined the pion beam at the target. Forward K- and π^- from reaction III-1 were detected by 20 channel picket fence counters V1, V2, V3 and V4, whose 4-fold coincidences defined trajectories emerging from the target into 20 coarse momentum channnel. Final momentum determination of the charged particles was accomplished by measuring particle trajectories photographed in the streamer chamber magnetic field. A K- trigger required an incident π^+ signal, a coincidence signal from corresponding elements of at least 1 picket fence momentum

channel, and a null signal from the appropriate channel of the 10 -cell "K-" threshold Cerenkov counter located behind the picket fence. This "K-" counter system was designed to distinguish π's from K's in the momentum range P>2.7 (GeV/C) and the rejection efficiency was measured to be 99.84% at 9 GeV/c. Trigger signal which coincided with a system ready signal pulsed the streamer chamber to permit the event to be photographed, and also recorded on magnetic tape other data including scintillation counter latches, pulse height in the Cerenkov counters, scalers and other information from the system. The data were passed partly via CAMAC to a PDP-9 processor which in addition to controlling the tape drive provided on-line monitoring of the various detectors. A second threshold Cerenkov counter, identical to that used to establish the K- trigger was mounted on the other side of the beam and pulse heights from its 10 cells were also recorded. This "K+" Cerenkov counter was used in the final data analysis to separate K+ mesons from particles whose trajectories extrapolated through the counter cells. Detailed descriptions of the different segments of the experimental apparatus are presented in following sections.

B-Beam

The π^+ mesons which comprised the beam for this experiment were produced by interactions of the SLAC primary electron beam, at energies of 19 to 21 GeV, in a beryllium target. Secondary particles were focused by a series of magnets, forming SLAC beam line 23, onto the successive focal

points, F1 and F2 (see Fig. III-2). Two scintillation counters, S1 and S2 monitored the beam flux at F2. A differential gas Cerenkov counter, Cf, was used to select π^+ from contaminating K+ and P at this point.

The last set of the quadrupole magnets 23Q7-9, focussed the beam onto the hydrogen target, in the streamer chamber. A scintillator S3 (Fig. III-1) was used to detect particles entering an area $1'' \times 1''$ ahead of the target. Two scintillation anti-counters, AS and AN, signalled beam halo particles. The beam came in 1.5 μ s bursts with about 7 particles per burst and a 1 μs duty cycle. For most of the data taking there were about 120 burst per second.

The beam signal " π^+ " was obtained by forming a coincidence between signals from S1, S2, S3, Cf and $\overline{AN+AS}$,

$$\pi^+ = S1 . S2 . S3 . CF . \overline{(AS+AN)} \qquad \text{III-2}$$

Beam momentum was determined by measuring 100 single beam tracks from streamer chamber pictures and was found to be 15.5±.8 GeV/c. The fraction of kaon and proton contamination in the beam was estimated from analysis of the data from the beam line Cerenkov counter($\check{C}f$). Table (III-1) gives the fraction of each of these particles in the beam. The momentum of the beam was also determined from this analysis to be 16±.13 GeV/C consistent with the beam track measurements. This analysis is described in detail in

reference 1.

The beam transport and monitoring system also included two small MPWC chambers, each constructed of four planes of X, Y, U and V with 1mm wire spacing. The information from these MPWC chambers was to have been used in the final data analysis for measurement of the coordinates and direction of the beam particles entering upstream of the streamer chamber. However, the use of these information was not possible due to inefficiency of the detectors and the relatively large beam flux.

C-The Streamer Chamber[2] and Target

The SLAC two meter streamer chamber was the major instrument in the experiment since it allowed geometrical parameters from interactions to be measured. The chamber was a box 2m long, .8 m wide and .6 m deep filled with a 90% neon and 10% helium gas mixture to which was added isobutane one part in 1000. Three planes of wires formed the transparent electrode. Electrode wires were of .25 mm diameter and 1 cm spacing.

The liquid hydrogen target was a 60 cm long cylindrical tube 3.17 cm in diameter placed just above the central electrode with its end cap at the center of the streamer chamber. The liquid hydrogen was in a vacuum jacket with outer and inner walls of thin mylar of thickness $\sim$ .01 cm. A foam and acrylic support was attached to the top of the vacuum jacket to serve as δ-ray absorber. Three

fiducial X-marks mounted on top of the δ-ray shield located the target optically in the streamer chamber photographs.

The streamer chamber was located in a 1 m gap between two circular coils which with an iron return yoke provided a magnetic field of 1.3 T. Three independent cameras were used to photograph the chamber from above with a streo angle of 18° from each part. Numerical values for various parameters in the streamer chamber photographic system are presented in Table III-2. Fig. III-3 shows a side view of the operational arrangement of the streamer chamber.

D- Cerenkov Counters[3]

The K- and K+ Cerenkov counters were two large-aperture, 10-cell threshold detectors. The counters were used as threshold detectors to separate π,s from K,s. The K- Cerenkov counter was used to veto pions and define the trigger particle. These counters have been described[3] in detail in Nuclear Instruments and Methods (see Appendix A). The Cerenkov radiation produced by charged particles traversing isobutane (CH(CH3)3) at atmospheric gas pressure was detected in each chamber by a system of 10 light collecting cells. The index of refraction of the isobutane radiator was ($n=1.000131$). Fig. III-4 showes a projected view of one of the identical counters. The pion rejection efficiencies of all twenty cells were measured during a test run, using a 9 Gev/c π^-

beam. The overall averaged efficiencies were 99.848±.006% and 99.717±.008% for the K- and K+ Cerenkov counters, respectively (see Appendix A). Statistical analysis of the pulse height spectrum from one of the Cerenkov cells for a 9 GeV/c π^- beam, suggests a value of 21 for the average number of photoelectrons generated at the photo-cathode. Given the following equation for Cerenkov light emission at angle θ,

$$\bar{n}=A\ L\ \sin^2\theta \qquad \text{III-3}$$

where

L= path length (225 cm)

and

A= 44 (from pulse height analysis)

then with θ =.02166 rd, corresponding to 3 GeV/c pions we would expect an $\bar{n}$ of 4 photoelectrons. Assuming a Poisson distribution we infer that this $\bar{n}$ would give rejection efficiency of ϵ >98.1% for pions of 3 GeV/c. This momentum value was used in subsequent cuts in the analysis.

The pulse height information from each of the 20 cells was used in the final data analysis to identify K- and K+ mesons emerging from photographed interactions in the target and extrapolated at a known momentum in a particular cell.

E- Trigger Hodoscope

Four sets of vertical "picket fence" counters, V1, V2, V3 and V4 were placed at 2, 3, 4 and 6.45 meters downstream of the streamer chamber respectively. These defined the trajectories of negative particles having momenta greater than 2.5 GeV/c(Fig. III-1). The momentum definition for a trigger particle was accomplished by requiring that corresponding elements in the 4 picket fence arrays be struck in coincidence. A null signal from the corresponding cell of the K- threshold Cerenkov counter excluded π^- and thus defined a K-(or P) as the trigger particle.

Each of the picket fence arrays consisted of 20 long scintillation counters. Tables III-3, 4 and 5 show the numerical values related to the physical configuration of the counters.

Each scintillation counter was viewed by a photomultiplier shielded with mu-metal and iron pipe against the 50-100 gauss magnetic field. The averaged efficiency of the picket fence counter set was measured to be ($\bar{\epsilon}$ =.482 +.001)(see section V-F for details). Efficiencies, channel by channel are given in Table III-4. Fig. III-2 displays the picket fence counters in place. The "Logical Trigger" was defined as a fast logical coincidence of corresponding elements in quadruple array of counters in anti-coincidence with the appropriate Cerenkov cell,

$$LT = \pi^{+} . \sum V1i . V2i . V3up/V3down . V4i . C1k- \qquad III-4$$

where π^{+} is defined in equation III-2.

F-Electronics and On-line Monitoring System

1-Fast Trigger Logic

The main purpose of the fast electronics in this experiment was to define a master trigger. This master trigger was a coincidence of logical trigger (III-4) with a system ready signal which indicated that camera and computer were free to record a new event,

$$MT = LT . SR$$

Schematics for beam and trigger logic are given in Fig. III-5 and Fig. III-6. Beam related signals were selected by a 2 μs wide gate, produced by a gate generator which was triggered by a machine gate received from SLAC accelerator control. The latter consisted of 1 μs pulses occurring at the same repetition rate as the primary electron beam, but $\sim$1 μs in advance of the beam. The output of the gate generator was vetoed by signals indicating any of the following conditions.

a) An event had already occured in the beam spill and a logical trigger had been generated.

b) The computer was busy recording the data from a previous event(20-60 ms dead time).

c) The manual beam switch was off.

Finally, a master trigger (III-7) was generated and the rest of the apparatus, including the streamer chamber pulser, camera and computer readout, were triggered by it as shown in Fig. III-7. As also shown in Fig. III-7, each time a trigger occurred, any further trigger was vetoed by a 200 ms signal generated by the main gate in order to allow for recharging of Marx generators that fired the streamer chamber.

2- Cerenkov Electronics

The K- Cerenkov counter circuits had two main functions:

a) to produce a logic level which would discriminate against π^- in the trigger generation (III-4), and

b) to measure the total charge in each photo-tube pulse in the corresponding channel of an ADC (Analog to Digital Convertor), for subsequent logging on the magnetic tape record of each event.

Ten additional units also recorded the pulse height information during the event gate for the 10 photo-tubes of the K+ Cerenkov counter.

The on-line monitoring system consisted of a PDP-9 computer and a CAMAC interface. The master trigger served as an interrupt signal for the PDP-9. When an interrupt signal was received the computer performed the following operations:

a) sent a 20-60 ms wide busy signal to veto the beam gate generator and further trigger;

b) recorded frame and roll number;

c) read into buffer all CAMAC data, including latches, scalars, ADC's, PWC data and the index of refraction of the isobutane gas, then wrote this buffer on to magnetic tape;

d) accumulated counter and other data for on-line monitoring of system performance

Data recording was completed when the streamer chamber was photographed by three independent cameras and the film was advanced.

REFERENCES

1-J.Hylen , Michigan State University, Doctral dissertation in Physics

2-F.Bulos, et al, SLAC Report NO.74

3-J.Hylen, Z.Ming Ma, A.Jawahery, T.Maruyama, and R.H.Milburn, Nucl. Inst. and Meth. 185(1981)107

TABLE III-1

Fractions of Various Contaminating Particles in the Beam

Particle	Fraction (%)	Fraction (%) After C_f
K^+	8.1	1.1
P	3.7	.04

TABLE III-2

Streamer Chamber Photographic System

Demagnification	70
Film	Kodak

TABLE III-3

Width of the Scintillation Counters Used in the Trigger Hodoscope (cm)

Elements	V_1	V_2	V_3	V_4
1	3.0	4.5	6	17.5
2	3.0	4.5	"	"
3	3.0	4.5	"	"
4	3.0	4.	"	"
5	3.0	3.75	5	"
6	2.5	3.75	"	"
7	2.5	3.75	"	15.5
8	2.5	"	"	"
9	2.5	"	"	"
10	2.5	"	"	"
11	2.5	"	"	"
12	2.5	"	"	"
13	2.5	"	"	"
14	2.5	"	4	"
15	2.5	3.25	"	13
16	3.0	3	"	"
17	3.0	"	"	"
18	3.0	"	"	"
19	3.0	"	"	"
20	3.0	"	"	"

TABLE III-4

Physical Configuration of the Picket Fence Counters

	V_1	V_2	V_3	V_4
Thickness (Inch)	.125	.125	.125	.25
Relative Distance to the Streamer Chamber (cm)	200	300	400	645
Distance Shifted to Left from Center Line (cm)	0	3	6	13.5
Length (cm)	40	60	40	125

TABLE III-5

Efficiency of the Various Elements in Trigger Hodoscope

Channel	Efficiency*	Fraction of Triggers†
1	0.430	0.0976
2	0.663	0.1219
3	0.445	0.1037
4	0.365	0.0936
5	0.408	0.0788
6	0.476	0.0734
7	0.703	0.0478
8	0.467	0.0492
9	0.467	0.0391
10	0.535	0.0458
11	0.514	0.0391
12	0.668	0.0492
13	0.527	0.0330
14	0.489	0.0175
15	0.283	0.0236
16	0.406	0.0209
17	0.142	0.0209
18	0.346	0.0128
19	0.387	0.0125
20	0.196	0.0108

* Efficiency is Averaged for Measurement Performed at the Beginning and End of the Data Taking for Up and Down Elements.

† The Fraction of Triggers into Each Element is Determined Using a Montecarlo Calculation.

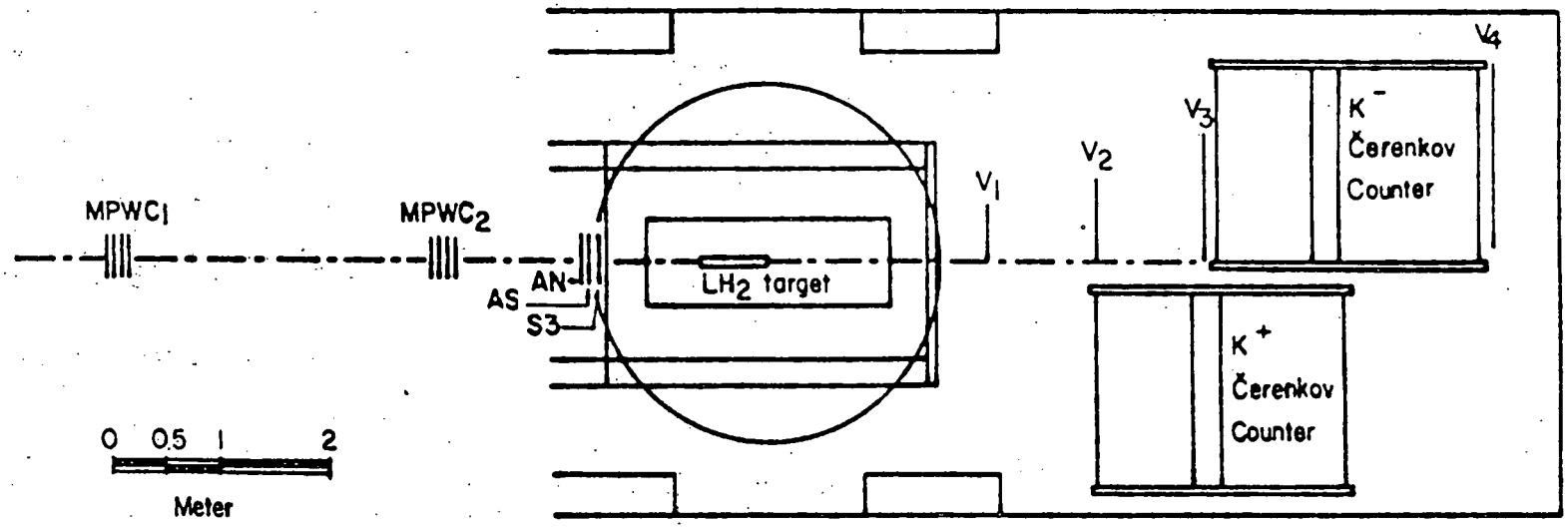

Fig III-1- Layout of Experiment

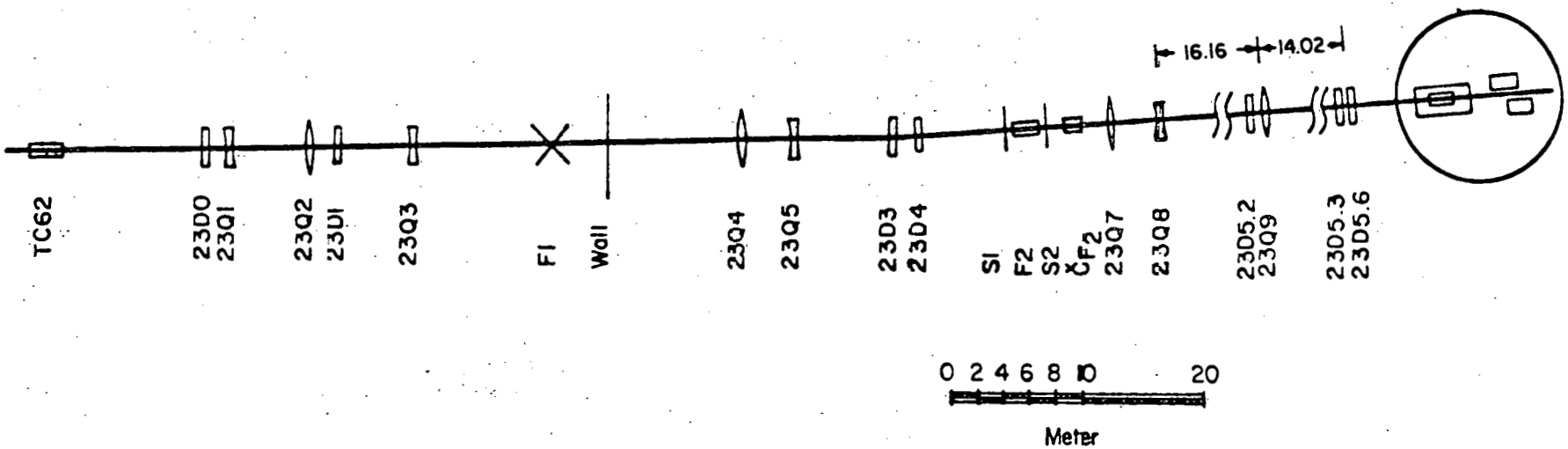

Fig III-2- SLAC Beam Line 23

(Note: D and Q stand for Dipole and Quadrupole magnet, respectively.)

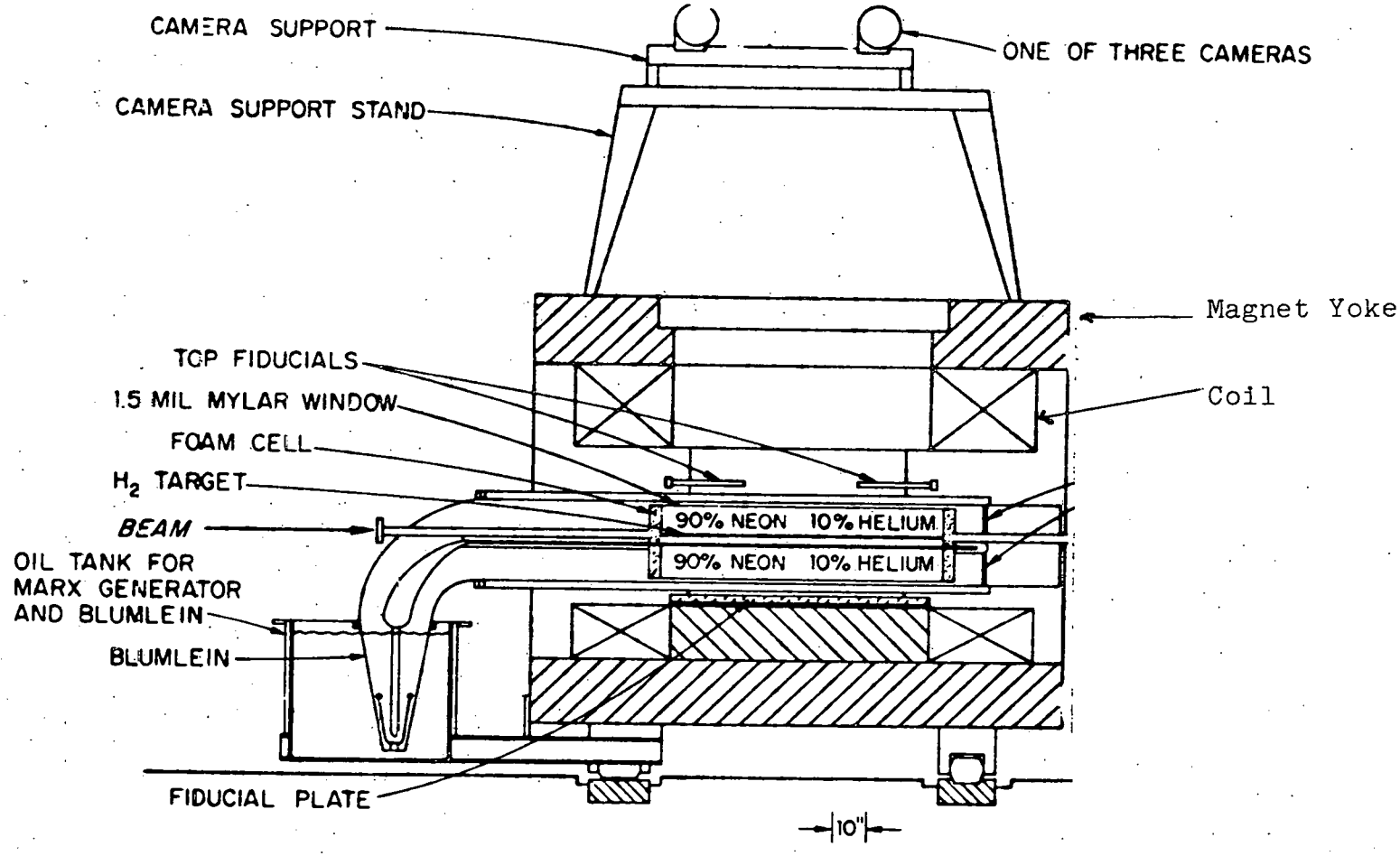

Fig. III-3- Side View of the Streamer Chamber

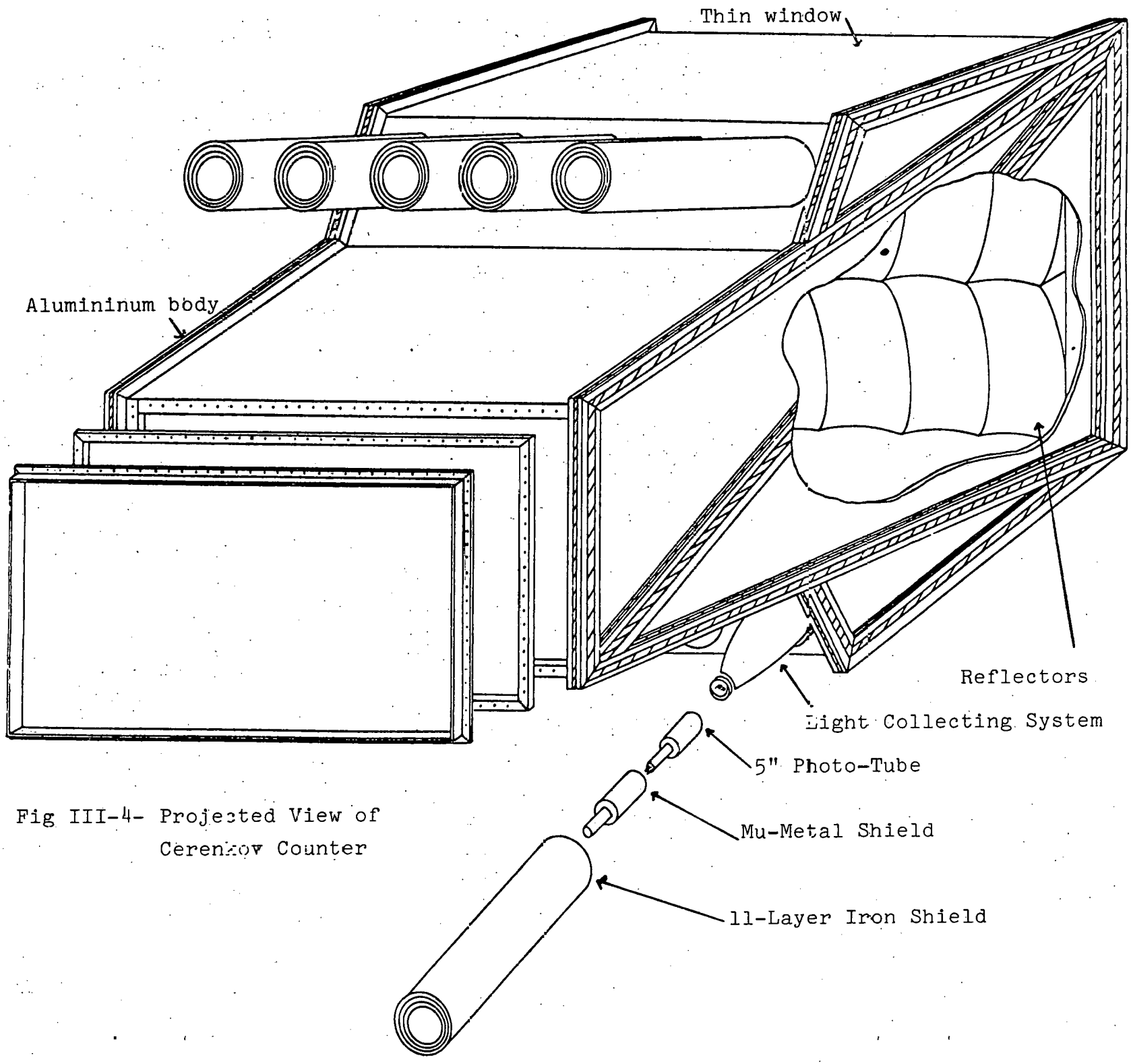

Fig III-4- Projected View of Cerenkov Counter

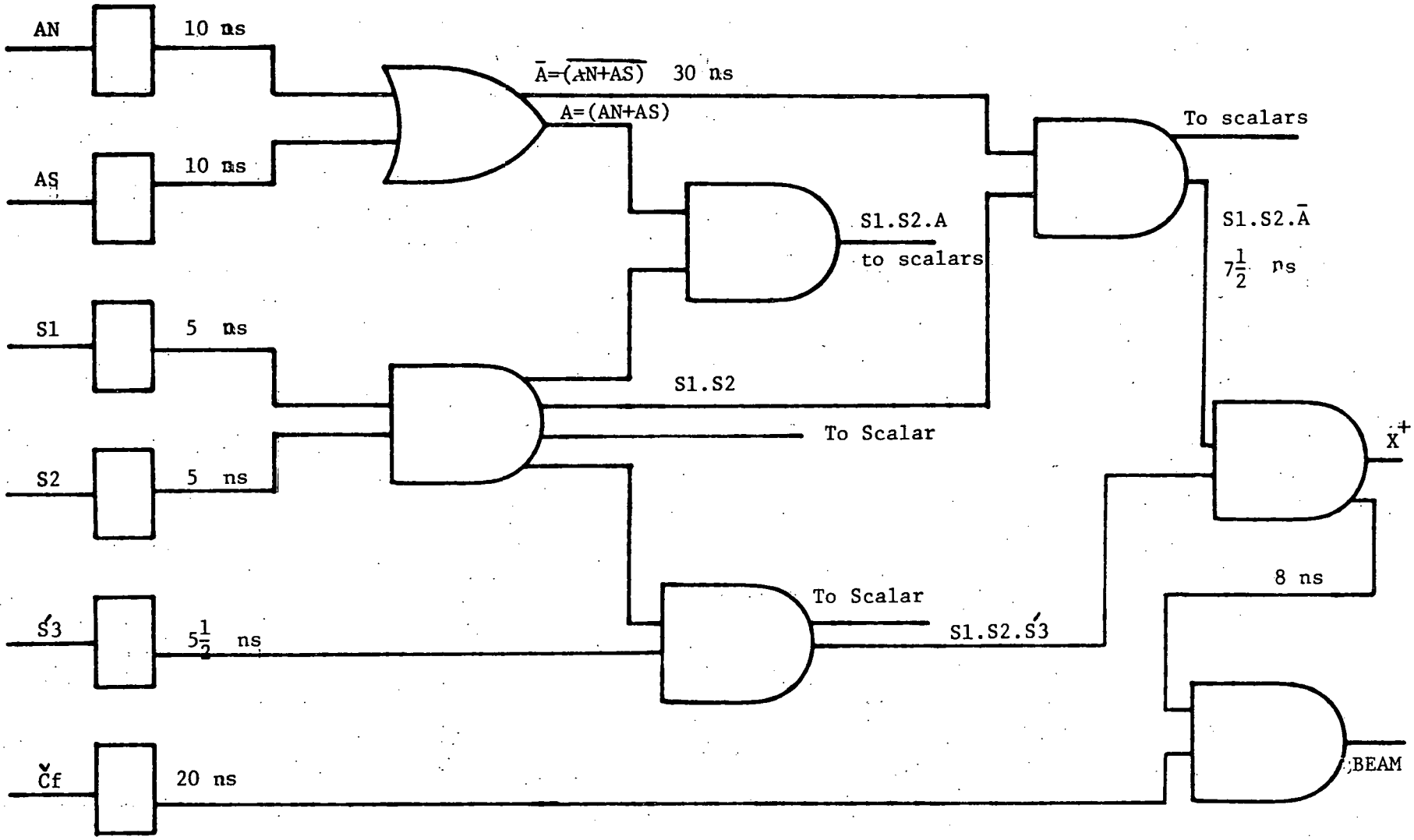

Figure III-5
Generation of Beam Signal

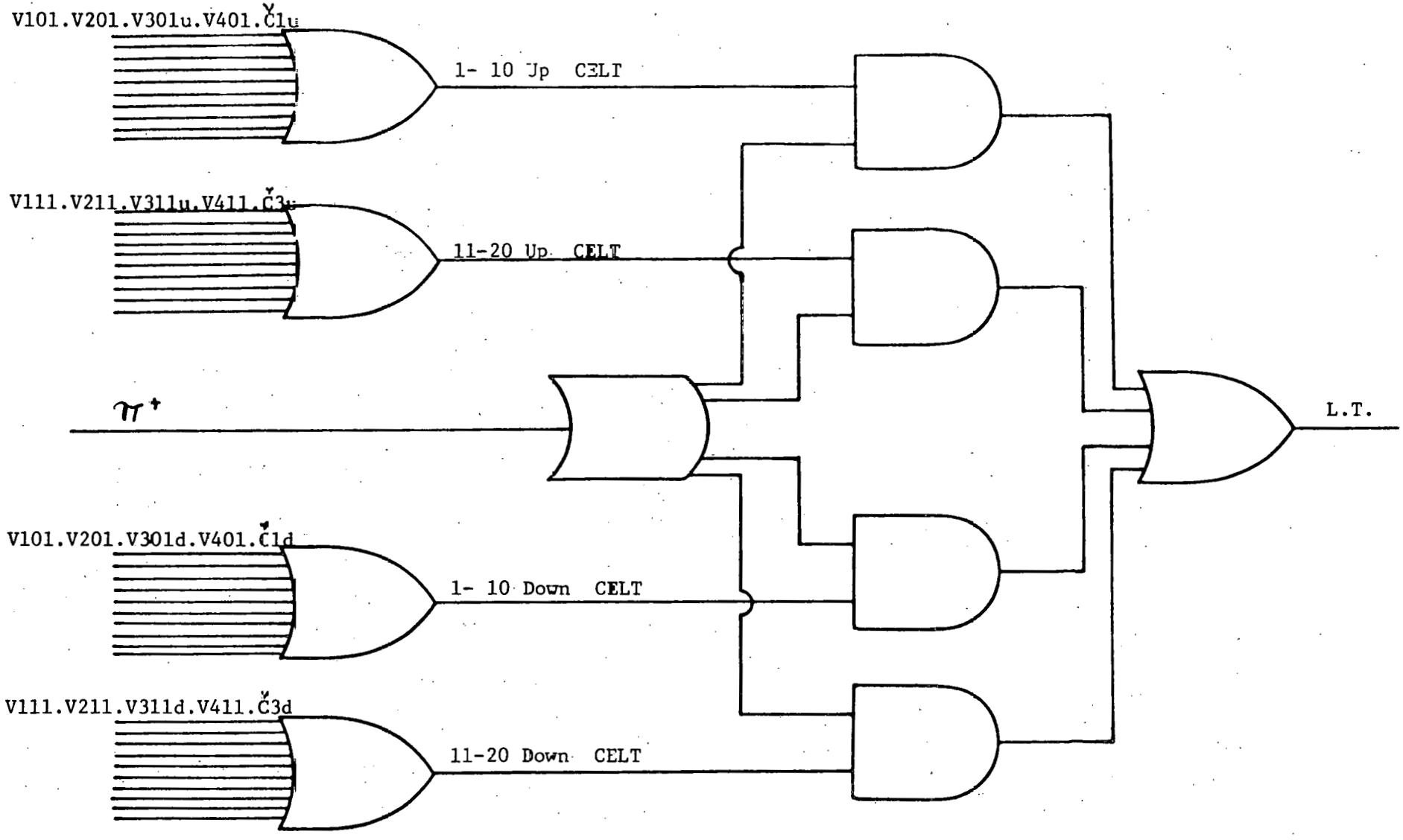

Figure III-6
Generation of Logical Trigger

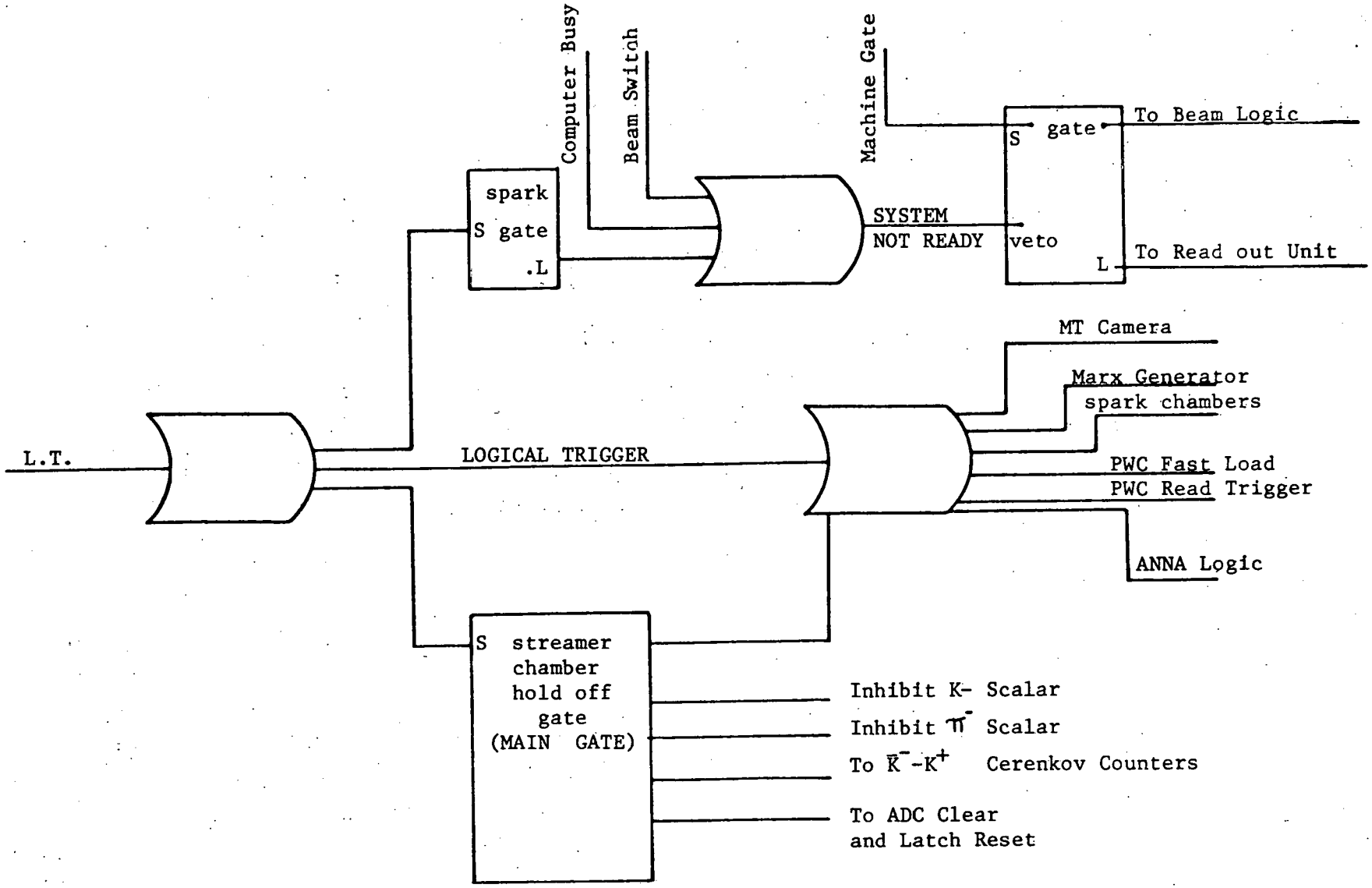

Figure III-7
Generation of Trigger Signal for
various Devices in the system
(S stands for "start" and L for "logic out")

CHAPTER IV - CONDUCT OF THE EXPERIMENT

A- Data Acquisition

During May and June of 1978 the SLAC two meter streamer chamber was exposed to the π^+ beam at 16 GeV/c(see section III-A). During the entire data taking period, routine checks were done to verify the operation of the equipment including the scintillation and Cerenkov counter high voltage supplies, the interferometer used to measure the index of refraction of the isobutane gas in the Cerenkov counters, the isobutane and nitrogen gas supplies used for the Cerenkov counters and the streamer chamber operating devices. An on-line display program was also written to plot counter information including the number of hits on each element of the picket fence and the pulse heights for each Cerenkov cell. The quality of the streamer chamber photographs was also checked daily to verify the operation of the photographic system. Scaler data were also recorded manually at the end of each roll to monitor trigger efficiencies. Test strips of film were examined and monitoring measurements were made and analysed at the SLAC film analysis facility.

Numerical values for various parameters related to data acquisition process are given in Table IV-1.

B- Scanning

Except for the off line monitoring analysis described above, the film scanning and measurement were carried out at Tufts by Tufts and Michigan State University scanners.

Scanning of this film was done in two separate passes. In the first pass the film was searched for events with a K- trigger track through the correct picket fence channels. In the second pass it was searched for events with visible neutral particle decays (Vees) and charged particle decays(kinks). The following sub-sections describe the scanning procedures and the methods used to correct for inefficiencies in the process.

1- Inclusive K- Scan

In this pass about 8 percent of the film (a total of 21787 frames) was scanned. Scanners were given a list which summarized recorded information about counters in the picket fence and Cerenkov arrays, for each frame. View-3 of each frame (taken by a camera centered on the beam axis) was first examined. All tracks in the picture were roughly checked to see whether a possible vertex existed within the approximate target area, which was marked by the two downstream target fiducials(Figure IV-1). When such an event candidate was found, further checks were made to find the track which caused the trigger in the counters. Each scanning table was provided with a template which displayed the approximate position of the 20 picket fence counter

channels relative to the target fiducials. It also showed most of the fiducial marks on the streamer chamber. All fast negative tracks were checked against the template. The impact point of the particle on the V1 counter array was found using a linear extrapolation from the end of the visible track in the photograph. Finally, an event was recorded as legitimate if the channel number inferred from the template was within ± 2 of the channel number which made the logical coincidence that triggered the streamer chamber for that frame. Note that in the scanning process, events which contained more than 14 charged tracks were recorded but not flagged for measurement. This rule was also applied to the " second pass"(Vee scan) as well.

One of the major difficulties which was encountered in the scanning and measuring of this film was the presence of multiple interactions in the pictures. Interactions to which the trigger track clearly did not point were excluded. Yet in most cases the resolution of these events was very difficult, because the trigger track was too straight and possible event vertices were located too close together. For such frames, the interactions were treated as one single event and the resolution of the problem was left to the analysis program which extrapolated tracks to vertices hidden in the target (APACHE see Section V-B).

2- Vee Scan

A complete pass was made on the film to search for visible decaying neutral particles associated with a triggering K-. In this pass was also recorded any event which contained a kinking track(a possible $K^{\mp}$ or $\Sigma^{\mp}$ decay).

The two clearest views of every frame were examined to find these Vees or kinks. A pair of positive and negative tracks was accepted as a Vee decay if the decay vertex was visible in at least two views. When a frame was found to contain a Vee decay or a kink, it was then examined as in the first pass, for trigger track legitimacy and for a primary event vertex. Finally, an event was recorded if the Vee or kink was approximately consistent with an otherwise legitimate charged particle event vertex within the target area. A summary of the results from two scanning passes is presented in Table IV-2.

3- Scanning Efficiency

a) Vee scan

To determine the detection probability of V0 events, 9 rolls, nearly 10 percent of the data sample (29000 frames) were rescanned, in each case by a scanner different from the one who had done the first scan. The two results were compared and a list of the events not found in common was prepared. These events were then rechecked by the author and by a senior scanner. Such events which were found to be

illegitimate were excluded. Finally the resulting records were compared and following information was extracted from them:

N1= number of events recorded in first scan,

N2= number of events recorded in second scan,

N12= number of events recorded in both scans.

The numerical values for these parameters are given in Table IV-3. If the loss of events were random, the probability that an event would be seen by a single scanner would be, following the Geiger-Werner method[1],

$$Ei=Ni/N \quad i=1, 2$$

where N is the total number of events present and Ni is the number of events observed by ith scanner. The probability that both scanners detect an event is similarly estimated as

$$E12= N12/N$$

Given that two scans were done independently and assuming that the losses are uncorrelated,

$$E12 = E1 \times E2.$$

Thus,

$$E12= (N1 \times N2)/N^2 ,$$

$$N=(N1 \times N2)/N12,$$

$$E1=N12/N2,$$

and

$$E2=N12/N1.$$

The global efficiency is defined as the probability that an event can be detected in at least one of the two scans, therefore,

$$Eg= NO/N =(N1+N2-N12)/N= E1+E2-E12,$$

where NO is the total number of events detected by two scanners.

To estimate the uncertainty in efficiencies, the following formula, based on statistical uncertainties in the number of detected events, is used:

$$\Delta E1 = \sqrt{E1(1-E1)/N}$$

and

$$\Delta E2= \sqrt{E2(1-E2)/N}$$

The results for scanning efficiencies are given in Table IV-4.

b- Inclusive K- Scan

To estimate the detection probability for a legitimate event(an event which lay within the target area and was associated with a legitimate trigger track) , 5410 frames

were rescanned from the film sample which had been scanned and measured during the "first pass" for inclusive K-events. The two scanning results were compared and numerical values for N1, N2 and N12, defined in the previous section, are given in Table IV-3.

Following the Geiger-Werner procedure, above, scanning efficiencies were estimated with the results presented in Table IV-3.

C- Event Measurement

Measurement of selected events was done on two 3-view IPD (Image Plane Digitizer) Projectors. The projection lenses used were of focal lengths 90 mm(Machine 3) and 105 mm(Machine 4). Magnified images of the three views of the film on a horizontal table were digitized in the X-Y plane using optical encoders with least count of 1 mil. The image to table magnification of the lenses was about 15. Corrections for distortion occuring in the projection process were originaly based upon measurements of a film on which was drawn a precision rectangular grid with 1/2 cm line spacing. However it was later decided to use a complete set of measurements of all visible fiducials(28 total). See Section V-A for detailed description of the method.

The measurement process was controlled and recorded by a PDP-8 computer. The events selected during the scanning process were re-examined by the measurer for trigger track legitimacy, for a possible event vertex and to establish the

overall topology of the tracks. In the case of the Vee scan events they were also checked for V's or kinks in the picture. If still acceptable the measurement of the event was carried out. Initialy the locations in each view of four streamer chamber fiducial marks were recorded. These marks are shown in Figure IV-1 as circled points. The measurement of the events was then completed by recording in each view the locations of six points along each track, starting at the visible exit points of the track from the streamer chamber and working as close to the primary vertex as the track remained visible. The maximum turning angle measured for each track was 60° reflecting a limitation in the track reconstruction programs. Tracks of visible length less than 1 inch were measured as "two point" tracks at the end and beginning. The decay vertex for Vees was measured as the last point on the negative track of the Vee decay. Kink vertices were measured as the last point on the outgoing track from decay vertex.

All of the selected events were measured. The measurement data which were on a 7-track magnetic tape, were edited on a PDP-1 computer. The resulting output data was processed through a program called PANEL which re-arranged the information to be acceptable for the track reconstruuction program TVGP(SLAC event format). The output data from PANEL was then processed through TVGP for event reconstruction. Events which failed to pass the requirements(described in Chapter V) in any of these

processes(PDP-1, PANEL and TVGP) were subsequently remeasured. Table IV-2 summarizes the pattern of the data flow through various processes.

D- Corrections for the Loss of Events in Measurement Process

1- To correct for the loss of events in obscured frames, we assign a weight factor 1/Em where,

$$Em=(Ntotal/(Nlost+Ntotal)$$

where Ntotal is the total number of events measured, and Nlost is the number of events recorded by scanners as unmeasurable, in this case obscured.

An estimation of Em was possible using the information from "K- inclusive scan" where Nlost=102 was estimated. Thus, using Table IV-2 we get,

$$Em=.98\pm.002$$

2- Another correction factor defined by

Ehm= (Number of measured events)/(Total number of legitimate events)

Ehm was used to correct the data for the loss of high multiplicity events (Note that the denominator includes the high multiplicity events (n> 14)). It should be noted that

this definition is based on the assumption that the fraction of the data that is of any interest in the rejected high multiplicity event set is the same as that in the measured data sample. Using the numerical values given in Table IV-2 Ehm was determined to be,

$$Ehm=.877\pm.004 \text{ For no Vee events}$$

and

$$Ehm=.923\pm.002 \text{ For Vee events}$$

3- A correction factor Ep was also calculated for the loss of events in PANEL-TVGP. To get Ep the following information was used:

G1= number of events which passed TVGP the first time, and

G2= number of events which passed after a second measurement, having failed the first time

Ep is then defined as

$$Ep=(G1+G2)/G$$

where G is the total number of measurable events in the sample. The procedure utilized here is based on the assumption that the losses occur in uncorrelated random processes such as:

a) appearance of a bad character in the measurement data record of an event (card images),

b) careless measurement of locations of fiducial marks,

c) bad measurement of a track,

d) wrong coding of event type,

or various other uncorrelated causes. In all these cases the losses can be characterized as random. However, to eliminate a possible correlated cause of event loss in reconstruction processes, tracks which would definitely have caused an event to fail, such as short (<1 inch) and thick tracks, were measured as "two point"tracks in the remeasurement process as well as the original measurement process.

Given the random loss assumption, the successful fraction of the first event measurements will be the same as that for the re-measurement set. Thus

$$G1/G = G2/(G-G1).$$

Therefore,

$$G = G1^2/(G1-G2),$$

so

$$Ep=(G1+G2)(G1-G2)/G1=(G1^2-G2^2)/G1.$$

A fraction of the inclusive K- event sample (10 percent) was used to estimate the processing efficiency. The numerical values for G1, G2 and Ep(processing efficiency) are given in Table IV-4.

E- Comments

The event selection, that is, the task of defining legitimate interactions in the scanning and measuring processes, was made complicated by the presence of multiple interactions in the pictures. The solution chosen for this problem was to treat them as single events in both scanning and measuring. However, this choice further complicated the process for the vertex finding program APACHE, and consequently increased the uncertainty in mass determination, as will be seen in following chapters.

The high density of beam particles (8 π^+/picture) obscured the region in the pictures where fast forward trigger tracks were to be found. This required close and careful examination of the beam region which could result in a scanning inefficiency. It also resulted in the poor measurement of those tracks which were partly obscured by the beam particles, giving large uncertainties in the track parameters as reconstructed by TVGP.

REFERENCES

1-H.Geiger and A.Werner, Z.Physik 21, 187(1924).

TABLE IV-1

Data Aquisition

Number of Beam Pulses	2.48101×10^7
Number of Beam Particle	1.279719200×10^9
Number of Particle per Pulse	5 to 8
Number of Triggers	$3 \quad 10^5$
Number of Trigger per π^+	1.6×10^{-3} to 2.5×10^{-3}
Dead Time	9%
Number of Rolls of Film	91
Number of Days of Data Taking	45

TABLE IV-2

Scanning and Measurement Pattern of the Analysed Events

Quantity	$\bar{K}$ Inclusive Scan	Vee Scan
Number of Rolls Analysed	7	72
Number of Frames Scanned	21787	253623
Number of Frames Recorded	8488	with Vee 25910 with Vee and Trigger 9333
Rejected as High Multiplicity	1044	2014
Number of Events Measured in First Pass	6094	6560
Number of Reconstructed Events from First Pass (PDP-1, PANEL and TVGP)	3715 + 865 (APAC)	3805 + 778
Number of Events Measured in the Second Pass	1559	1619
Number of Events Measured in the Second Pass which were not Measured in the First Pass	501	377
Number of Reconstructed Events from the Second Pass (TVGP)	918 + 167 (APAC)	1102 + 186

TABLE IV-3

Scanning Efficiency for Vee and Inclusive $\bar{K}$ Scan

Quantity	Inclusive $\bar{K}$ Scan	Vee Scan
# Frames Recorded in First Pass (N_1)	1713	751
# Frames Recorded in Second Pass (N_2)	2041	846
# Frames Recorded in both Pass	1478	625
Scanning Efficiency in First Pass	72 ± 1%	73 ± 1%
Scanning Efficiency in Second Pass	86 ± 1%	83 ± 1%
Global Efficiency	96 ± 1%	95 ± 1%

TABLE IV-4

Processing Efficiency

G_1	G_2	G	E_p
339	61	413	.968

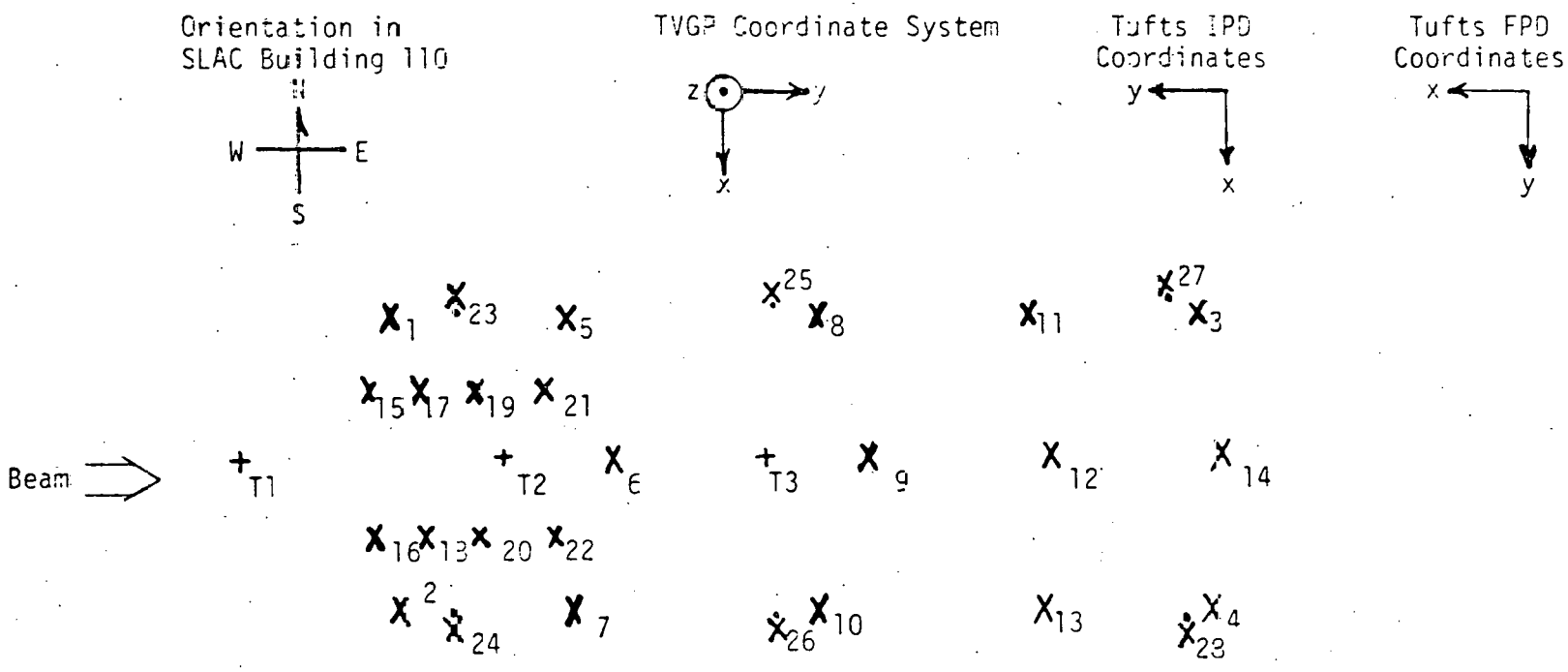

Fig IV-1- E 131 Coordinate Systems
and
Fiducial Numbering

CHAPTER V-ANALYSIS OF THE MEASURED DATA

A-Geometrical Reconstruction of Photographed Events

The analysis was carried out, first by reconstruction of the tracks in real space, using a modified version of the SLAC Three View Geometry Program (TVGP)[1].

A program PANEL, was written to translate measurements from Tufts card image format into the SLAC TVGP input format. For each event , the four measured fiducials were used in TVGP as the bases for the transformation from the projector's image plane into a standard film plane. The first part of the transformation was done in subroutine ENGINE to correct for magnification of the lenses and for alignment distortions arising from the projection of the filmed images onto the table where measurements were made. The following procedure was developed to generate the necessary mapping functions.

1) Several times during the event measurement process on each of the two tables the locations of all 28 streamer chamber fiducial marks were measured carefully and repeatedly. Alternatively, the locations were measured of the intersections of lines drawn on a piece of film with a precision 1/2 cm grid spacing. However, the finer resolution of the intersection points in the fiducial marks made their measurement more appropriate for use in the mapping process.

2) These points were mapped into the corresponding points as measured on the same film by a film plane engine, through the transformations:

$$\begin{aligned} Xfilm &= f(Ximage, Yimage) \\ Yfilm &= g(Ximage, Yimage) \end{aligned} \qquad V\_1$$

These functions were realized as third order polynomial expansions whose coefficients {ai} and {bi} were determined by a least squared method.

$$\begin{aligned} Xfilm &= a1+a2X+a3Y+a4X^2+a5XY+a6Y^2+a7X^3+a8X^2Y+a9XY^2+a10Y^3 \\ Yfilm &= b1+b2X+b3Y+b4X^2+b5XY+b6Y^2+b7X^3+b8X^2Y+b9XY^2+b10Y^3 \end{aligned} \qquad V\_2$$

These fitted constants were put into the TVGP subroutine ENGINE which transformed every measured data point into the corresponding film plane. Each time the projection lenses of the image plane digitizers were adjusted, a new set of optical constants was generated from the fiducial measurements and used with the corresponding data. During the measurement process special care was taken to ensure that the filmed image was correctly located with respect to the origin of measurement coordinates.

A TVGP subroutine, TYPSUB, was written for this experiment. All negative tracks were reconstructed as K-, $\bar{P}$ and π^- and positives as K+, P and π^+. charged tracks from Vee decays were reconstructed as $e^{\pm}$, $\pi^{\pm}$ and P. Kinking tracks were tried as π, Σ and K. The TVGP analysis was

standard, with allowance for the gas filling and the absence of glass window in the streamer chamber. A parametrized map of the non-uniform ($\sim$ 1.3 T) magnetice field of the streamer chamber was provided for TVGP in subroutine FIELD.

The geometrically reconstructed track output from TVGP was a standard data record containing the values of all track parameters and an additional data record containing detailed spatial error matrices for the reconstructed tracks which were needed later by the vertex finding program APACHE.

Measurement data were first processed through TVGP to establish and select events requiring remeasurement. The resulting intermediate data were then processed through APACHE (next section). As a test of measurement quality the "Film Root Mean Square" (FRMS) generated by TVGP for each reconstructed track, was used. Fig. V-1 shows the distributioin of the FRMS for measured tracks. These figures show a clear dependence of FRMS on measurer. As it can be seen in Fig. V-1a the average FRMS for measurer number 1 is much less than that for all others. The effect of the FRMS in vertex reconstruction will be discussed further in the next section. TVGP assumed a constant film setting error of 4 least counts (least count = 1 mil on IPD table), to carry out the fitting process.

An overall test of the accuracy of the magnetic field and optical constants and the measurement process was made by reconstructing KO and Λ° masses from the charged tracks in Vee decays. Using 712 K^0_s and Λ°, their invariant masses was measured to be 497.83±.8 and 1115.89 ±.25, respectively, which are consistent with current accepted values[2] 497.67±.13 and 1115.60±.05. Figures V-14 and V-15 show the mass distribution for K^0_s and Λ° analysed.

B- Vertex Finding

The interactions of interest occurred in the hydrogen target centered in the upper half of the streamer chamber and their tracks did not become visible until they emerged into the chamber volume some centimeter from the vertex. Thus the second step in event reconstruction was extrapolation of the appropriate measured tracks to find the coordinates of a unique production vertex and then to correct the track parameters given this additional constraint. The program APACHE had been developed earlier for the SLAC streamer chamber to do this. Selecting the tracks to extrapolate was a major feature of APACHE.

Program APACHE[1] used a chi-square minimization method to obtain the best common vertex point in space for observed tracks extrapolated back in the magnetic field and through target materials. The basic mathematical method is summarized in Appendix B.

The main driving routine in APACHE was GTYPE which through subroutine DOIT performed the following steps in deciding which tracks should enter into the vertex calculation and whether or not a vertex so fitted was acceptable,

1) All negative forward going tracks were extrapolated into the picket fence counter array to check if they passed through the picket fence elements. Tracks which did, were flagged as candidate trigger tracks. Note that this was just a linear extrapolation from the end of the track and required only that it hit the V1 array somewhere.

2) To prevent primary beam halo tracks, which might have been measured, from being considered, all positive particles with momentum greater than 10 GeV/c were omitted. Positive particles above this momentum could not arise in 16 GeV/c π^+P interactions giving a legitimate K- trigger of momentum greater than 3 GeV/C.

3) A vertex track bank was set up starting with tracks 1 (trigger), 2 and 3. When any of these tracks had been excluded in preceding steps the next track in order was used. In subsequent steps additional tracks were appended one at a time.

4) A vertex was reconstructed as described in Appendix B.

5) Given the χ^2_v for the vertex of n tracks, and given (χ^2_{TK}, k=1, n), where χ^2_{TK} is defined as,

$$\chi^2_{TK} = (\chi^2_v)_n - (\chi^2_v)_{n-1}$$

APACHE had to accept or reject the vertex. This was done on the basis of the vertex χ^2_v and of the χ^2_{TK} calculated for the last track added to the vertex. Note that the errors entering into the χ^2_v determinations were calculated in TVGP assuming a fixed film-setting error of 4 least counts, thus the actual errors resulting from the dispersion of the measurements were not present in the TVGP error matrices. To correct for this over-simplification in TVGP, the χ^2_v,s were multiplied by a parameter "Fscale" to reflect the actual measurement uncertainty of the event, where,

$$\text{Fscale} = \left(\sum_{i=1}^{n} (\text{FRMS})^2/n \right)/16.$$

Here FRMS is the "Fit Root Mean Square" of each of the n tracks as reconstructed by TVGP.

A detailed study of the χ^2_v dependence on FRMS is given in Appendix C. In consequence the following criteria were imposed on an n-track vertex for it to be acceptable:

a) Given 2n-3 as the number of degrees of freedom (NDF), then χ^2_v/NDF should be less than 3. This limit, for five degrees of freedom (4 tracks), corresponds to a confidence level of 1 percent.

b) χ^2_{Tk} for the last track added to the vertex should be less than 5.

6) Each time a vertex was accepted, another track was added to it and the process was repeated until all tracks had been tried and a final acceptable vertex was formed for them. When adding a track yielded an unacceptable vertex, the preceeding acceptable combination was noted and a new sequence started.

7) When a final vertex of 3 or more tracks was found, APACHE generated a data record similar to that from TVGP but with the vertex point included for each of the tracks coming from it and with track momenta and directions recalculated to give their extrapolated values at that point (Appendix D). This process was repeated for all other possible combinations of tracks (n>3) which included a trigger candidate. An event record was generated for each such successful combination.

Track parameters for Vees (K^0/Λ°) were obtained by attempting a 1- constraint kinematical fit to the Vees given the reconstructed charged tracks from them (see Section V-D).

All events successfully reconstructed by TVGP were processed through APACHE, and the data output from APACHE were then merged with corresponding counter information to generate a final data summary tape. This was used for further analysis of the events.

C- Charged Kaon Identification

1- K- Identification

In order to reduce the pion contamination of the triggering particles, the following conditions were required for a negative particle to be accepted as a K- :

a) The track had to be negative and forward with measured momentum greater than 3 GeV/C.

b) When extrapolated through the streamer chamber magnetic field, the track was required to pass through those elements of the picket fence whose latch bits were recorded as having contributed to the event trigger. A discrepancy of $\pm$ 1 counter for V1, V2, V3, V4 was allowed.

c) The pulse height from the Cerenkov counter cell or cells hit by the extrapolated track was required to be the established pedestal value. The value of pedestal for each ADC channel corresponding to a Cerenkov cell varied slightly during the data taking period, therefore it was established separately for every 1500 frames of the data by making use of the pulse height distribution and averaging over pedestal values.

The pion threshold of the Cerenkov counter was 2.7 GeV/c and a 98.1 percent rejection efficiency for pions of momentum 3 GeV/c was estimated.

The momentum distribution for trigger particles selected by the above criteria is given in Fig. V-2.

2- K+ Identification

In order to identify the K+ among the positive particles which entered the K+ Cerenkov counter the following criteria were applied:

a) The track was required to be that of a forward going positive particle of momentum greater than 3 GeV/c

b) The pulse heights over pedestal from the cells hit by the Cerenkov radiation cone of the track were required to vanish.

A test of the procedure was possible by utilizing the $\bar{K}^{*\circ}$ production. In a histogram of masses of $(K-\pi^{+})$ pairs for which the π^{+} has produced Cerenkov radiation in the "K+" counter, a strong $\bar{K}^{*\circ}$ signal was seen with a small background For comparison, Fig. V-3b shows a histogram of invariant masses of (K-K+) pairs for which the K+ was identified by the above criteria but was assigned a pion mass for the invariant mass calculation. No clear $\bar{K}^{*\circ}$ signal is evident in the plot. However, by assuming a smooth fall off for background, an excess of about 60 events can be detected around the $\bar{K}^{*\circ}$ mass ($800<m(K-\pi^{+})<960$ MeV) which confirms the possible $\bar{K}^{*\circ}$ production due to pion contamination in positive tracks. Considering the ratio of pion to kaon production[4] ($\sigma_{\pi^{+}}/\sigma_{K^{+}} = 46$) and the measured pion rejection efficiency of

the Cerenkov detector (Eck= 99.717 percent)[3], the contamination of π^+,s in the identified K+ sample can be estimated from,

$$N_{\pi^+}(1-.99717)/Nk+$$

where $Nk+=N_{\pi^+}/46+N_{\pi^+}(1-.99717)$, giving 11.5 percent corresponding to 85 K+,s for the sample of events plotted in Fig. V-3b. Thus the possible K* production observed in the spectrum of Fig. V-3b is consistent with the expected contamination of π^+,s in the sample of positive tracks identified as K+.

D- Event Selection in the Streamer Chamber

Given the hydrogen target location and size and the total charge (+2) of the incident particle and struck proton, the vertex of a (π^+ P) event ought to lie within the target boundary and the reaction products should have a total charge (+2). However slow protons may have not emerged from the target , or they and similar low momentum tracks may have been excluded from event by the APACHE algorithm. Also associated fast tracks may have been obscured by the beam tracks and thus missed. Therefore, the total charge seen in 63 percent of the final events was not +2. Subsequent cuts also had to be made to exclude events outside the hydrogen target and also to suppress fake APACHE solutions. Acceptable events had to meet the following criteria, applied to each set of APACHE vertices for a

measured event:

1) The coordinates of the production vertex of the event as fitted by APACHE had to satisfy the following conditions,

$$-65 \text{ cm} < Yv < -5 \text{ cm}$$

$$R=(Xv^2+Zv^2)^{1/2} < 1.58 \text{ cm}$$

in the coordinate system shown in Fig. V-4. The full hydrogen volume extended (-65 cm <y<-5 cm) and had a radius 1.58 cm.

2) The event must have had a fast forward negative track flagged as a trigger track by the criteria of section (V-C).

3) The tracks associated with the vertex of the event had to satisfy the following conditions on charge balance:

$$0 < \text{Net charge of the event} < 4.$$

This condition allowed for as many as 2 missing negative or positive tracks. Since APACHE would not necessarily associate a poorly measured track with its actual vertex, this criterion increased the effective APACHE efficiency for event detection.

After these cuts (V.D.1-3) were applied the surviving events were divided into two categories:

a) Events for which only a single APACHE solution remained in the data sample. The vertex of this solution and its associated tracks thus defined the event for further analysis.

b) Events with multiple APACHE solutions sharing one track as the trigger particle. For these the remaining problem was to select, if possible, the actual solution to which the identified trigger track belonged. The following parameters were used to resolve the ambiguities in these events:

i) The APACHE chi-square per track, χ^2_{PT} (χ^2_ν /no of tracks). (This reflects the overall goodness of fit to a single vertex).

ii) The trigger track χ^2_{tg} (The contribution of the trigger track to the above, reflecting the fit of this track to a particular vertex).

iii) The total charge of the final event (insofar as all relevant tracks have been measured the better fit might be expected to have net charge closer to 2).

Given these parameters, the following tests were made on each group of APACHE solutions formed from a single measured event (using the program APCUTS).

4) If the χ^2 pt for one solution was greater than 2 $\times \chi^2$ pt of all other solutions, then that solution was excluded.

5) If χ^2 tgp (χ^2 tg/χ^2 total) was greater than .5, and was also greater than χ^2 tgp of all the other solutions, then that solution was excluded from the data.

6) Among the remaining APACHE solutions for the event, those were selected whose track had a net charge differing least from the total charge of the incident particles, (+2).

7) A weight defined as

APWT=1/ (number of unresolved APACHE solutions)

was assigned to each of these solutions remaining after all the above cuts were made.

It is to be noted that the cuts 4) through 6) above do not reduce the total number of triggered events in the data, but serve to define more precisely the composition of the events. Distributions of APACHE χ^2_ν for the whole data set before and after cuts are shown on figures V-5a, b (Note that in Fig. V-5a each point represents a solution).

E- Identification of Neutral Strange Particles

The TVGP event reconstruction provided all track parameters for the charged particles from VO-decays. The measurement procedure required that the beginning point of the negative track in a Vee be the closest point in space to the decay vertex. However, for a large number of VO decays, the vertex was not clearly visible in all three views and consequently only a poor measurement of the decay vertex was possible. To overcome this problem APACHE was used to reconstruct the decay vertex by extrapolation of the two outgoing tracks back to a point in space.

After the decay vertex had been determined, the VO events were processed by a kinematical fitting program (SQUAW), where 1-constraint fits were attempted to the hypotheses,

i) $K^0 \longrightarrow \pi^+ + \pi^-$

ii) $\Lambda^\circ \longrightarrow P + \pi^-$

iii) $\gamma + P \longrightarrow e+ + e- + P's.$

The single constraint was the assumed mass of the decaying neutral particle.

If both KOs and Λ° hypotheses were unsuccessful, that event was deleted from the VO sample. Events with successful fits to KO and Λ° were further processed through APACHE for reconstruction of the primary vertex and then

through SQUAW for 3-constraint fits (neutral particle mass and direction), using a primary vertex determined from other charged tracks by APACHE and the VO vertex. At the conclusion of this process a set of KOs and Λ° events was obtained which had successful 3-c fits to a production vertex. After application of the cuts described in Section V-D, a total 887 were left. Ambiguities among these events are summarized in Table V-1.

1- Selection of KO, Λ° and γ Events

Table V-1 shows that 71 percent of the VO's were uniquely determined to be KO, Λ° or γ by 3 and 1-constraint fits. The remaining 29 percent were ambiguous.

To obtain a clean sample of Λ°'s and KOs's the γ's had to be removed from the VO sample. Figure V-6 shows the distribution of the depth coordinate Zv for the vertices of all fitted Vees (Z is measured parallel to the electric field in the streamer chamber). There is an obvious peak at the location of the streamer chamber electrode consisting of a set of fine wires. This is expected because of the very small probability of pair creation (γPs $\rightarrow$ e-e+Ps) in neon-helium gas. Photon conversion is expected only in the dense material in the chamber, i.e, the electrode wires and the target.

Figure V-7 shows the $\bar{P}_\perp$ distribution for all VO,s. Here, $\bar{P}_\perp$ is the transverse momentum of the negative particle of a VO decay relative to the direction of flight of the VO. The transverse momentum $\bar{P}_\perp$ has definite maximum values of 0 105, and 206 MeV/c for γ, Λ°, and KOs decays respectively.

Fig. V-7 shows peaks at 0. , 100 and 200 MeV/c which correspond to γ, Λ° and KOs decay respectively. In order to remove the γ,s from our ambiguous sample, any VO which had a successful fit to γ and satisfied any of the following conditions was called a γ :

a) $\bar{P}_\perp$ was less than 20 MeV/c

b) The decay vertex was in the streamer chamber H.V. electrode, i.e,

$$-7 \text{ cm} < Zv < -6 \text{ cm}$$

c) The decay vertex was on or within the target, i.e,

$$R=(X^2+Z^2)^{1/2} < 1.587 \text{ cm}$$

Figure V-8a,b show the Z distributions for VO events after these criteria were imposed and the resulting gammas were removed. One observes that the peak at the H.V. electrode has been eliminated.

The remaining problem was to separate the Λ^0's and K^0_S's in the ambiguous V0 sample. The transverse momentum distribution $\bar{P}_\perp$ for uniquely fitted Λ° decays shows a peak at 100 MeV/c. Thus a simple method based on $\bar{P}_\perp$ can be used to select Λ° from (Λ°/KOs) mixture, as follows:

V0's with $\bar{P}_\perp < 110$ MeV/c are treated as if they were Λ° and, those with $\bar{P}_\perp \geq 110$ MeV/c, as if they were K^0_S.

2- Test of the Consistency of the Method

A test of the consistency of the method may be performed as follows:

a) assuming that KOs's decay isotropicly in their rest frame, one can calculate the expected number of KOs's with $\bar{P}_\perp < 110$ MeV/c

$$N(\theta)d\theta = N_0 \sin\theta\, d\theta,$$

$$N(P_\perp) = N_\theta \left(P_\perp/p^* \right)\left(d\bar{P}_\perp/\left(P^{*2} - \bar{P}_\perp^2 \right)^{1/2} \right).$$

$$0 \leq \bar{P}_\perp < P^*$$

Defining f as,

f= Number of KOs's for $P^* > \bar{P}_\perp > 101$ MeV/c, then for $P^* = 210$ (MeV/c)(KOs),

$$f = N_\theta \int_{P_{Min}}^{P_{Max}} \left(\bar{P}_\perp / P^* \right)\left(d\bar{P}_\perp/\left(P^{*2} - \bar{P}_\perp^2 \right)^{1/2} \right),$$

$$f = N_\theta \sqrt{\left(1 - \left(P_{Min}/P_{Max} \right)^2\right)}$$

and

$$f/N_\theta = \sqrt{\left(1 - (P_{min}/P_{max})^2\right)}$$

From Figure V-10a,

$$f=431$$

and

$$f/NO=.851$$

giving

$$NO= 506$$

Therefore the number of KOs' s expected for the region $\bar{P}_\perp$ < 110 is

$$N1=NO= 431= 75$$

Fig V-10b shows the $\bar{P}_\perp$ distribution for KO's after final cuts. From this plot the number of KO in the region ($\bar{P}_\perp$ <110) is 61, consistent with the expected number of K^0_S's determined above using an isotropic decay angular distribution for KO in rest frame.

b) Life time of Λ° and KOs:

The proper life times for VO's were calculated using the primary vertex, the decay vertex and the momentum of the VO. Distributions of life-time in length unit $c\tau$ for KOs and Λ° are given in figures V-12 and V-13 respectively.

Exponential fits to these distributions give the following values:

$$c\tau = 2.78 \pm .11 \text{ cm for KOs}$$

$$c\tau = 6.8 \pm .72 \text{ cm for } \Lambda^\circ$$

These values for the mean lifetimes of the KOs and are in agreement with other measured values[2].

$$c\tau_{KOs} = 2.675 \pm .0066 \text{ and } c\tau_{\Lambda^\circ} = 7.89 \pm .06$$

The 5-10 percent error in our measured values can be attributed to the decay of VO's (KOs/Λ°) in the target and to the low statistics. To correct for target loss, each VO is weighted by the inverse of detection probability of the event in which it occurred, that is, the probability that the VO would decay inside the sensitive and visible region of the streamer chamber.

c- Mass of KOs and Λ°

Figures V-14 and V-15 show invariant mass distributions for the resolved KOs and Λ°. The mean values were

$$m_{\Lambda^\circ} = (1116.49 \pm .3) \text{ MeV}$$

$$m_{KOs} = (497.69 \pm .8) \text{ MeV}$$

to be compared with values from the particle data handbook, $(497.67 \pm .3)$ and $(1115.60 \pm .05)$ for KOs and Λ° respectively[2].

An alternative method to calculate these masses used a χ^2 minimization. The Chi-Square was defined as,

$$\chi^2 = \sum_{i=1}^{n} \left((m_i - m_{V^0}) / \sigma_i \right)^2$$

where mi and σ_i were the measured V0 mass and its uncertainty respectively. Minimizing the χ^2 gave mV0 as the mass of the V0. From this method was obtained,

$$mV0 = \frac{\sum_{i=1}^{n} m_i / \sigma_i^2}{\sum_{i=1}^{n} 1 / \sigma_i^2}$$

then,

$$mK0 = 497.83 \pm .8 \text{ MeV}$$

$$m\Lambda^0 = 1115.89 \pm .25 \text{ MeV}$$

3- Losses and Correction Factors

a) Losses from V0 decays in the target or outside the streamer chamber

Any V decay near the walls of the streamer chamber was excluded by defining the scanning fiducial volume of the streamer chamber to be:

$$-90 \text{ cm} < Y < +90 \text{ cm}$$

$$-30 \text{ cm} < X < +30 \text{ cm}$$

$$-20 \text{ cm} < Z < +20 \text{ cm}$$

in the coordinate system defined in Figure V-4. The probability for detection of a Λ^0 or K0s is defined as the

probability that a KOs/Λ° with the given direction and momentum would be detected had the event occurred anywhere in the target. Note that scanning rules required that a Vee be recorded, whether or not a vertex was seen. To estimate the losses, production vertices and azimuthal angles of the VO were generated randomly and for each given squared transverse momentum $\vec{Pt}$ and the Feynman variable Xf defined as $(Pl/\sqrt{s})$, the direction of flight of VO particle and its laboratory mean flight distance, LO, were determined. The detection probablity for a VO with a given production vertex, Xf, $\vec{P_t}$ and azimuthal angle is

$$Et=(Exp\ (\ -Lmin/LO)-Exp\ (\ -Lpot/LO)),$$

where Lmin is the distance travelled by VO in the target and Lpot is the potential path along the VO direction from the production vertex to the edge of the streamer chamber fiducial volume. The average of Et over azimuth and X, Y and Z of the production vertex was taken as the detection probability for a VO with a given $\vec{Pt}$ and Xf. Finally each KOs/Λ° in the data was weighted by the inverse of the detection probability corresponding to its $\vec{Pt}$ and Xf.

b) A weight Wneut was used to account for the neutral decay modes of KOs and Λ°,s

Wneut=1.55 Λ°

Wneut= 1.46 KOs

Finally, every "KOs" or " Λ° " with a proper life time ($c\tau > 5\, c\tau_{\circ}$) was excluded from the sample. VO's with 3c-fit χ^2 greater than 16 were also removed from the VO sample (Note, χ^2 =16 for 3 degrees of freedom corresponds to a confidence level of .001). These cuts were not expected to affect significantly VO's produced in the target events, but should reduce strongly accidental coincidences.

c) After applying the above corrections, there was still observed a loss of VO decays in the region where the beam track density is high. The loss can be seen in Fig. V-16 where Xbm is defined as:

Xbm =Xv- Xbeam

where Xbeam is approximated as, Xbeam=.05Yv, from a study of the primary beam track spatial distribution. Using the average number of events in neighbouring bins , the number of VO events lost (Nloss), in the beam region was estimated to be 57 . Thus a weight, Wbeam defined as

Wbeam=(NO+Nloss)/NO=1.04±.006

was used to correct overall cross-sections, where NO is the total number of weighted VO's.

F- Correction Factors:

To correct the data for the loss of events in various processes in collection and analysis of the data, several correction factors, each corresponding to the loss in a single process, were estimated. Table V-4 summarizes the losses from these factors. The description of procedures used in their estimation were presented in appropriate sections describing the process. The remaining correction factors are estimated as follows:

1- CELT Efficiency

The Average efficiency of the picket fence counters performance in triggering process was defined as,

$$E = \sum_{i=1}^{20} Fi \cdot Ei$$

where Ei and Fi are the efficiency of the ith channel and the fraction of trigger tracks passing it. The values of these parameters are given in Table III-5.

3- Correction for Beam Scattering in $S3'$ and Target End-Cap:

Scattering of the π^+ beam particle in the 1/4 inch thick beam counter $S3'$ was accounted for by a correction factor estimated as

$$E = (EXP\ (-w/\ \lambda I)$$

where w=.635 cm and λ_I=84.94 cm are the thickness of the scintillator and the mean interaction length of π^+ beam at 16 GeV/c in scintillator respectively.

To correct for interactions of the beam particles in the endcap of .02 cm thick mylar of the liquid hydrogen target container, a factor was estimated as

$$Ecap = EXP\ (-.02\ cm/\lambda'_I\ ) = .9997$$

where λ'_I =69.44 is the interaction length of π^+ beam in mylar.

4- Correction for Decay of Trigger Particles (K-)

The detection of an event followed the passage of a forward K- through the picket fence counter and Cerenkov detector (Ck-). Thus an event would not be recorded if the K- decayed before it hit all four picket fence arrays.

Given the momentum and direction of the detected K- trigger particles, a correction factor was estimated as follows:

For each detected K- trigger a factor was defined as

$$Edk- = EXP\ (-LO/\gamma ct0),$$

where LO=the distance travelled by K- trigger to hit the array V4, t0 is the mean life time of K-, c velocity of light and γ=Ek-/mk-. Here Ek- is the energy of the trigger particle. The average value of Edk- was used in final cross-section calculations (Table V-4).

5- Dead Time

A factor Edead=.923±.0004 was estimated, using beam counts recorded by scaler during the data taking period, to correct the cross-sections for the unused beam particles (see Reference 3 for detail of the method).

6- APACHE Efficiency

In order to correct for the loss of events in the process of vertex finding, a factor Ea was estimated:

Ea= The probability that a track is included in an event formed by APACHE

In order to determine, Ea, a sub-sample of V0 events was selected. Starting with 1744 events as input to APACHE from this sample of events, the following information was obtained:

N1 (number of events with some final fits) = 1547

N2 (Number of events with at least one APACHE fit which included a VO)= 1144

N3 (total number of events which after final selection still included a VO)= 742

Assuming that APACHE will try all of the possibilities for vertex formation, it can be argued that N1 is the (or at least is close to) total number of true interactions with a VO. Then the APACHE efficiency can be defined as,

Ea= The probability that a VO is included in an interaction vertex.

Given that the average number of π^+/burst =8, and that the interaction probability Pi=(1-EXP $(-Lt/\lambda I)$)=.059, then the probablity of occurence of n interactions would be,

$$Pin=(8!/n!(8-n)!)Pi^{n}(1-Pi)^{8-n}$$

Thus,

P_{in}^{1} (probability of only one interaction)=.308,

P_{in}^{2} (probability of 2 interactions)=.067,

P_{in}^{3} (probability of 3 interactions)=.008 $\sim$ .01.

^{1}Pin, ^{2}Pin and ^{3}Pin are then normalized to total probability of occurrence of a trigger which is proportional to,

$$Pnor= {}^{1}Pin +2{}^{2}Pin +3{}^{3}Pin=.472$$

Then, fractions of the data which are expected to contain respectively, single, double and triple interactions are

$$^{1}Fin={}^{1}Pin \quad ,{}^{2}Fin=2{}^{2}Pin \quad \text{and } {}^{3}Fin=3{}^{3}Pin.$$

The probability that a V0 will be included in either of the two or three interaction vertex events is 1/2 and 1/3 respectively, thus the total number of final interaction vertices containing a V0 would be,

$$Nvv=(Fin+1/2Fin+3Fin)xN2$$

and therefore the APACHE efficiency is

$$Ea=N3/Nvv=.796\pm.03$$

The error in this number is based on the statistical uncertainties in N2 and N3.

REFERENCES

1-A.Seidon, Ph.D. Thesis, University of California Santa Cruz (1975), University Microfilms No. 74-23,015

2-C.Bricman, et al, Review of Particle Properties, LBL-100, 1978.

3-See Reference 1, Chapter III

4-See Reference 3, Chapter VI

TABLE V-1

Pattern of Events Before and After Final Cuts

Before Apcuts and Trigger Check	Inclusive Sample	Vee Sample
Number of Events	4624	1347
Number of APACHE Solutions	6512	1503
Number of Events with Single Solutions	3290	733
After all Cuts		
Number of Events	3245	887
Number of APACHE Solutions	3372	919
Number of Events with Single Solutions	2327	502

TABLE V-2

Ambiquity Pattern of 3C-Fitted V^o Events

	K_s^o			Total
K_s^o	530 (Unique)	107	58	695+18 ($K^o/\Lambda/\gamma$) (80%)
Λ^o	107	95 (Unique)	72	274+18 ($K^o/\Lambda/\gamma$) (32%)
γ	58	72	7 (Unique)	137+18 ($K^o/\Lambda/\gamma$) (17.4%)

TABLE V-3

Selection of Λ^o and K^o After Final Cuts

	After , $\bar{P}$, Life Time, Fiducial and χ^2_{3c} Cuts
K_s^o	492
Λ^o	220

TABLE V-4

Correction Factors

Correction Factors	Inclusive	V^o Events
CELT	.482	.482
Dead Time	.923±.0004	.923±.0004
π^+ Scattering in S_3 and Target End Cap	.99	.99
Scanning	.72 ± .01	.73 ± .01
Measuring (Obscured Frames)	.98 ± .002	.98 ± .002
(Cut on High Multiplicity Events $n_t > 14$)	.877 ± .004	.923 ± .002
Processing (PDP-8, PDP-1, PANEL, TVGP)	.96	.89
APACHE	.80 ± .03	.80 ± .03
$\bar{K}$ (Trigger) Decay	.864 ± .03	.864 ± .03
Loss for Special Measurement of Events with Trigger on High Number CELT Channals ($n > 8$)	.97	---------
Loss of V Decay in Beam	----	.961 ± .006
Neutral Decay Mode of V^o	(Λ : .64 ± .008 / (K^o_s : .68 ± .0024)	

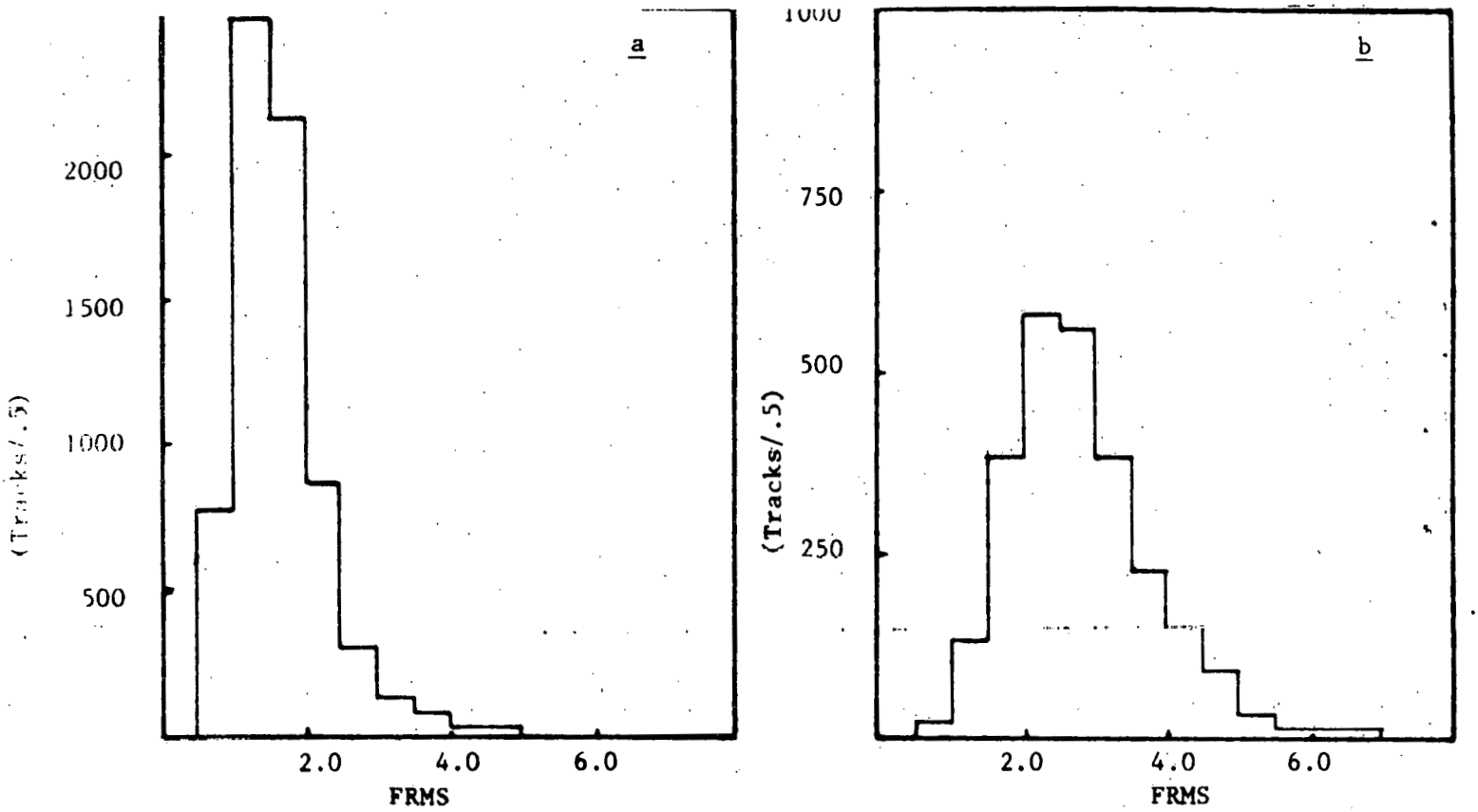

FIG. V-1 FRMS Distributions for Four different measurers, showing typical dependency of FRMS on measurers

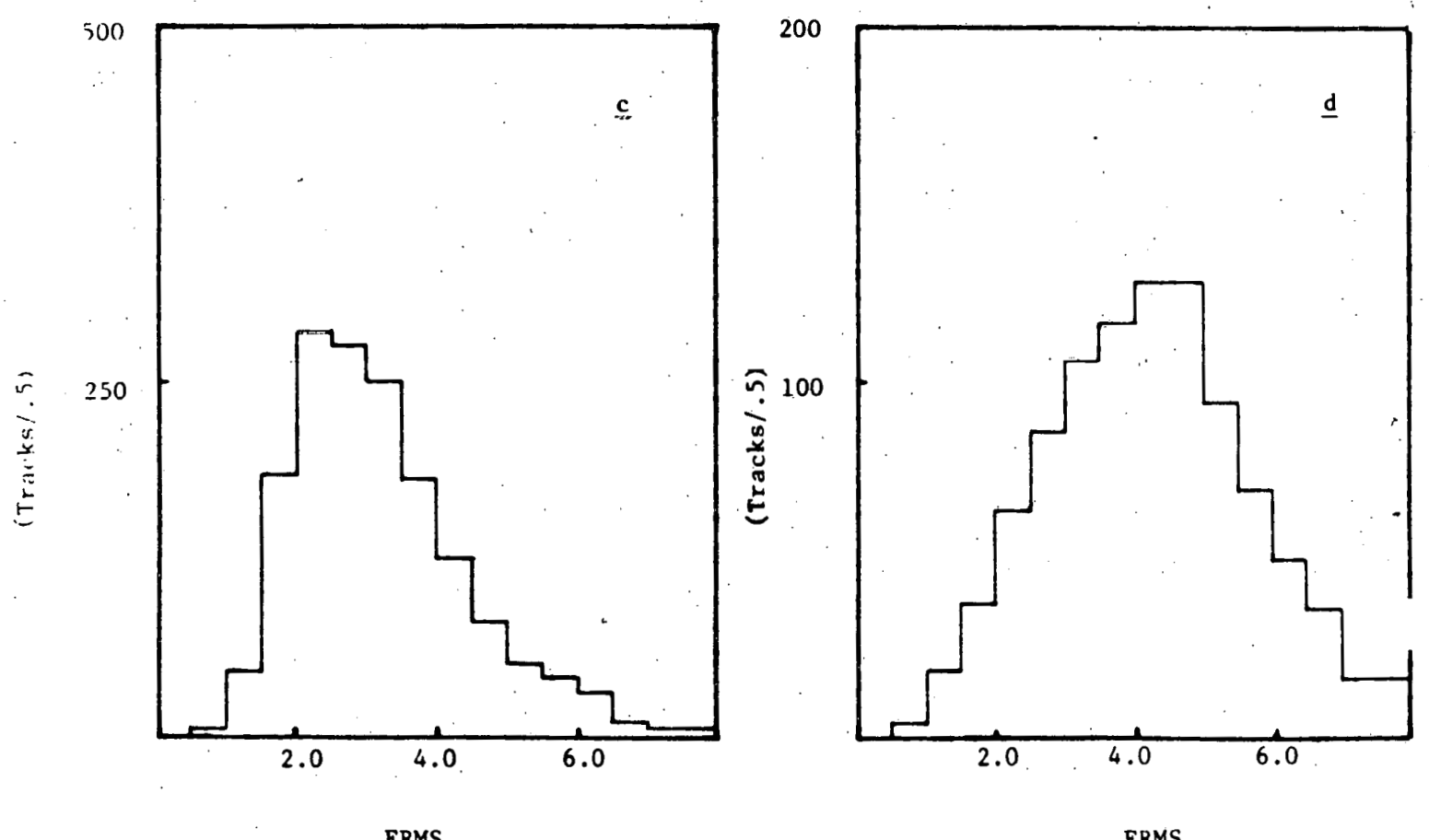

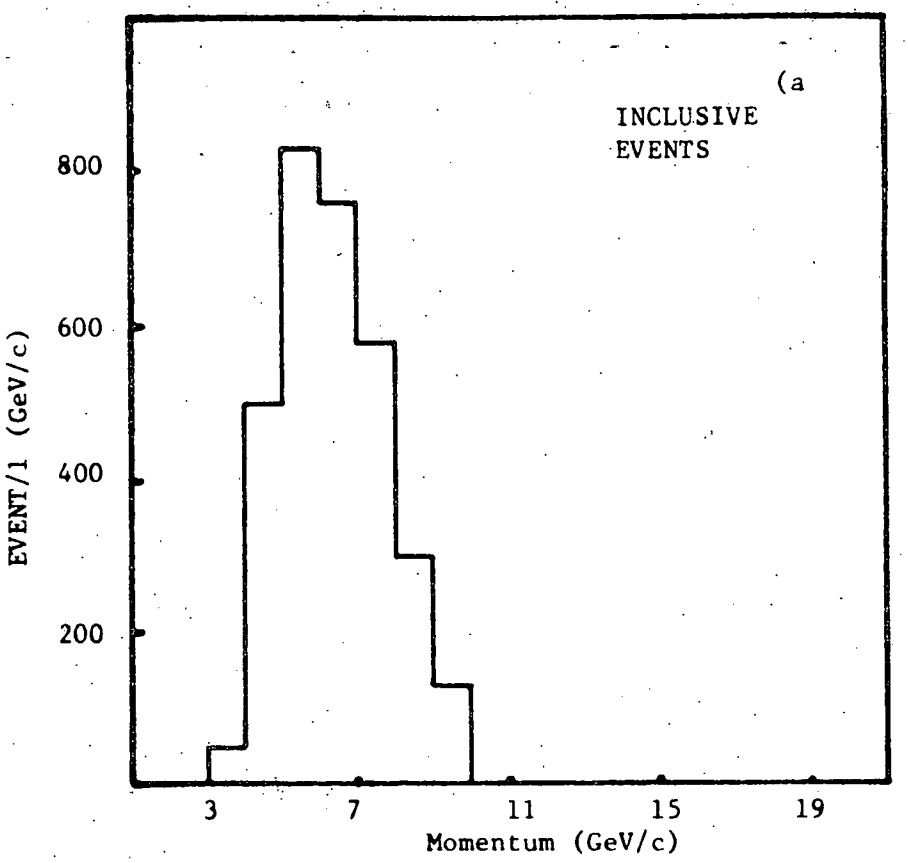

FIG. V-2 Distribution of trigger track momentum for Inclusive and Vee events

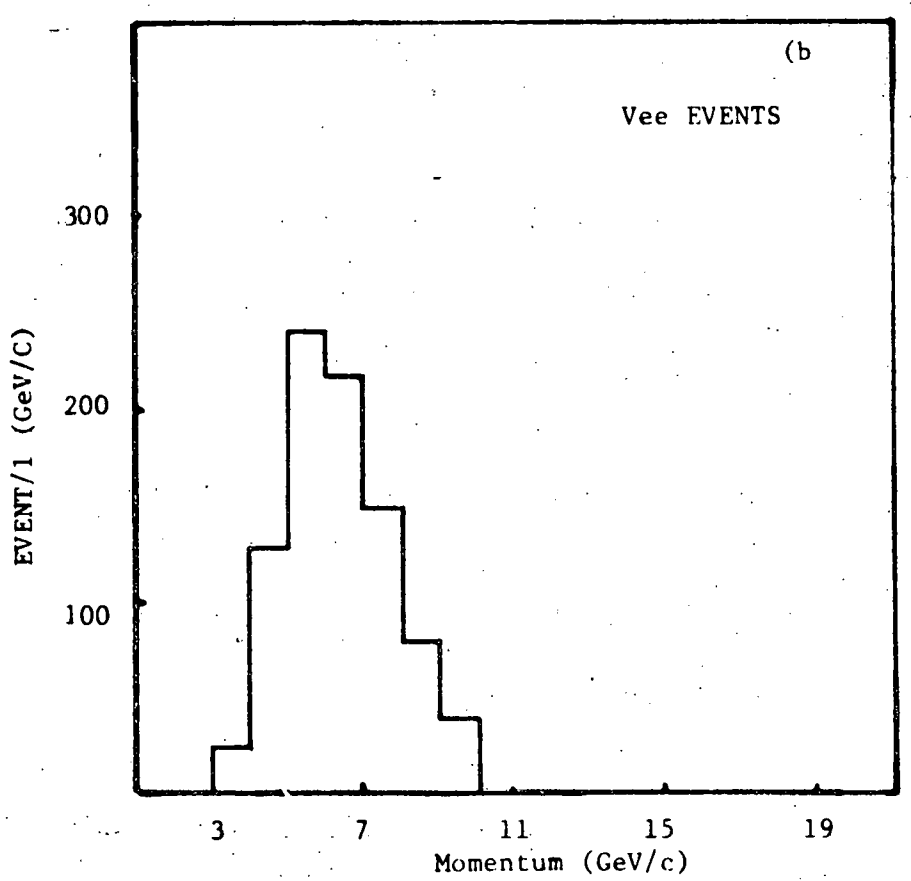

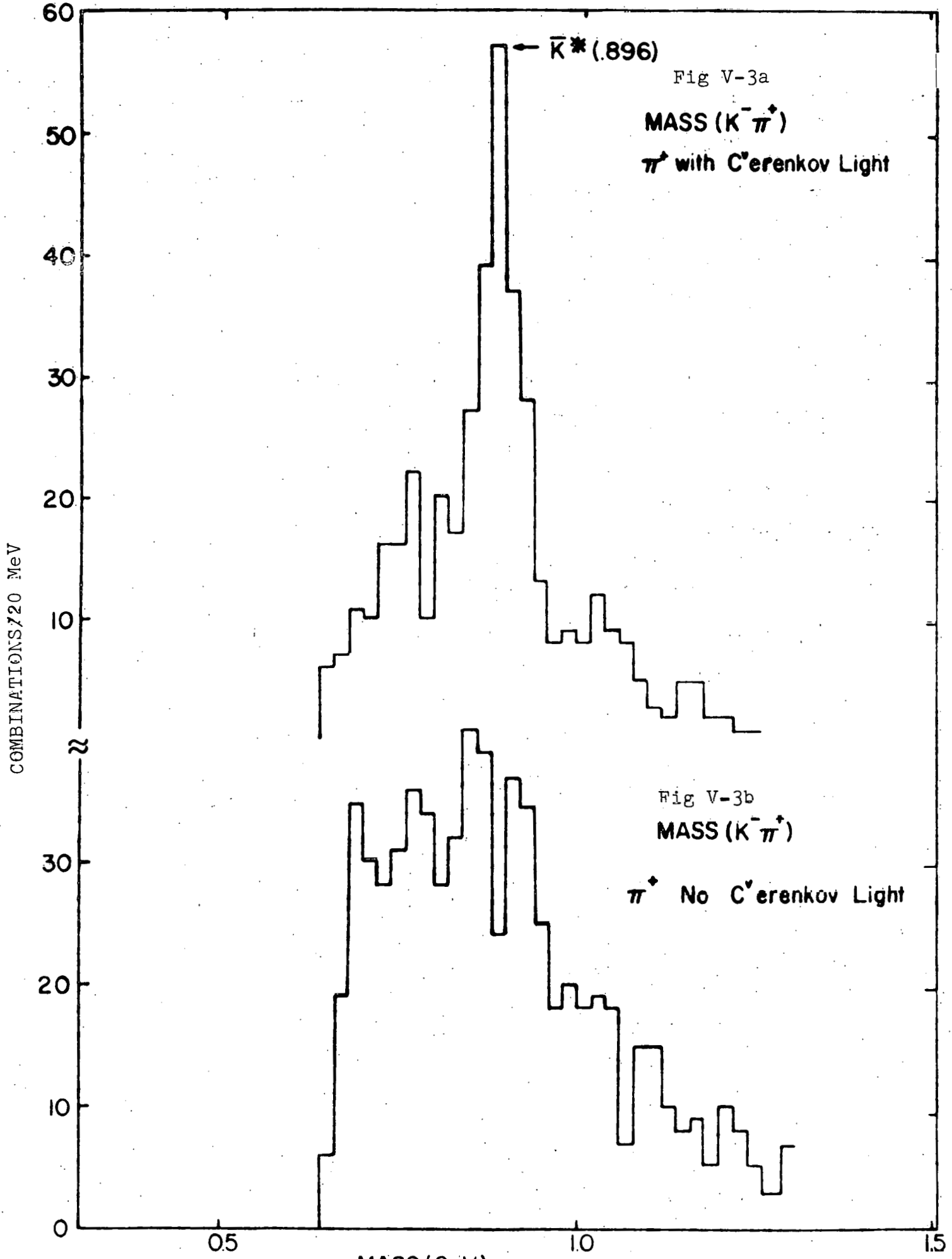
$\bar{K}^*$(.896)
Fig V-3a
MASS ($K^-\pi^+$)
π^+ with Cerenkov Light
Fig V-3b
MASS ($K^-\pi^+$)
π^+ No Cerenkov Light
COMBINATIONS/20 MeV
60
50
40
30
20
10
30
20
10
0
0.5
1.0
1.5

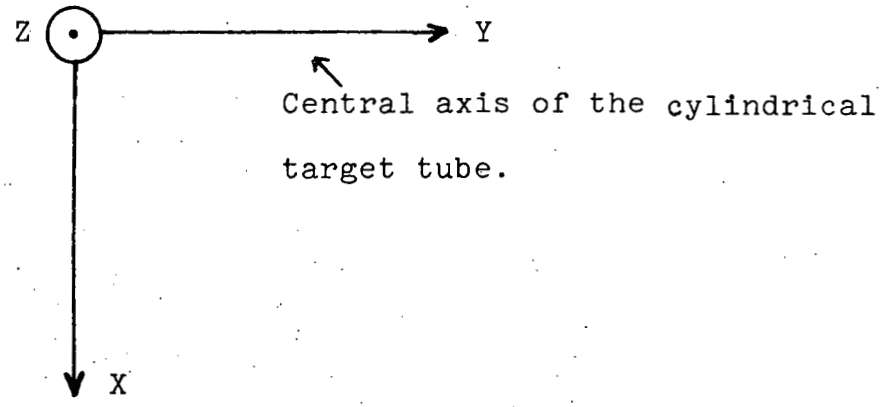

Fig. V-4- Target Coordinate System

Note: The cylindrical target extended $-65 \leqslant Y \leqslant -5$ cm and had a radius of 1.58 cm

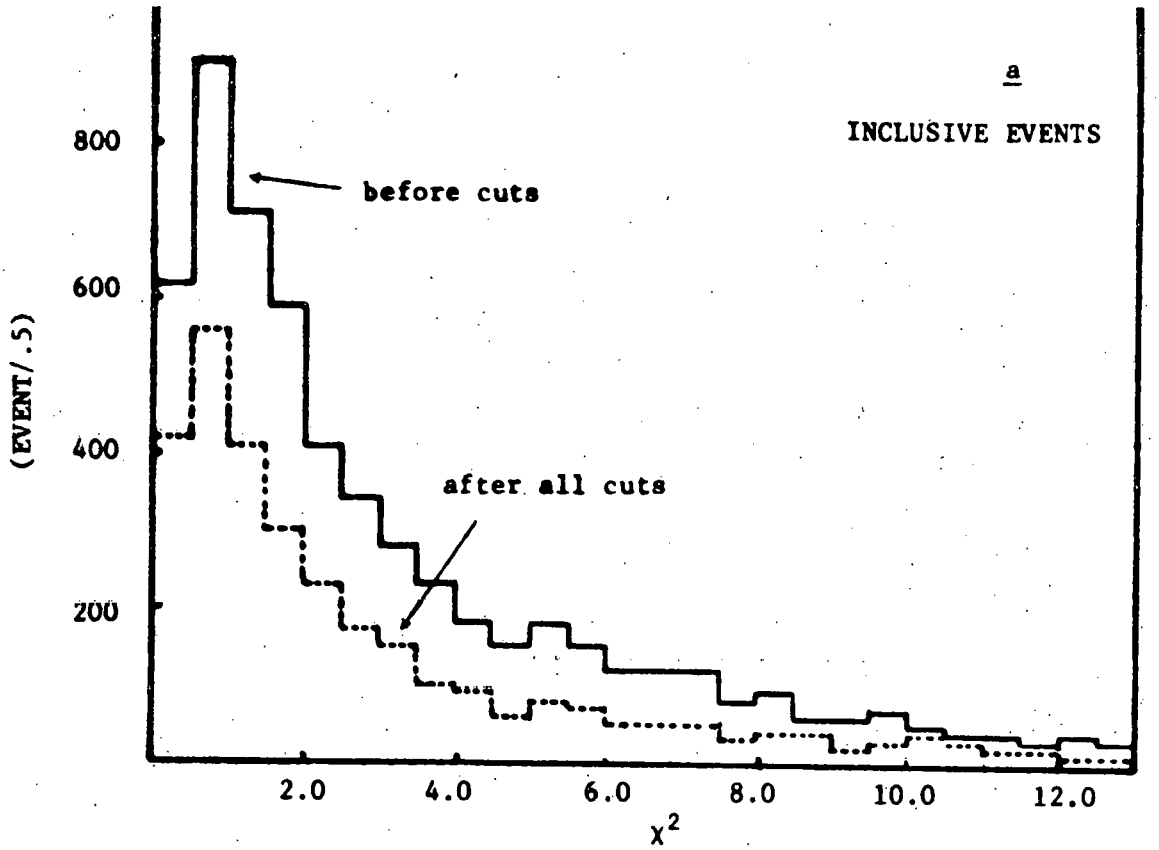

FIG. V-5 Distributions of APACHE χ^2 for inclusive and vee events.

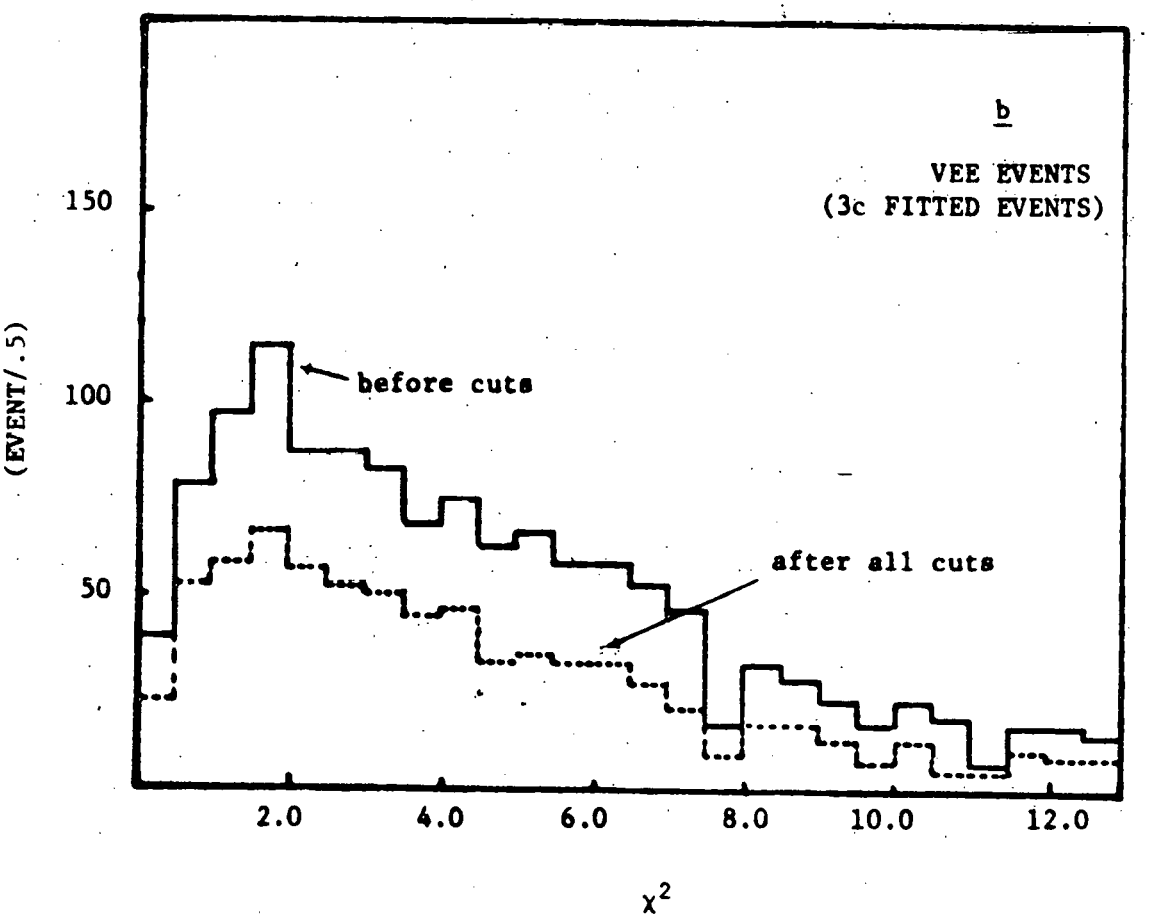

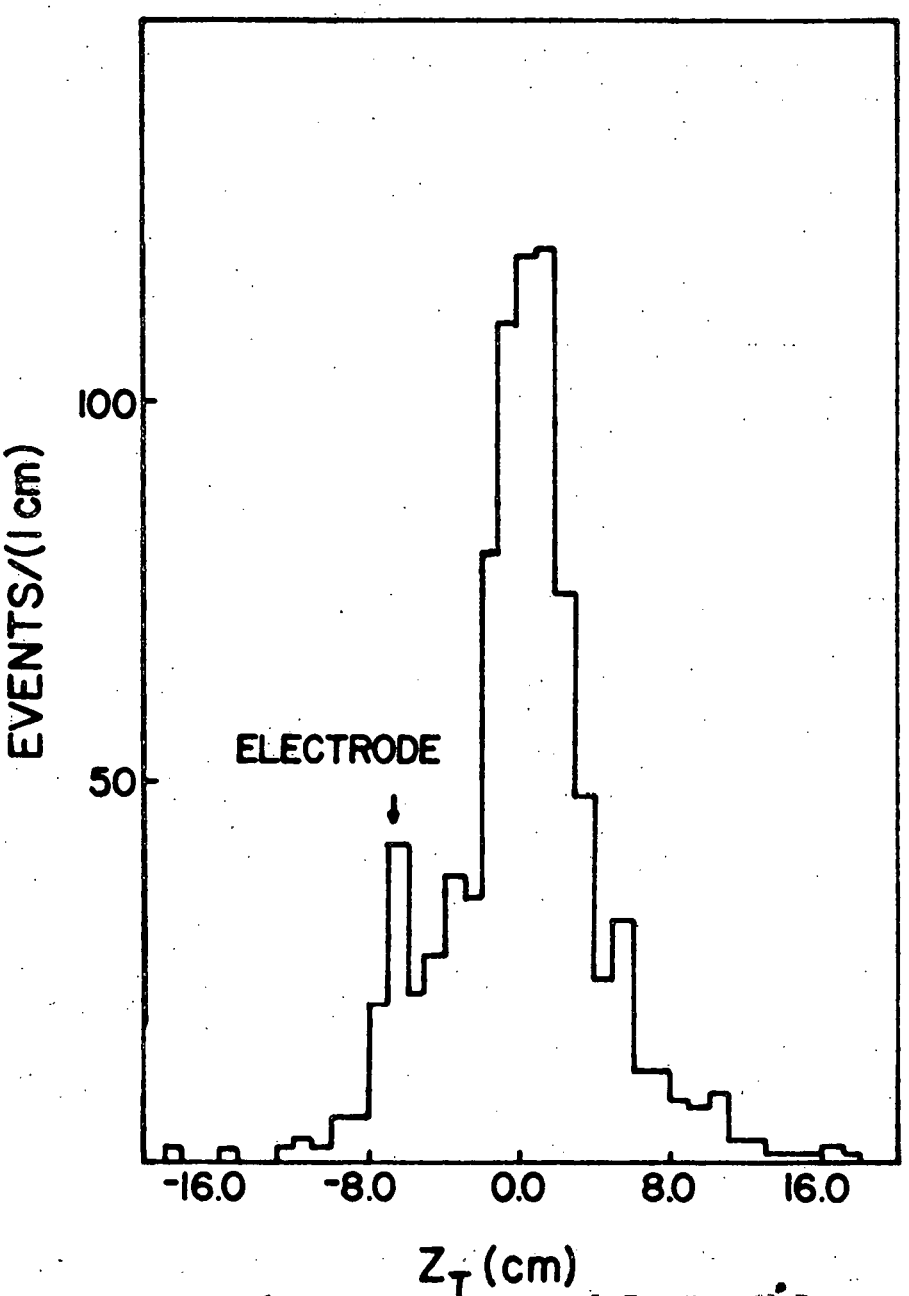

Fig. V-6- Distribution of Z_T for V^0 Decays

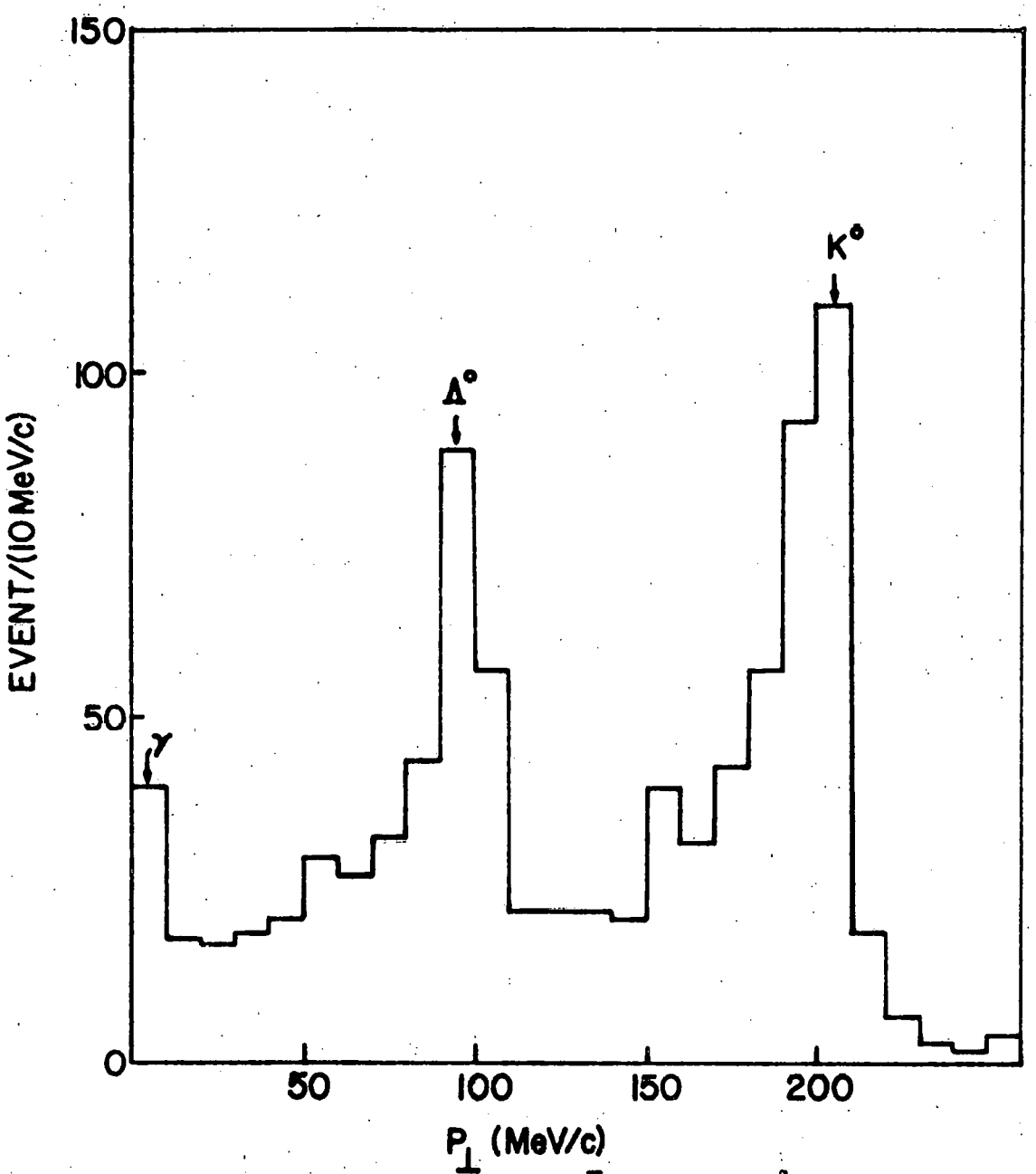

Fig. V-7- Distribution of $\bar{P}_\perp$ for all V° decays

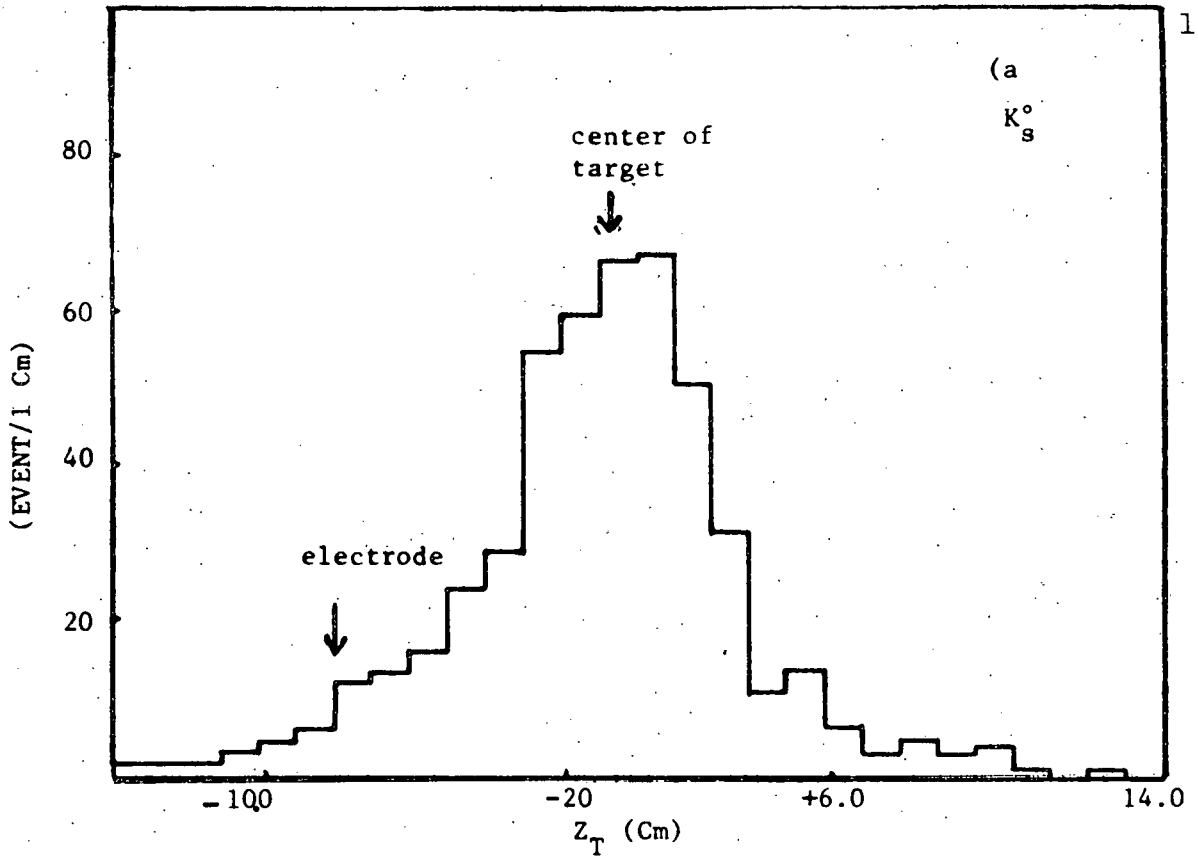

FIG. v-8 a) Z_T distribution of K°_{s}'s after all cuts
b) Z_T distribution for Λ°s after all cuts

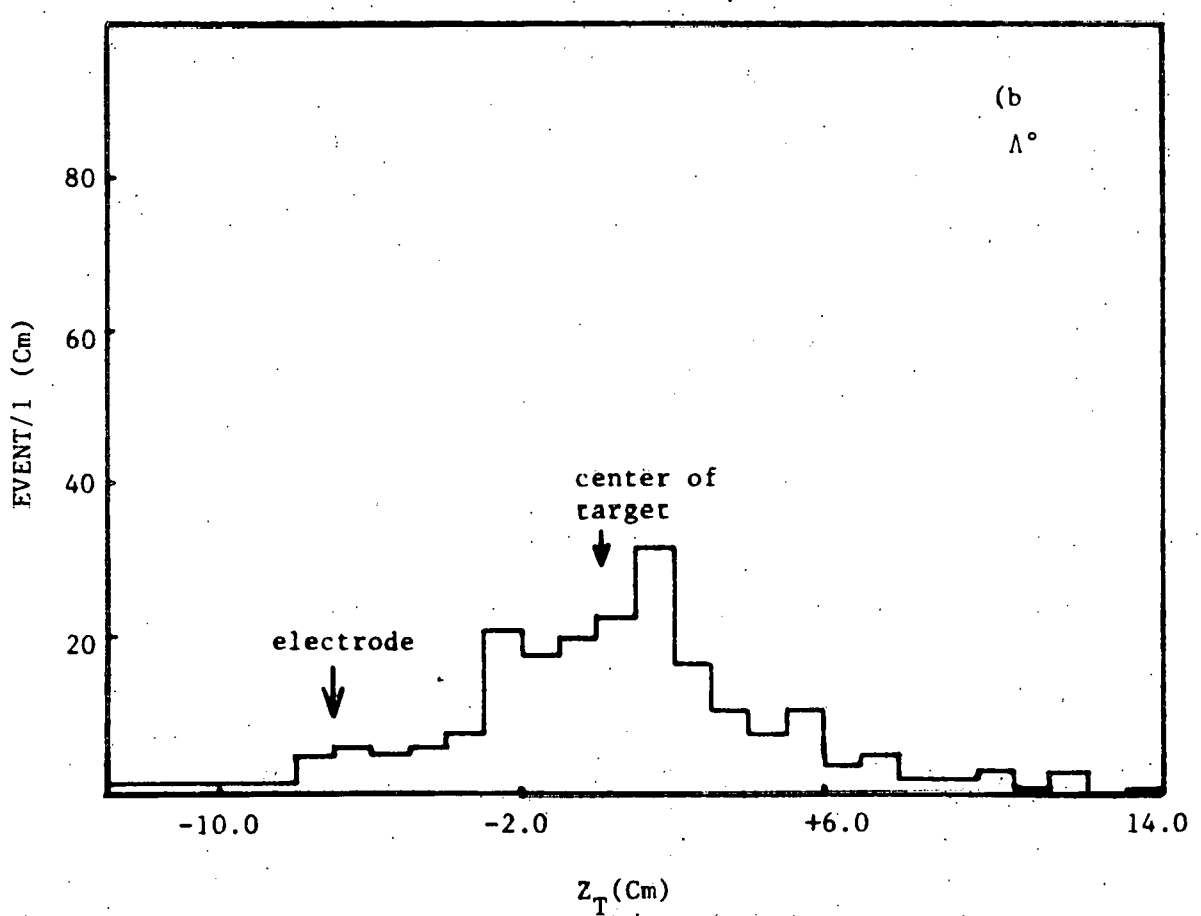

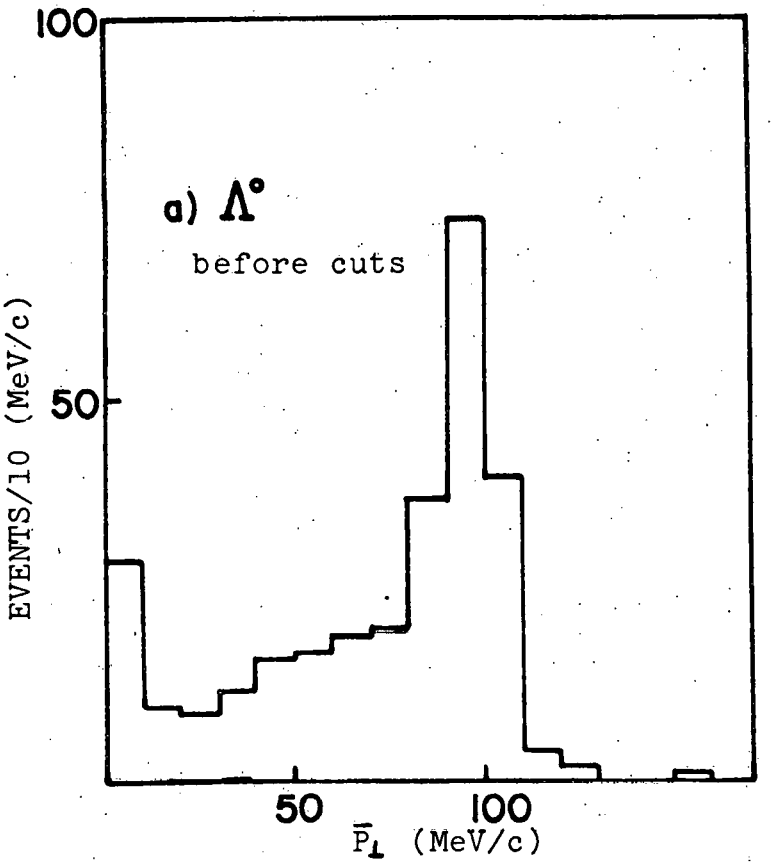

Fig. V-9- Distribution of $\bar{P}_\perp$ for Λ° before and after cuts

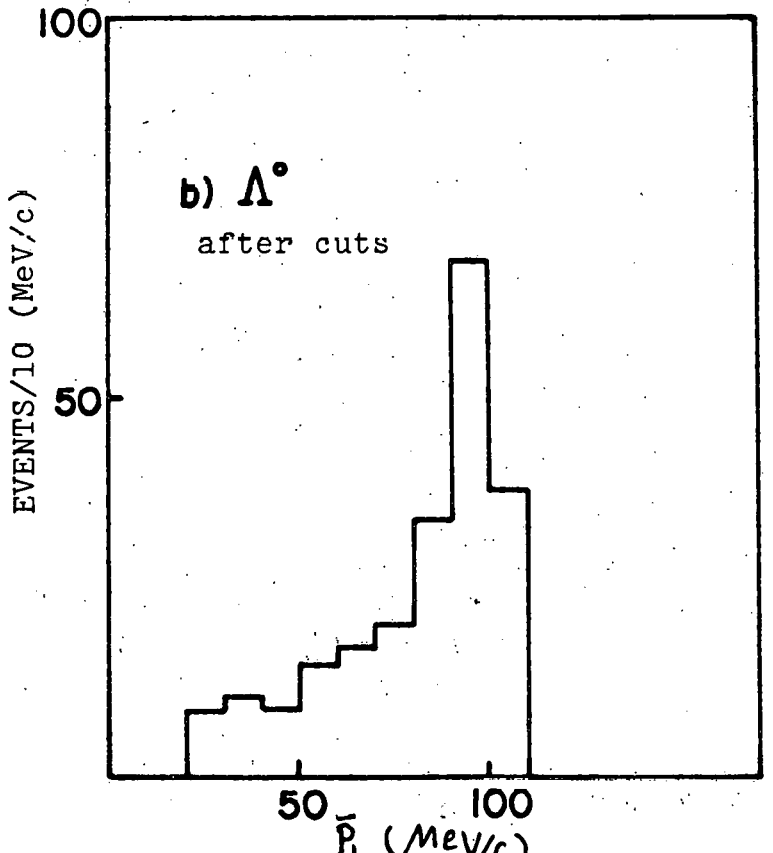

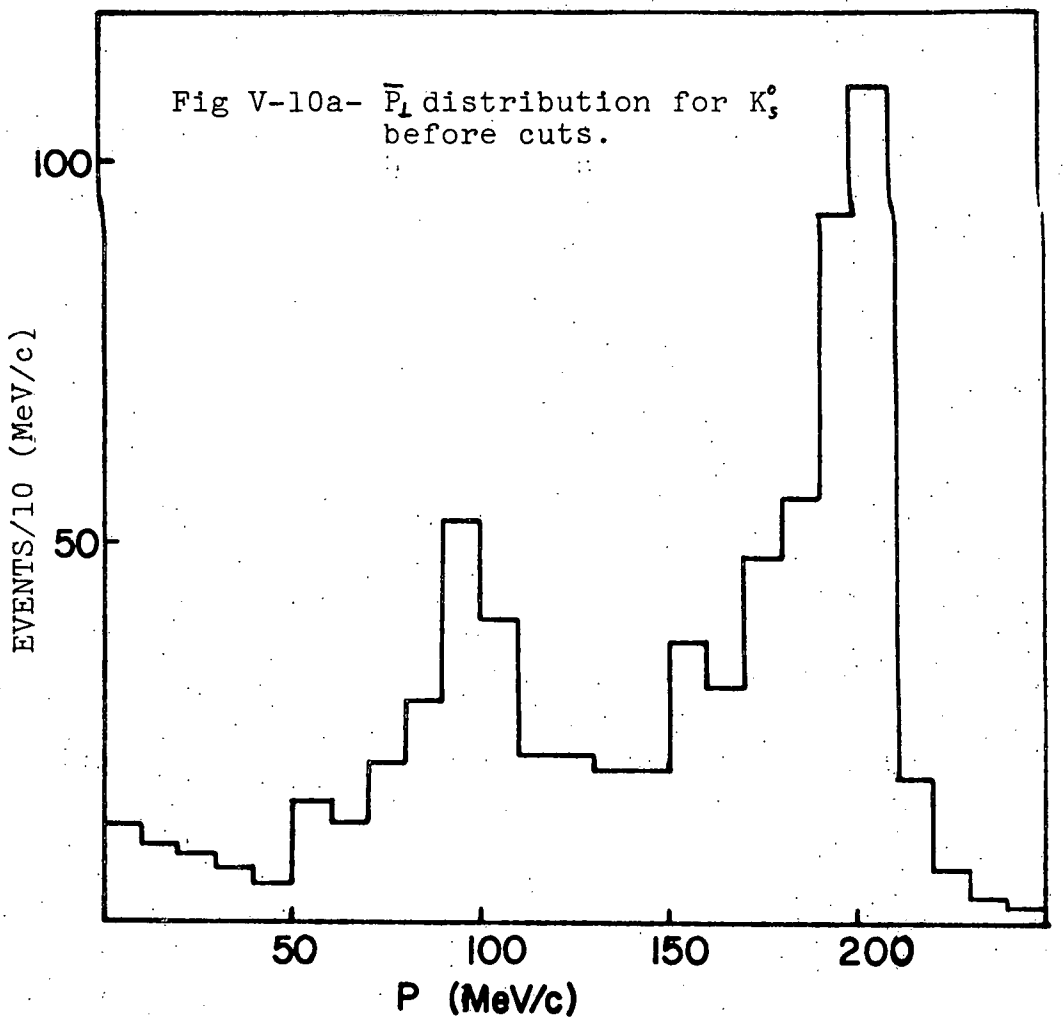

Fig V-10a- $\bar{P}_t$ distribution for K^o_s before cuts.

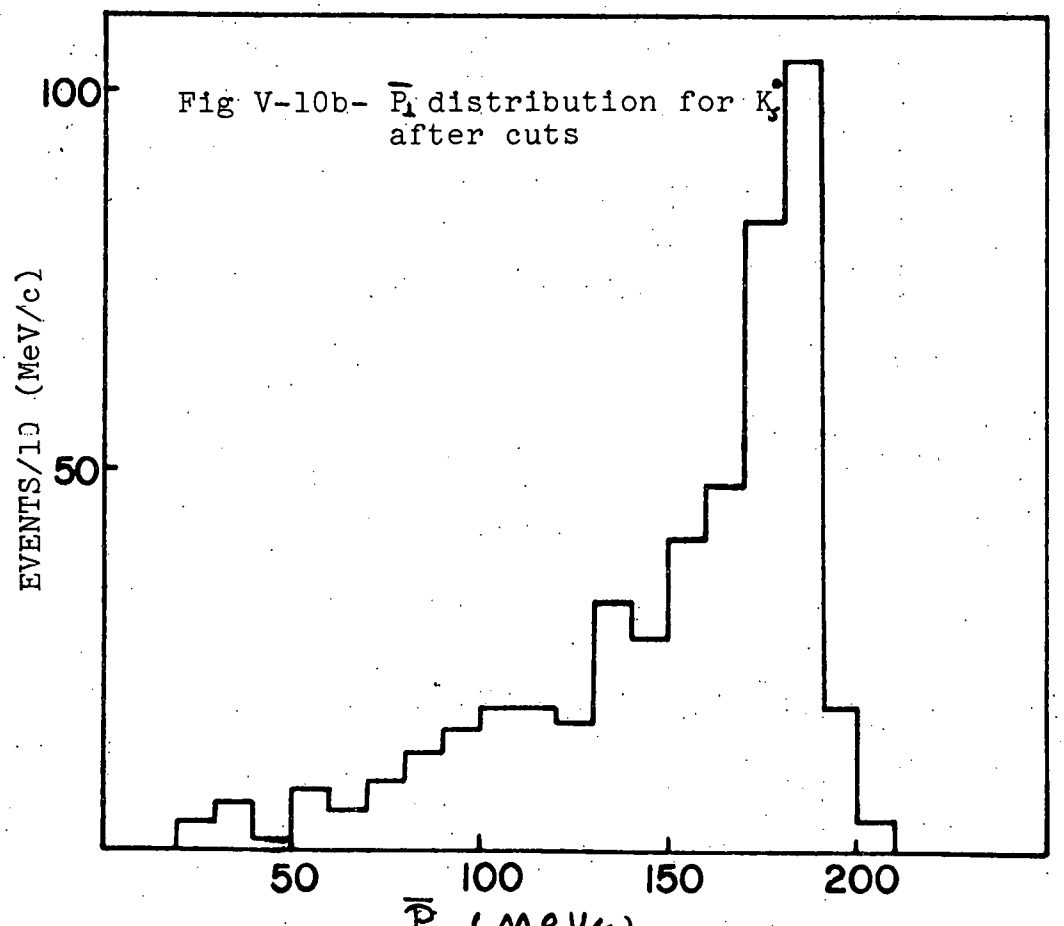

Fig V-10b- $\bar{P}_t$ distribution for K^o_s after cuts

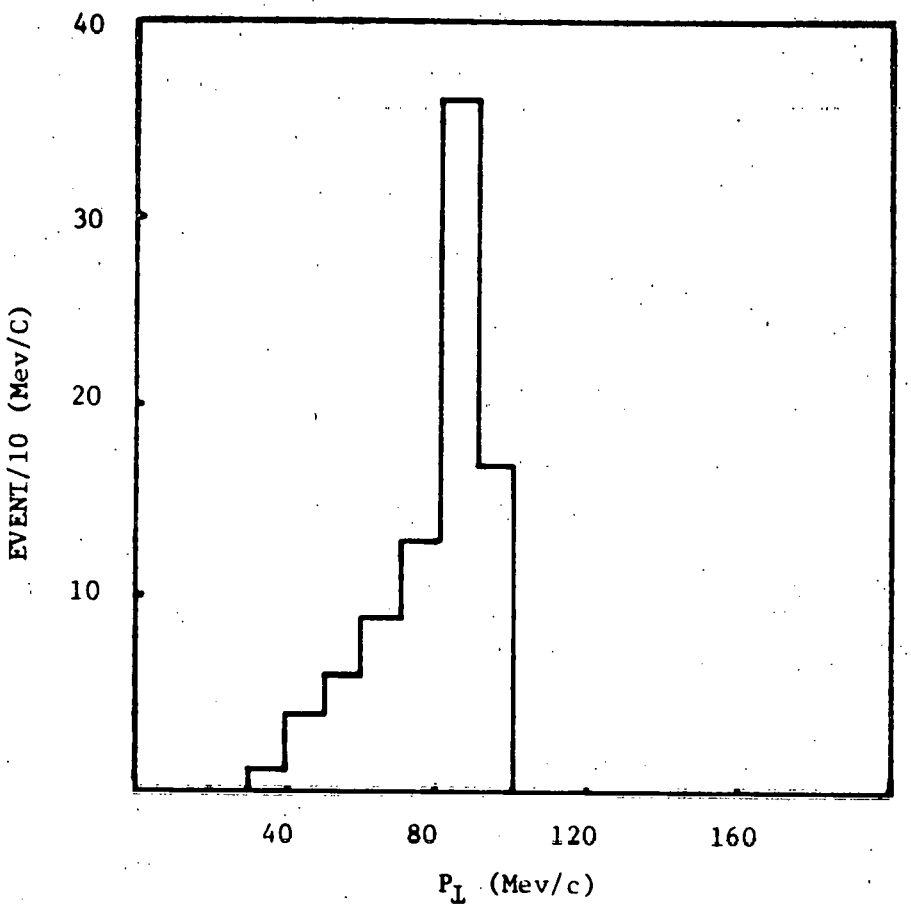

FIG. V-11 Distribution of P_L for uniquely fitted Λ°

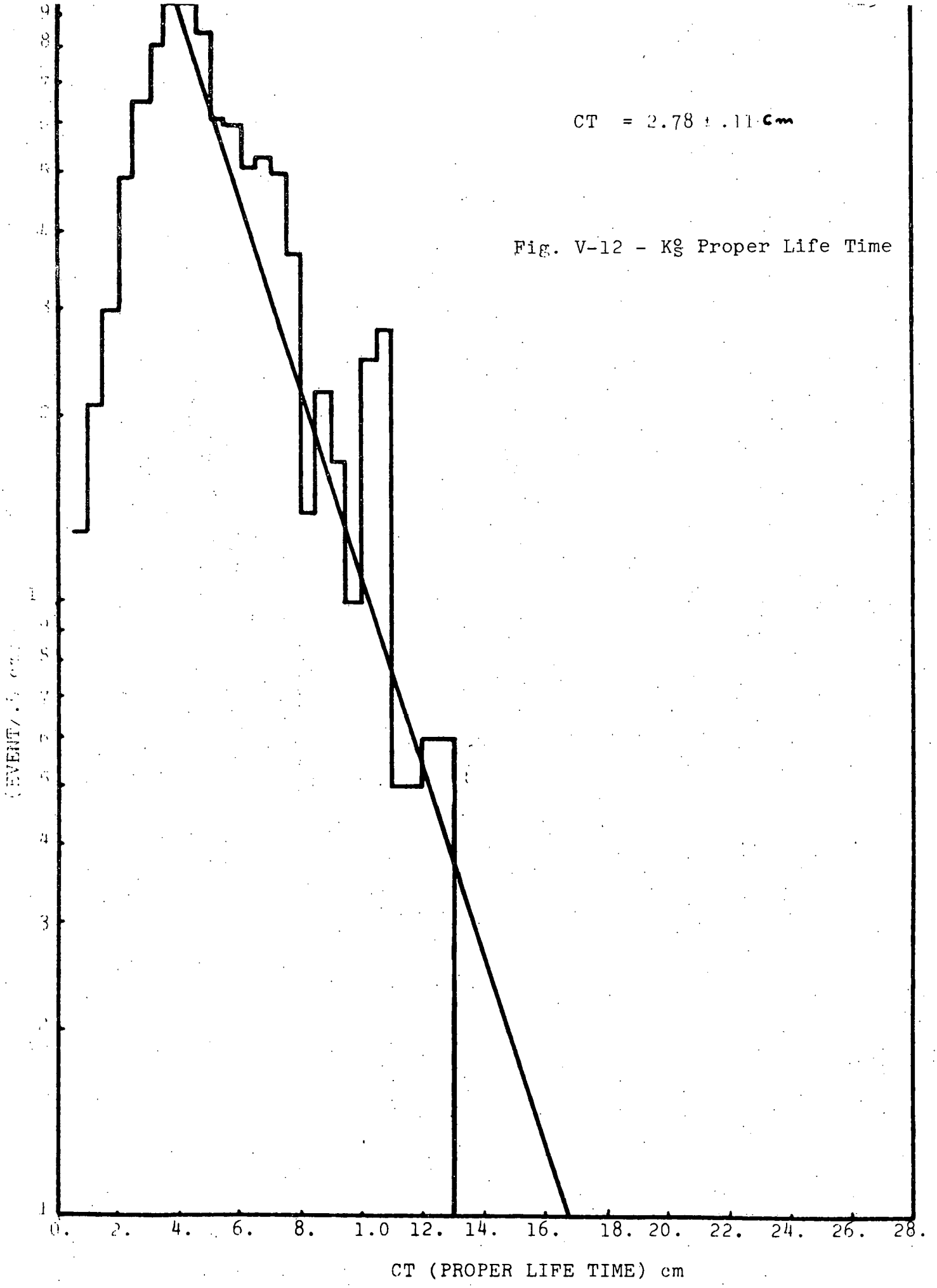

Fig. V-12 - K^0_S Proper Life Time

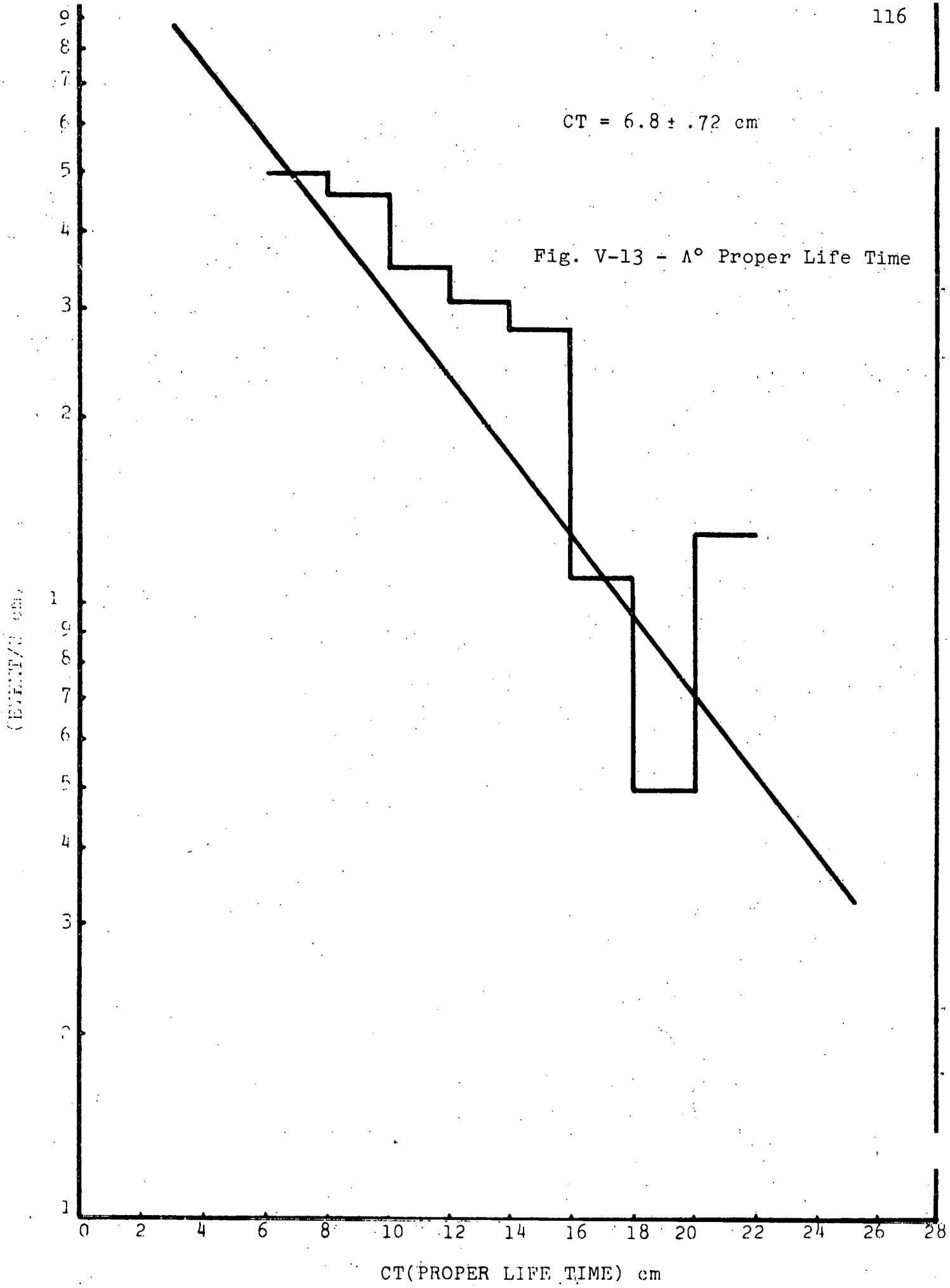

Fig. V-13 - Λ° Proper Life Time

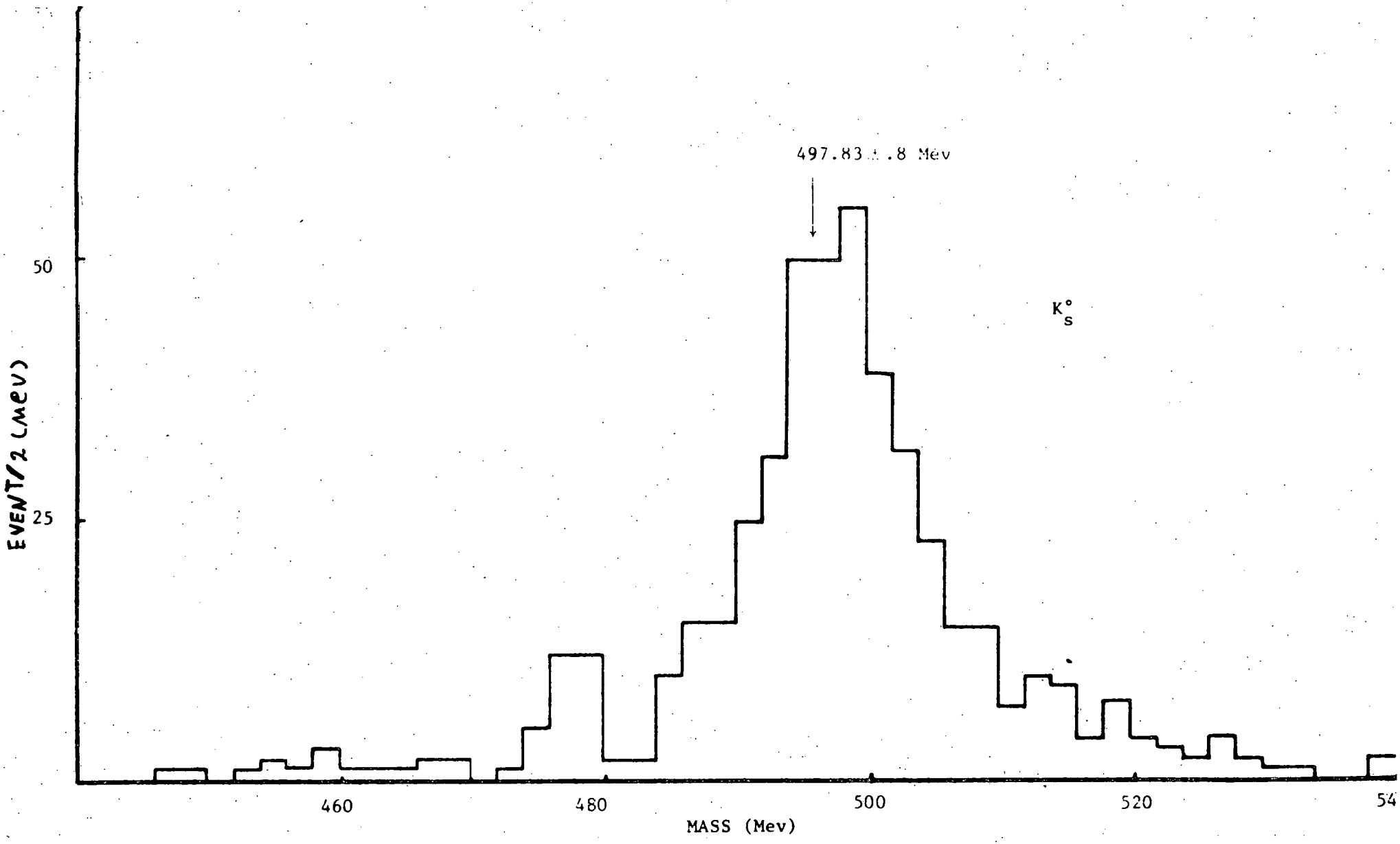

FIG v-14 Distribution of measured K°_s invariant mass

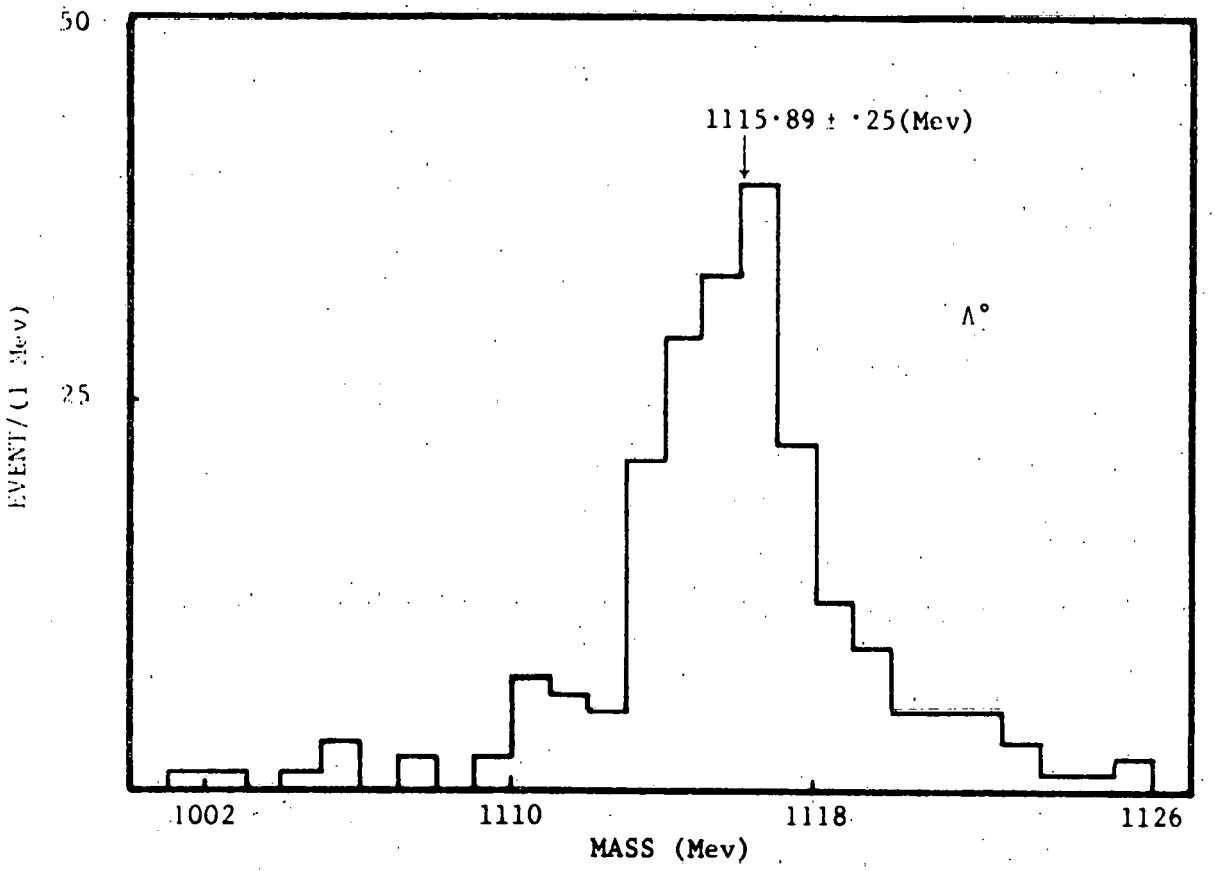

FIG. V-15 Distribution of measured Λ°_{s} invariant mass

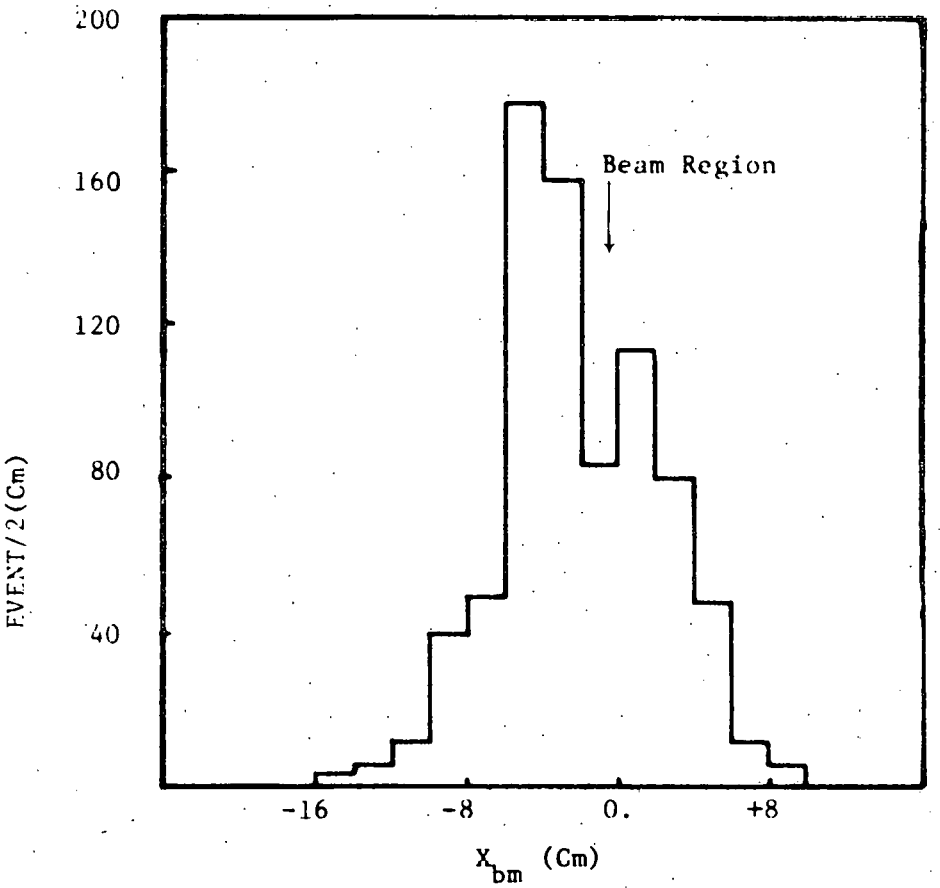

FIG. V-16 Distribution of $(X_{bm}=X_v-X_{beam})$ For V0 decay vertices in the streamer chamber

CHAPTER VI- ANALYSIS OF THE Φ (1020) AND $\bar{K}^{*\circ}$(896) PRODUCTION

SUMMARY

In this chapter, results are presented for the semi-inclusive reactions:

$$\pi^+ + P \longrightarrow \Phi(1020) + K_S^\circ + X \,, \qquad VI-1$$

$$\pi^+ + P \longrightarrow \Phi(1020) + \Lambda^\circ + X \,. \qquad VI-2$$

and

$$\pi^+ + P \longrightarrow \bar{K}^{*\circ}(896) + X \qquad VI-3$$

where X represents any additional particle.

A-Conjoint Production of $\Phi(1020)$

1-Invariant Mass Spectra

As described in chapter II, much of the motivation for this experiment was to study production of the Φ-meson in conjunction with strange particles. Invariant mass distributions of (K-K+) combinations were used to search for the Φ-meson resonance. Here K- and K+ respectively are trigger particle and a positive track identified as a K+ (see section V-C). Figure VI-1 shows the (K-K+) invariant mass spectrum for events which contain a visible neutral strange particle decay, i.e., a K_S° or Λ° . An enhancement is seen at the Φ mass (1020 MeV). These events were separated into events containing a K_S° or Λ° .

The (K-K+) mass spectra for both sets of events are shown in figs. VI-2A, B, . The peak at the Φ mass enhancement is evident in both distributions. To determine the Φ contribution to this distribution quantitatively, it was necessary to estimate the shape of the background in this (K-K+) mass spectrum.

To generate the background mass distribution the invariant mass of a set of pseudo-combinations was calculated. A K- trigger particle from one event was matched with a K+ from another event, with the condition that the two primary vertices have the same charged particle multiplicity. Following this method a large number of combinations were generated and a smooth distribution of invariant masses was obtained. One possible source of inaccuracy of the method would be that momentum and energy conservation were not obeyed properly in generating the events. However it can be argued that the shape of the background will not alter because most events have missing neutrals anyway. The resulting combinatorial background is shown in Fig. VI-3.

Given this background distribution BG(m), the combined mass spectrum of Fig. VI-1 was taken to have the form,

$$dN/dm=BG(m)+BW(m)PS(m) \qquad \text{VI -4}$$

where BG, BW, PS represent background, Breit-Wigner and phase-space distributions, respectively. The resonant signal Φ was described by a simple Breit-Wigner function,

$$BW(m) = \frac{\Gamma^2/4}{(m-M_0)^2 + \Gamma^2/4} \qquad \text{VI\_5}$$

where MO and Γ are, the mass of thc resonance and its width respectively. Note that a relativistic Breit-Wigner fuction with a mass dependent width is not appropriate, because the natural width for the Φ(1020)-meson (Γ=4 MeV) is much less than the experimental mass resolution. Thus the observed width is mainly the effect of uncertainty in measurement of the invariant (K-K+) mass, expressed as a Breit-Wigner function.

The background BG(m) and phase-space factor PS(m) were assumed to have the mass dependence of the combinatorial background. The fit was then carried out over the range from 980 to 1400 MeV, over which there was a substanial number of events present. The Particle Data Group value was used for the resonance mass(M_Φ =1020 MeV). The variables in the fit were the width of the Φ(1020) mass peak and the numbers of background and resonance combinations. The width of the resonance, which was adjustable, was found by MINUIT to be 17 MeV.

Fits were also carried out for KOs and Λ° associated events by fixing the values of the Φ mass and width at 1020 and 17 MeV respectively.

2-Cross-Sections

Table VI-1 contains the numbers of Φ and background events determined from fitting the reactions VI-1, VI-2.

In order to determine the production cross-sections for these reactions, the data had to be corrected for geometrical acceptance as well as for the inefficiencies in triggering, scanning, measurement and analysis.

To estimate the geometrical acceptance of the system as a function of the longitudinal Xf variable (Feynman Xf=Pl/Pmax) and the squared transverse momentum, $\hat{Pt}$, of the Φ-meson, the following procedure based on a Monte Carlo method was used.

a) Assume that the differential cross-section for Φ production can be parametrized as

$$F(Xf, \hat{Pt}) = f(Xf)EXP(-B\hat{Pt})$$

b) Fix the value of B at an arbitrary but typical value of $3.5(GeV/c)^{-2}$. (Note:Several Monte Carlo calculations for different values of B ranging from 2 to 5 showed that the geometrical acceptance was not sensitive to the choice of B.)

c) Generate Xf with values of 0. ,.1,.2,.....,.9

d) With each (Xf and $\hat{P}t^2$) for the Φ , an isotropic decay angular distribution was assumed for its decay in the rest frame. Momentum vectors for the K- and K+ decay products were then determined in the LAB frame.

e) Trajectories of the product K- and K+ mesons were simulated , using the above momentum vectors and coordinates of the interaction vertex located randomly in the target.

f) By extrapolating these trajectories, it was determined whether the K- and K+ would have hit a picket fence channel and $\check{C}k$, respectively. The K- , and K+ were required to have momenta of greater than 3 GeV/c, which was the momentum cut applied to the data as well.

Figures VI-4 shows the geometrical acceptance as a function of Xf , as determined by this process.

To correct the data for the geometrical acceptance, each (K-K+) combination with an invariant mass less than 1100 MeV and a given longitudinal momentum variable Xf was weighted by the inverse of the corresponding geometrical acceptance for the same Xf. Finally, an averaged correction factor was determined for combinations with $m(K^- K^+) < 1100$ MeV.

Each event was also weighted by the inverse of the detection probability for Λ°/Ks, W (see Section V-E for detail of the method used to determine W)

A complete list of all the other correction factors used in the calculation of the cross-sections is presented in Table VI-2.

With the correction factors so applied the cross-sections were calculated from the formula

$$\sigma_x = (N_x / F \prod_i E_i) \qquad \text{VI-6}$$

where Nx=number of events found in interaction channel x, Ei are efficiency factors and F denotes the total incident π^+ flux per unit cross-section (VI--7).

$$F = n_{\pi^+} (1/\sigma_{TOT})(1 - e^{-L_t/\lambda I}) \qquad \text{VI-7}$$

where n_{π^+} =number of incident π^+ $= 1.20303 \times 10^{9}$

and $$\lambda I = (A/Na\rho)(1/\sigma tot)$$

A= Atomic weight= 1.01

Na= Avogadro's number $= 6.023 \times 10^{23}$

ρ = Target density = .0708 gm/cm^3

σ tot= Total π+p cross-section at 16 GeV/C=24.05 mb [2,3]

L_T= Target fiducial length =60 cm

The interaction length is, therefore,

λ_I=984.5 cm

and

$F=2.95584 \times 10^{23}$ event/cm^2.

Final results for the cross-sections are given in Table VI-3.

B - Search for Inclusive Production of The Φ-meson

Fig. VI-5 shows the distribution of invariant mass of (K-K+) combinations from the inclusive data sample (see Chapter V). Here K- is the trigger track and K+ a positive particle identified as K+ by the procedures of chapter V. No clear Φ signal is apparent. An estimate of the upper limit for the possible $\Phi(1020)$ contribution was made by normalizing the combinatorial background spectrum described in the previous section to the inclusive distribution. The normalization was carried out for the mass range of 1500<m(K-K+)<1800 MeV, and then the resulting factor was used to normalize the background to the entire mass spectrum. This is presented in Fig. VI-5. No more than a few events can be detected above the background in the mass range of 980<m((K-K+)< 1100 MeV, thus the resonance

contribution is consistent with zero and its upperlimit can be determined based on statistical error, i.e., to be of order of 10 events. An estimation of the expected number of Φ,s in the inclusive sample, as might be contributed by conjoint production processes, will be presented in chapter VII.

The excess of events observed in the mass range of 1150 MeV $<m(K^-K^+)<1350$ MeV can be attributed to $\bar{K}^{*\circ}$ production due to pion contamination in positive tracks identified as K^+ resulting from inefficiency of the Cerenkov detector (see Section V-C). An indication of the presence of these contaminating particles is seen in Fig. VI-7b where ~60 $\bar{K}^{*\circ}$ are observed in the mass distribution of $(K^-\pi^+)$ pairs for which the positive particle is identified to be K^+ but is assigned the pion mass.

C-INCLUSIVE PRODUCTION OF $\bar{K}^{*\circ}(s\bar{d})$

1-Mass Spectrum

Study of the inclusive production of the $\bar{K}^{*\circ}$ is based on the inclusive data sample described in chapter VI, whose $\Phi(1020)$ content was discussed in the preceeding section. The invariant mass distribution of $(K^-\pi^+)$ combinations consisting of a trigger particle (K^-) and a positive particle assumed to be π^+, was used to examine $\bar{K}^{*\circ}$ production. This spectrum is shown in Fig. VI-6. The spectrum for $(K^-\pi^+)$ combinations for which positive particles passed through the K+ Cerenkov counter and were identified to be π^+ is also given in Fig. VI-7a. The $\bar{K}^{*\circ}(896)$ resonance is seen in both mass spectra. No clear high mass resonance $(\bar{K}^{*\circ}(1420))$ is present in the spectrum.

2-Inclusive Cross-Section

The resonance production was determined by fitting the mass spectrum to,

$$dN(m)/dm = BG(m) + BW(m)PS(m) \qquad VI\_8$$

where BG(m), BW(m) and PS(m) represent background, resonance and phase-space contributions respectively. The resonance signal was described by relativistic Breit-Wigner functions with mass dependent width[1]:

$$BW(m) = \frac{m M_R \Gamma(m)}{(m^2 - M_R^2)^2 + M_R^2 \Gamma^2(m)} \qquad VI-9$$

where

$$\Gamma(m) = \Gamma_R (q/q_R)^{2L+1} \frac{\rho(m)}{\rho(M_R)}$$

and

$$\rho(m) = (q_R^2 + q^2)^{-1} .$$

Here Mr is the resonance mass, Γ_R its width, q the momentum of the decay products in the rest frame of the resonance, qr its value at M=Mr and L =1, the relative angular momentum.

To describe the background, the function

$$BG(m)=A(m-mt)^{\alpha}EXP(-\beta m) \qquad VI-10$$

was used. The choice of this functional form for the background was made because it was consistent with the low mass rise and with the overall shape of the combinatoral background, generated for ($K^- \pi^+$) combinations. (It should be noted that the resonant ($\bar{K}^{*0}$) peak is not at the peak of the background, thus an exponential decline for the background would have sufficed to estimate the resonance contribution to the spectrum.)

Given the background shape and assuming the same mass dependence for phase-space factor PS(m), then the MINUIT fit was carried out over a large mass range $640<m(K^-K^+)<1800$ MeV.

A Chi-square of $\chi^2/NDF=.2$ was obtained. These fits are shown in Fig. VI-6.

Values of the resonance mass and width were also determined from the fit to be,

$$M_{\bar{K}^{*\circ}}=896.2\pm5 \text{ MeV}$$

and

$$\Gamma_{\bar{K}^{*\circ}}= 100.4\pm12 \text{ MeV}$$

The mass and width of the resonance is consistent with its established values considering the mass resolution ($M_{\bar{K}^{*\circ}}= 896.1$, and $\Gamma = 49.5$).

The cross-sections were evaluated using the formula (VI-6) and the number of $\bar{K}^{*\circ}$,s obtained from the fit . Table VI-4 shows the final results and also the correction factors used in the cross-section calculation.

3-Differential Cross-Sections

The $\bar{K}^{*\circ}$ longitudinal and transverse momentum distribution were found by dividing $(K^-\pi^+)$ combinations into suitable bins in Xf and P_t^2. The $(K^-\pi^+)$ mass spectrum for each range of Xf and P_t^2 was then fitted to the equation (VI-8) by fixing the resonance mass and width to be 896

MeV and 100 MeV, respectively.

The resulting dN/dP_t^2 and dN/dx_f distributions for $\bar{K}^*(896)$ production are shown in figs VI-8 and VI-9 respectively.

4-Geometrical Acceptance

The geometrical acceptance for the K- trigger from the $\bar{K}^*$ was a function of Xf and $\vec{Pt}$, and also of the decay angles of the $\bar{K}^*$. The following method was used to simulate the $\bar{K}^*$ production, and to determine this acceptance.

a) Assume that the differential cross-section for $\bar{K}^*$ production can be parametrized by Xf and $\vec{Pt}$ as

$$F(Xf, \vec{Pt}) = f(Xf)EXP(-B\vec{Pt})$$

b) Fix the value of B at 3.5. (Note :several Monte Carlo calculations showed that the geometrical acceptance is not sensitive to the value of B for the $\bar{K}^*$, as it also was not for Φ production.)

c) Assume an isotropic decay angular distribution for the $\bar{K}^*$ decay in rest frame.

$\bar{K}^*$'s were then generated for the fixed values of Xf in the range of 0.0 to 0.9. The geometrical acceptance was determined by extrapolating the decay product K- into the trigger hodoscope. Fig. VI-10 shows the geometrical acceptance as a function of Xf.

The longitudinal momentum distribution of $\bar{K}^{*\circ}$ was corrected for the geometrical acceptance at each Xf and the resulting spectrum is also shown in Fig. VI-9.

To obtain the dependence of the geometrical acceptance upon the transverse momentum of $\bar{K}^{*\circ}$, the $\bar{K}^{*\circ}$ production was simulated using the distribution of Xf obtained above after the acceptance corrections were applied. The acceptance as a function of P_t^2 is shown in Fig. VI-11. The data were then corrected for geometrical acceptance and the resulting distribution is presented in solid lines in Fig. VI-8.

The cross-section calculations were performed by adjusting the data for the correction factors and the geometrical acceptances. Figures VI-12 shows the distribution of $d\sigma/dx_f$.

REFERENCES

1-J.D.Jackson, Nuovo Cimento 34(1964)1644;
F.Selleri,Phys. Lett. 3(1962)76

2-C-Baltay, et al, Phys. Rev. D17 62(1978)

3-D.Pisello, Columbia University, Doctral Dissertation (1976)

4-See References 1and 2, Chapter VII.

5-See Reference 2, Chapter V.

*

TABLE VI-1

Estimated Number of Φ in Associated Channels

Reaction	Number of Φ
$\pi^+ + P \longrightarrow \Phi + K_s^o + X$	7 ± 3
$\pi^+ + P \longrightarrow \Phi + \Lambda^o + X$	9 ± 3

TABLE VI-2

Correction Factors Used in Estimation

of Cross-Section for Φ

Production Peocesses.

Correction Factors	$\pi^+ + P \longrightarrow \Phi + K^o_s + X$	$\pi^+ + P \longrightarrow \Phi + \Lambda^* + X$
1- Averaged Geometrical Acceptance for Φ Production	13.46 ± 2.5	17.4 ± 3.8
2- Averaged Correction for Loss in Detection of V^o Accompaning Φ Meson	2.47	1.49
3- V^o (K^o_s/Λ^*) Neutral Decay Mode	1.47	1.55
4- Other Decay Modes of Φ Meson	2.08	2.08
*5- All Other Correction Factors for Losses in Experimental Processes	5.98 ± .52	5.98 ± .52

* This Correction Factor E_5 is Defined as $(1/E_5 = \Pi_i e_i)$, where e_i are summarized in Table V-4.

TABLE VI-3

Estimated Cross-Sections for

ϕ Production Processes

$\pi^+ + P \longrightarrow \phi + K^0_S + X$	$\pi^+ + P \longrightarrow \phi + \Lambda^0 + X$
$1.43 \pm .92$ μb	$1.44 \pm .91$ μb

TABLE VI-4

Numerical Values Used in Estimation of the Cross-Section for Inclusive $\bar{K}^*$ Production

1- Number of $\bar{K}^{*o}$	953 ± 35
2- Number of π^+ Incident Beam	9.31249×10^7
3- π^+ Flux	2.28807×10^{32} events/cm^2
4- Correction Factors	$5.74 \pm .75$
5- Correction for Other Decay Modes of $\bar{K}^{*o}$	1.5
6- Inverse Sensitivity (mb/event)	37.62 ± 4.9 (nb/Event)
7- Averaged Geometrical Acceptance for $\bar{K}^{*o}$ Production	$31.1 \pm 2\%$
8- Estimated Cross-Section $X_f > .3$	115.29 ± 26.6 μb

Fig VI-1- Invariant Mass Distribution of (K⁻K+) Combinations

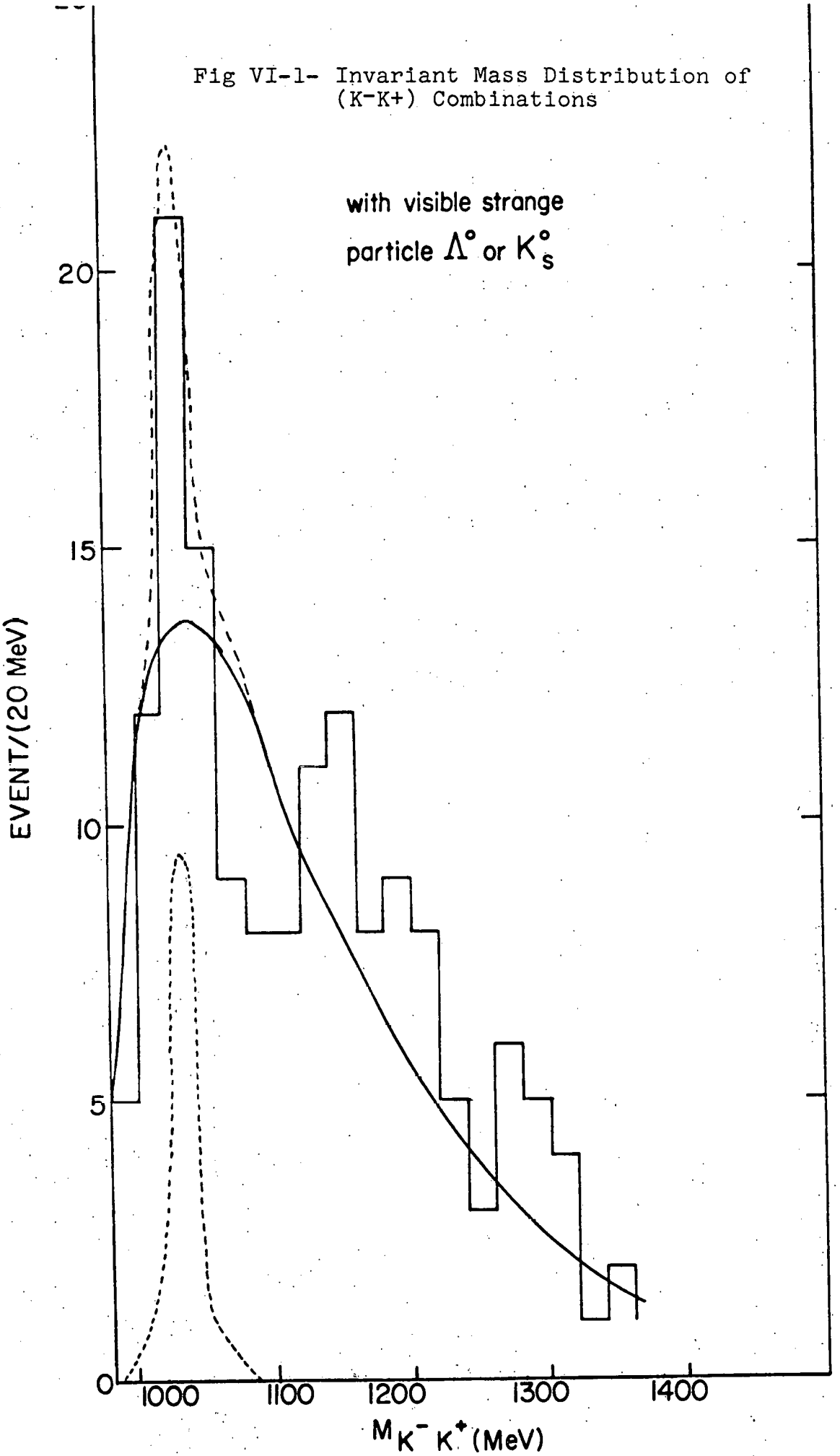

Fig VI-2- (K^-K^+) Invariant Mass Dist. for K°_S and Λ° Associated Events

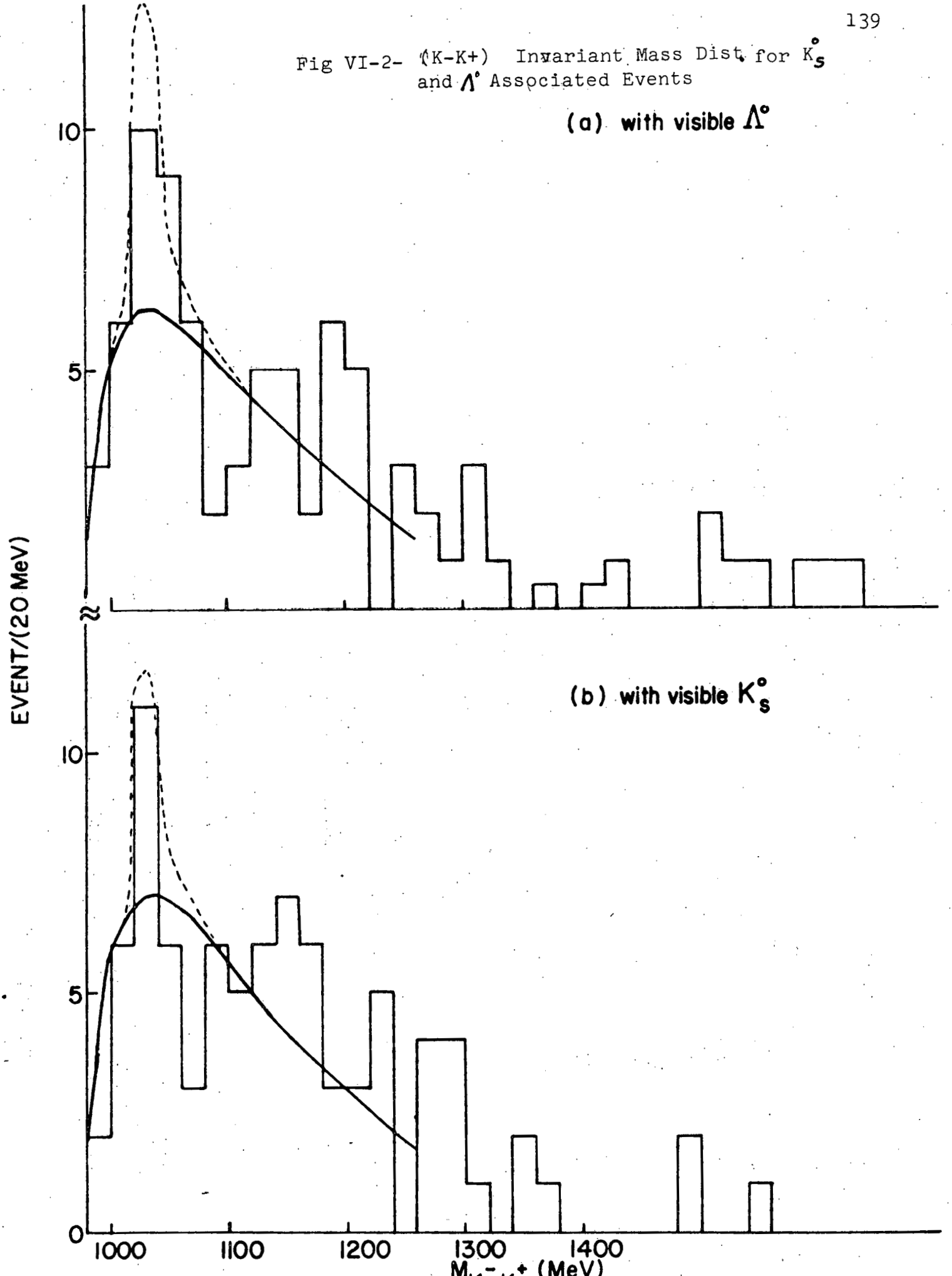

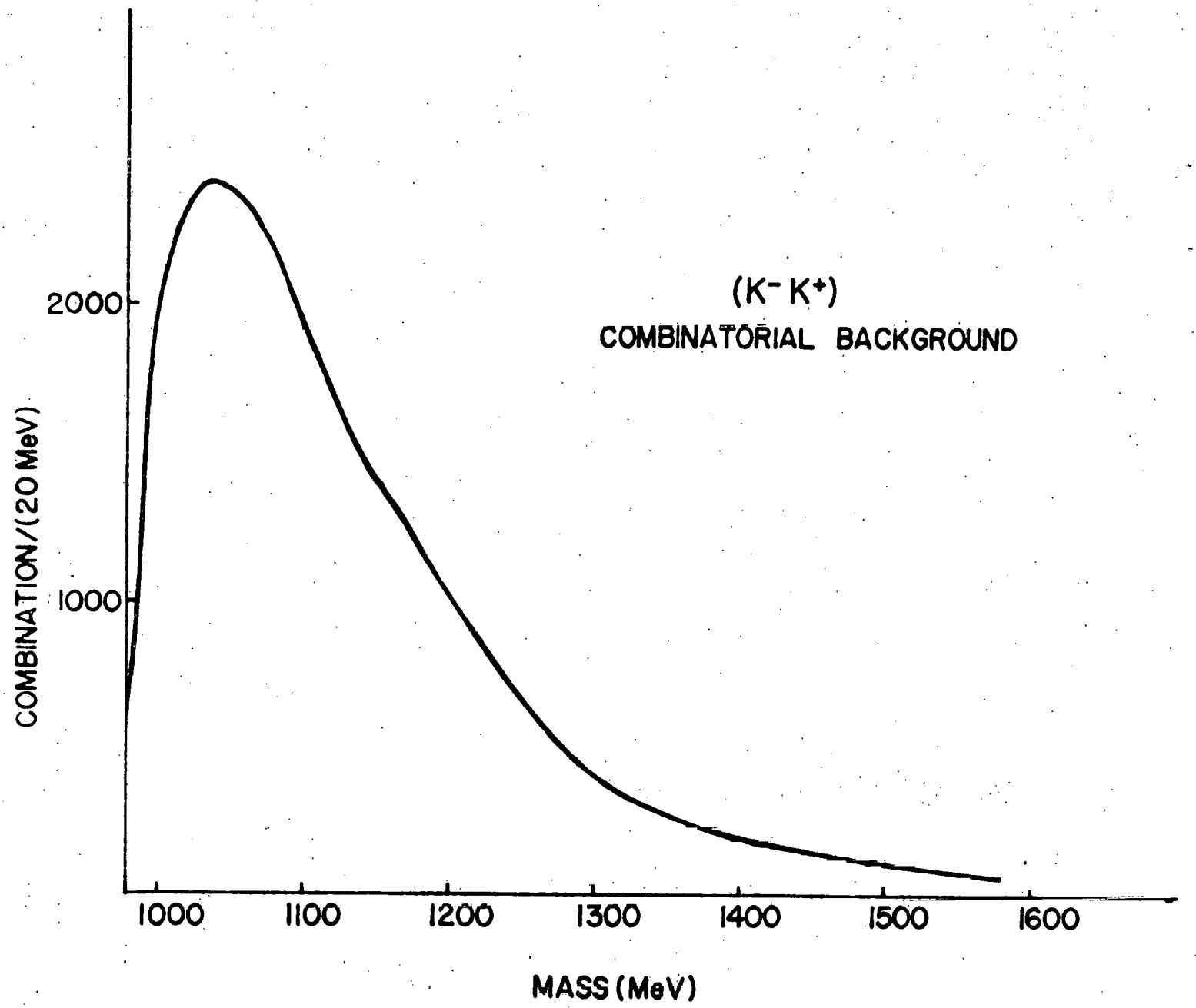

Fig. VI-3- (K-K+) Combinatorial Background

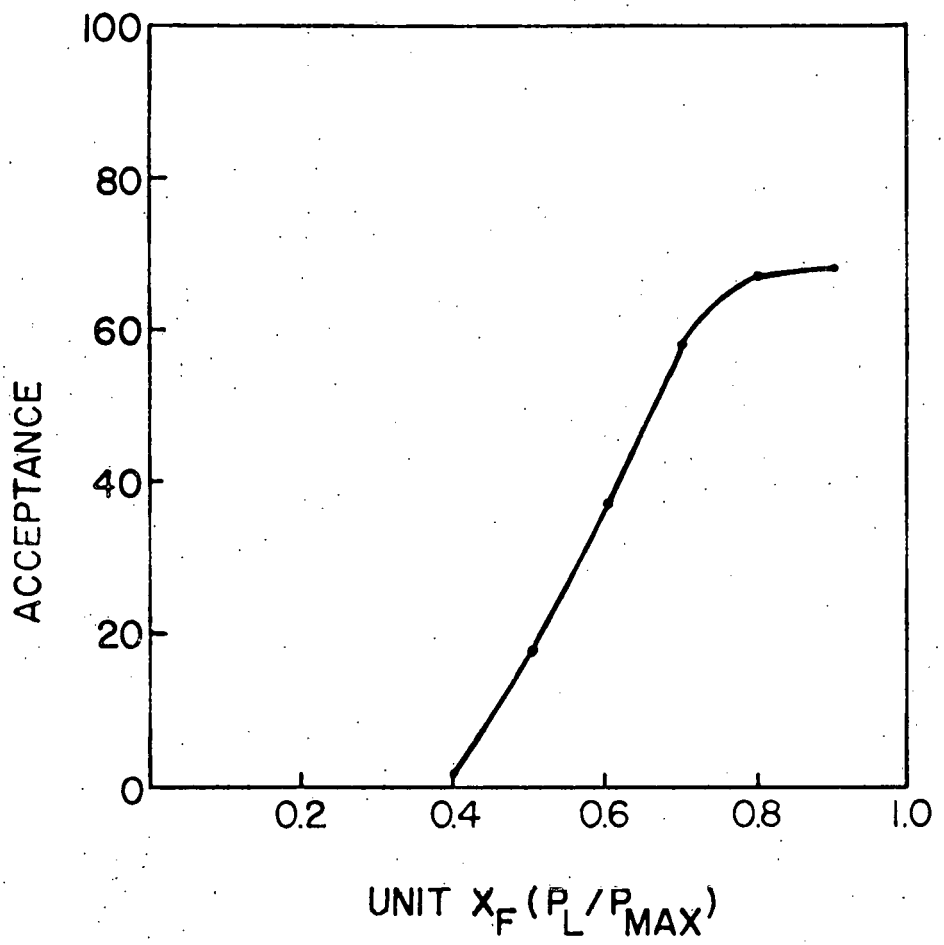

Fig VI-4- Dependence of Φ(1020) Acceptance on X_f

Fig VI-5- (K-K+) Invariant Mass Distribution for Inclusive Events

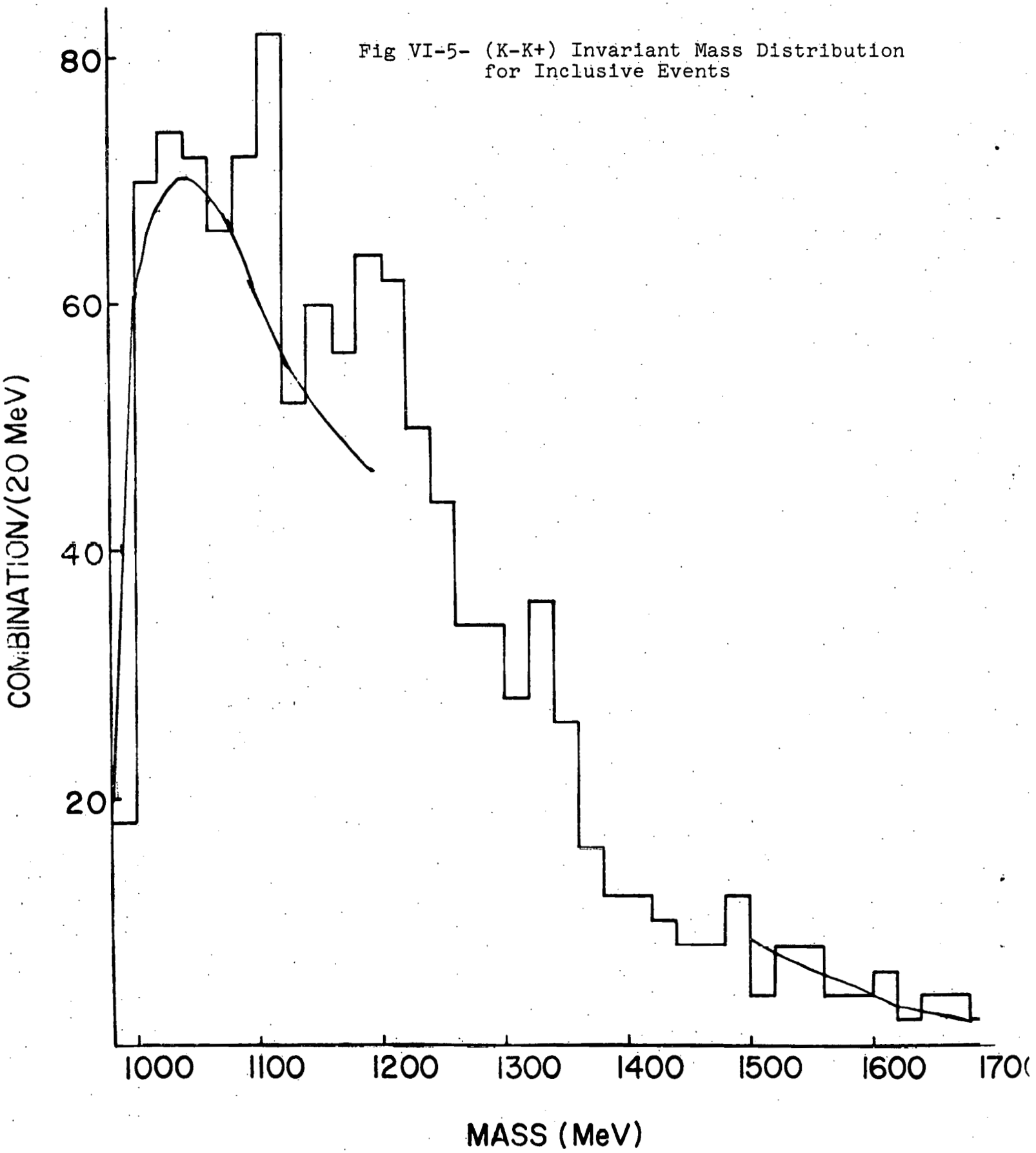

Fig. VI-6- ($K^-\pi^+$) Mass Distribution

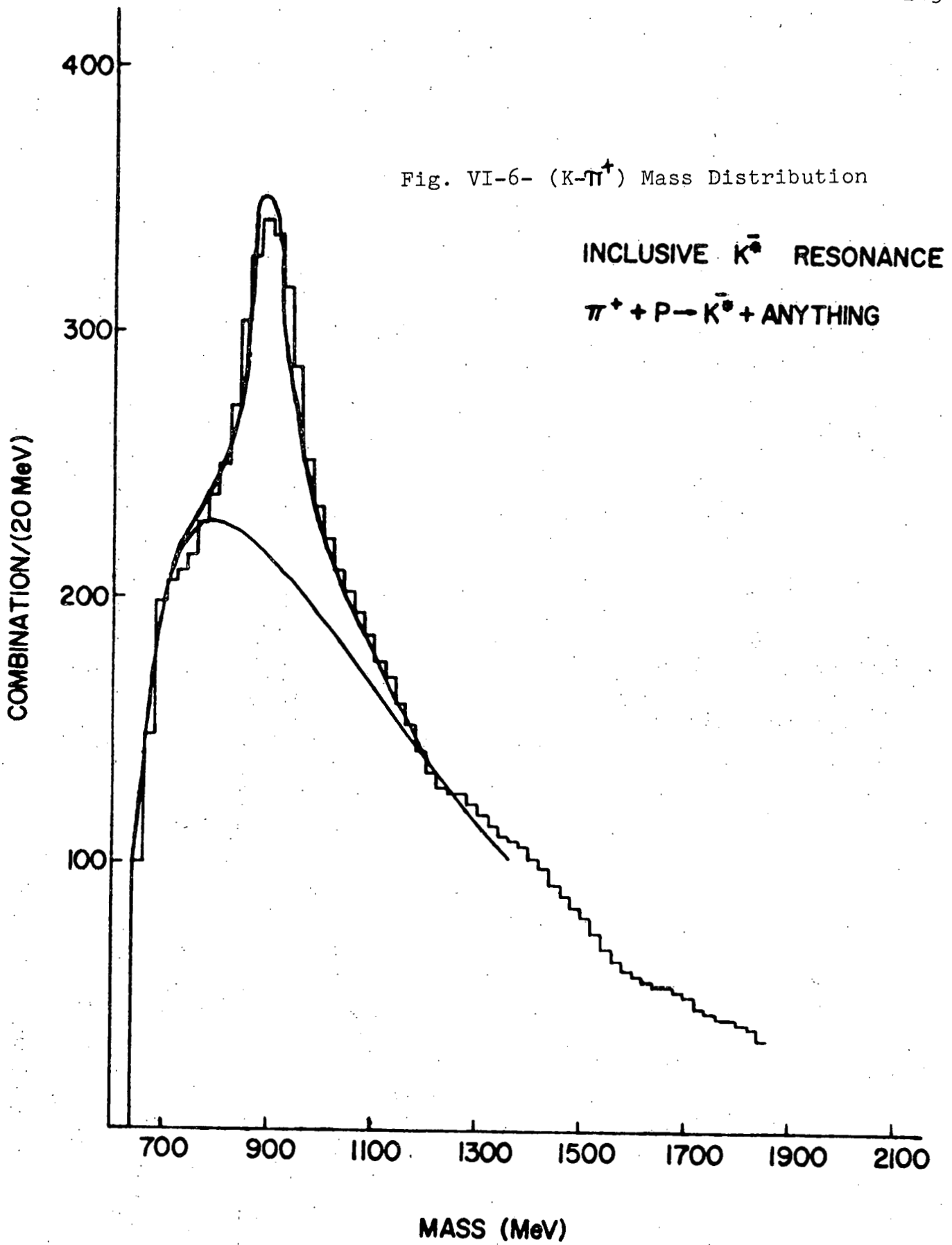

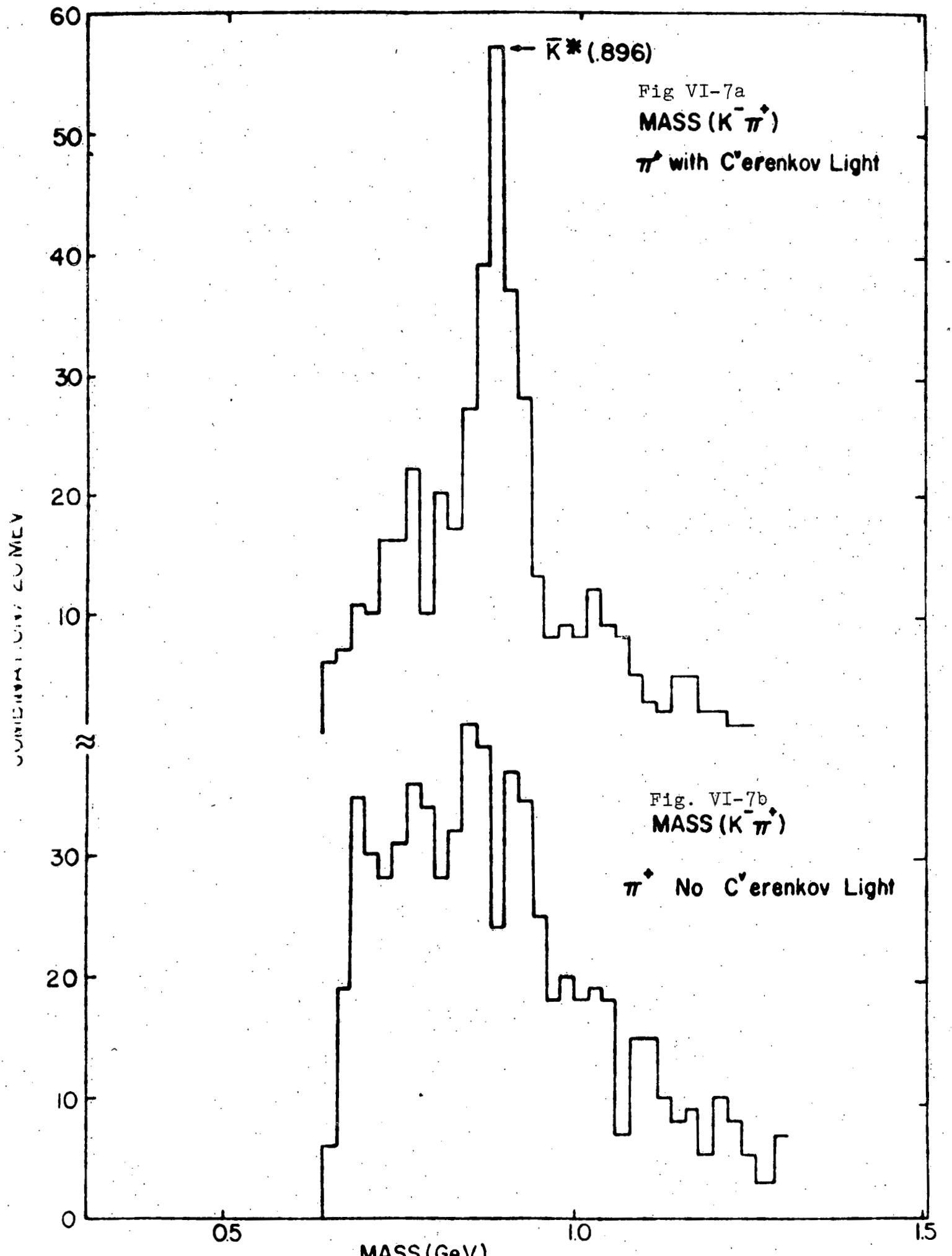
$\bar{K}^*$(.896)
Fig VI-7a
MASS ($K^-\pi^+$)
π^+ with Cerenkov Light
Fig. VI-7b
MASS ($K^-\pi^+$)
π^+ No Cerenkov Light
60
50
40
30
20
10
0
30
20
10
0.5
1.0
1.5
MASS (GeV)

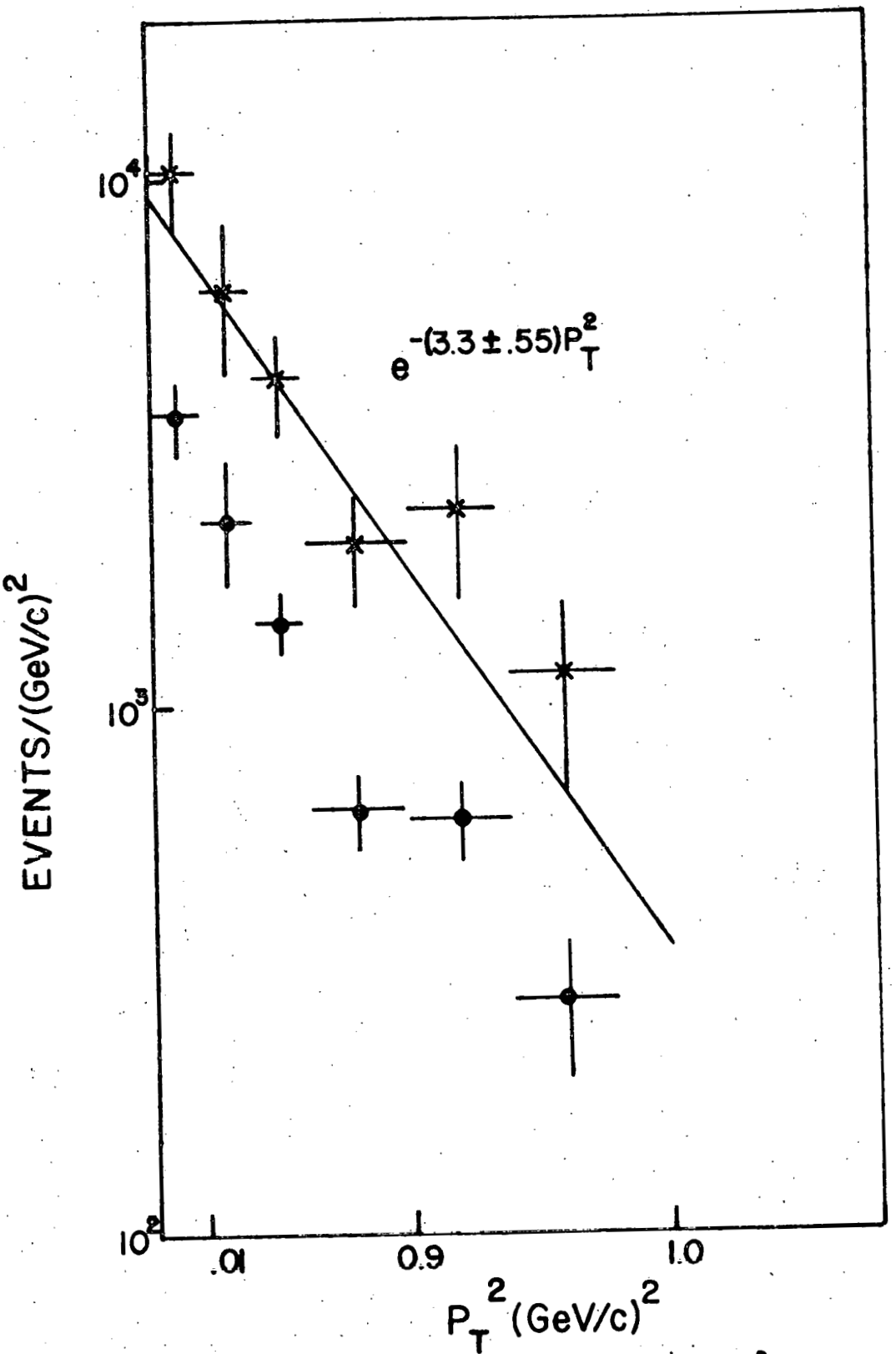

Fig. VI-8- P_T^2 Distribution for $\overline{K^{*0}}$

Fig. VI-9- X_f Distribution for $\bar{K}^{*0}$

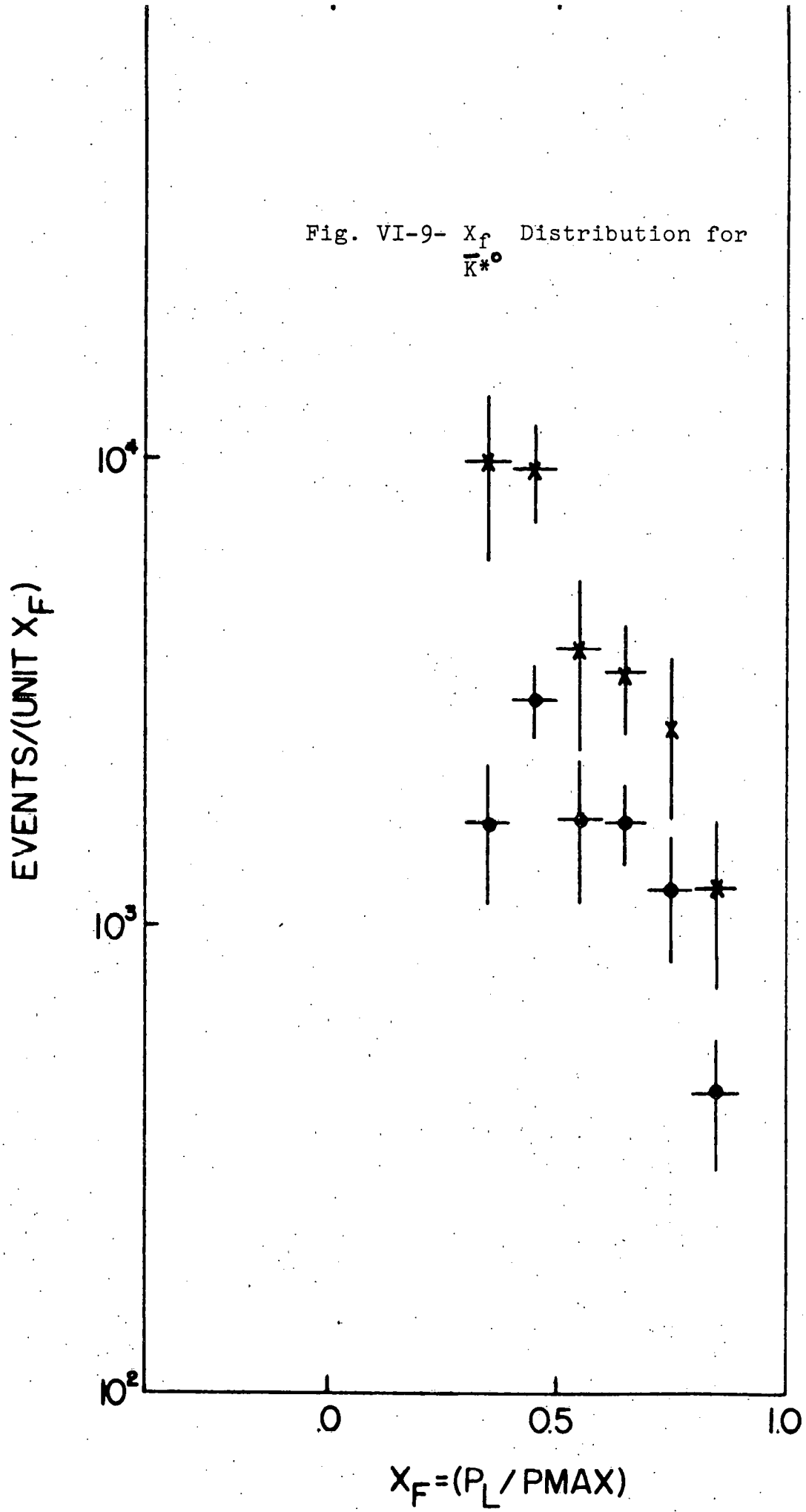

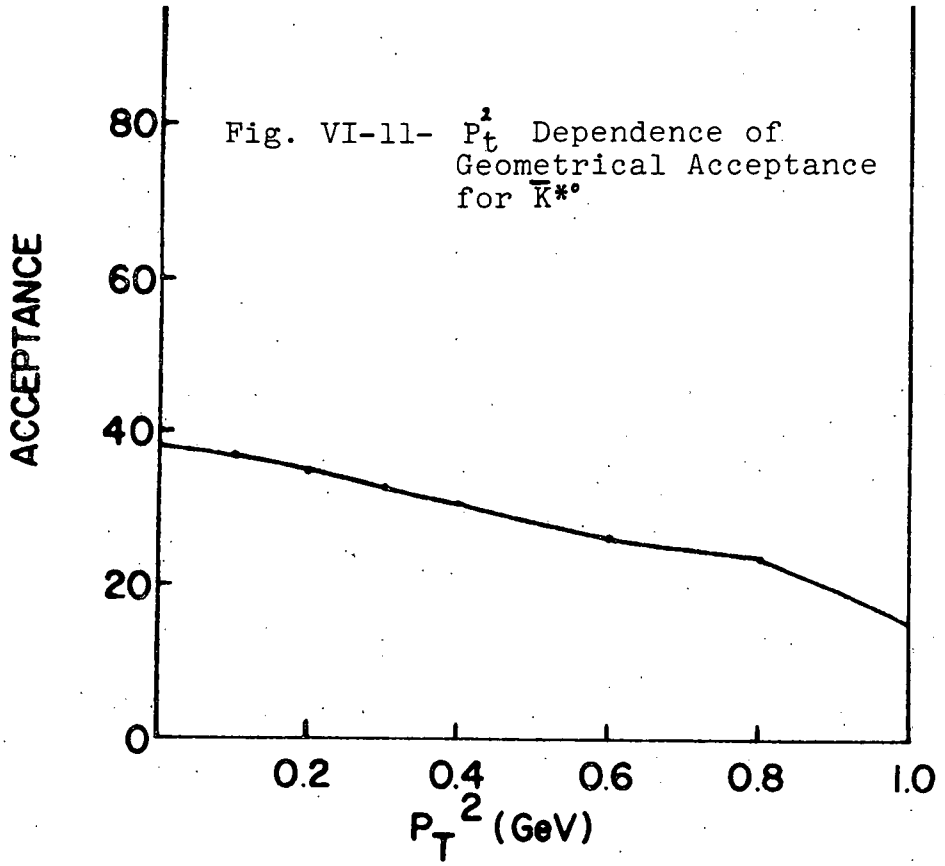

Fig. VI-11- P_t^2 Dependence of Geometrical Acceptance for $\bar{K}^{*\circ}$

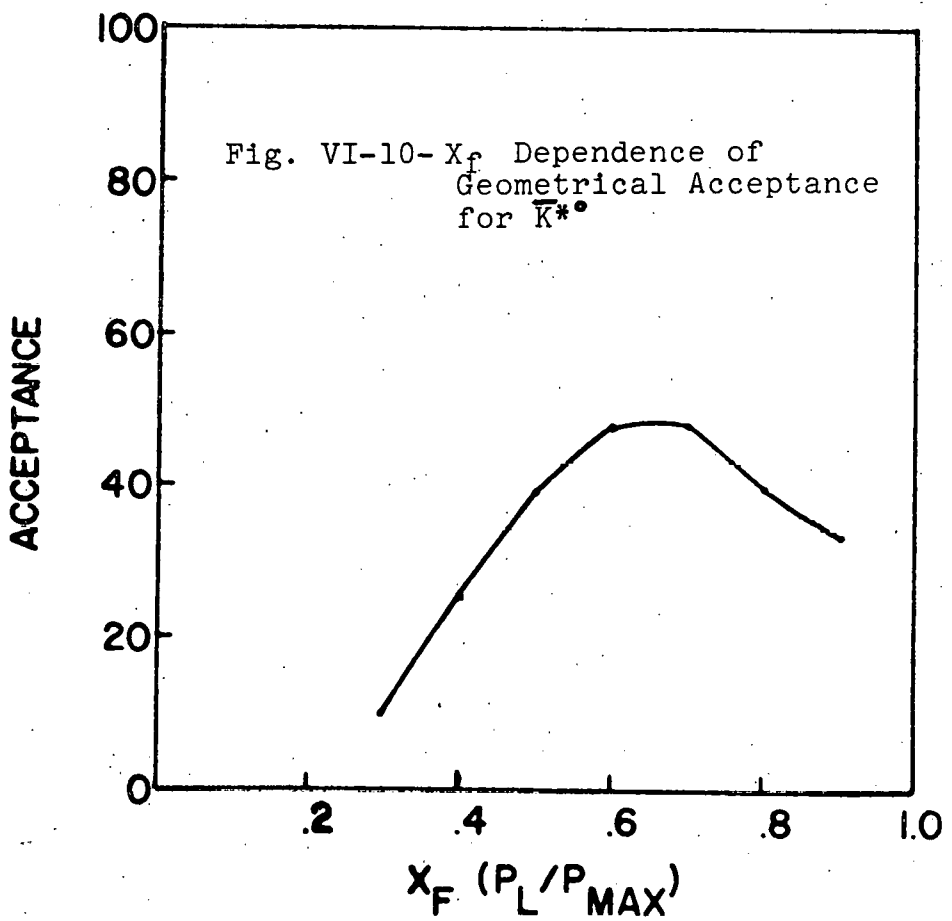

Fig. VI-10- X_f Dependence of Geometrical Acceptance for $\bar{K}^{*\circ}$

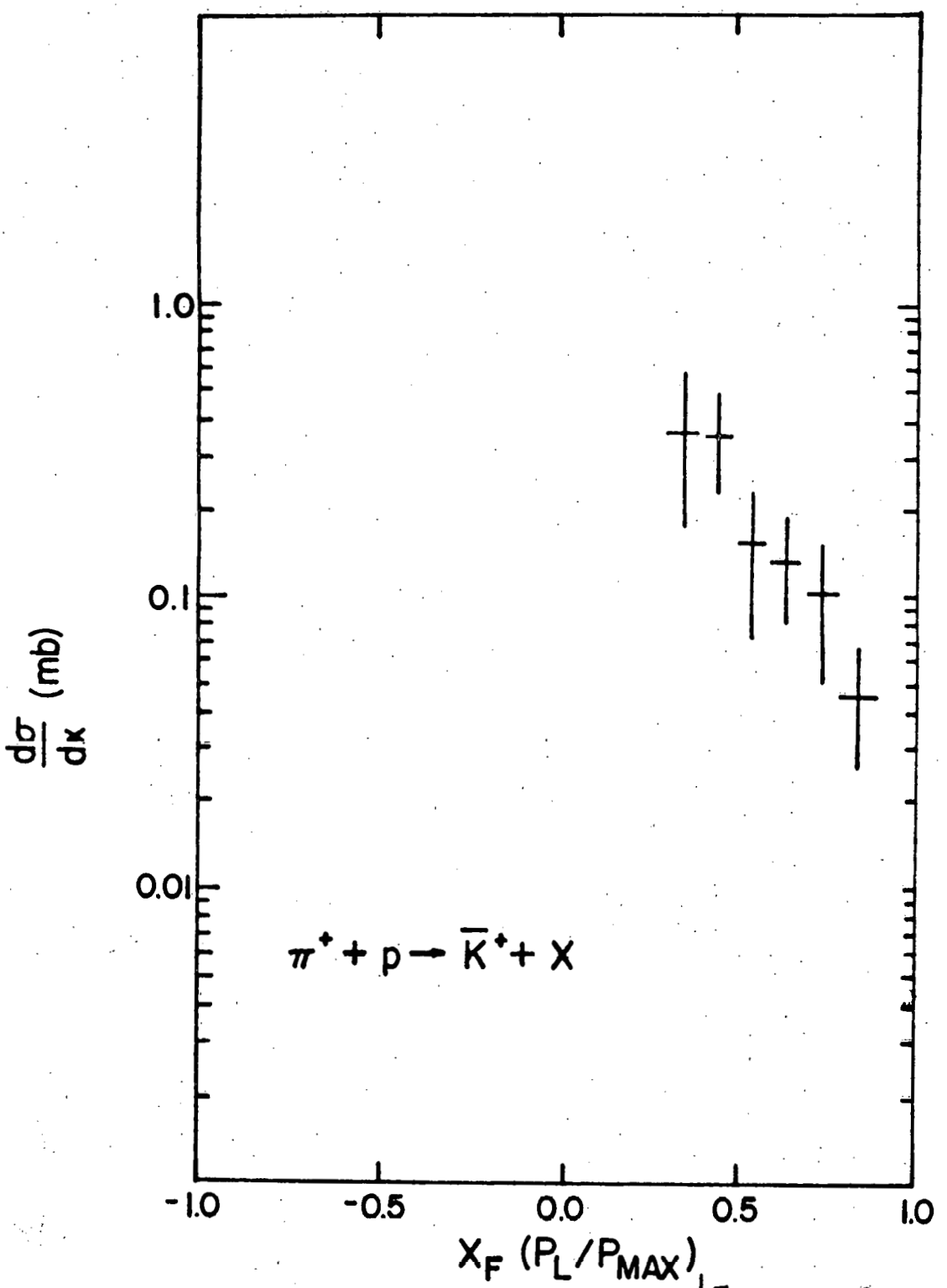

Fig. VI-12- Distribution of $\frac{d\sigma}{dx_F}$ for $\bar{K}^{*0}$ Production

CHAPTER VII- CONCLUSION

A- The OZI Rule

As described in Chapter-II, the main objective of this experiment was to investigate the validity of the OZI rule and determine the strength of the rule as it applies to Φ production processes.

A search was carried out for reactions of the type,

$$\pi^+ + P \longrightarrow \Phi + X \qquad \text{VII-1}$$

$$\pi^+ + P \longrightarrow \Phi + K_s^\circ + X \qquad \text{VII-2}$$

$$\pi^+ + P \longrightarrow \Phi + \Lambda^\circ + X \qquad \text{VII-3}$$

where VII-1 denotes the inclusive production of the Φ and VII-2 and VII-3 denote the conjoint production.

As described in Chapter VI no obvious Φ signal was seen in the inclusive reaction VII-1 (Fig. VI-5), however, clear Φ resonances were observed in the semi-inclusive reactions of VII-2 and VII-3 (see figs VI-1, 2 and tables VI-1, 3).

In order to estimate the contribution of the semi-inclusive channels (VII-2 and VII-3) to the inclusive production of the Φ-meson, possible conjoint processes involving an extra pair of ground state strange particles may arbitrarily be assumed to possess equal probability of

occurrence. Thus, if all high mass strange resonances decay strongly into stable kaons(K or $\bar{K}$) or hyperons(Λ or $\bar{\Sigma}$), then conjoint processes could be observed in reactions of the form,

$$\pi^+ + p \longrightarrow (K^+/K^\circ)\,\Phi\,(\bar{K}^\circ/K^-) \qquad \text{VII-4}$$

$$\pi^+ + p \longrightarrow (K^+/K^\circ)\,\Phi\,(\Sigma/\Lambda) \qquad \text{VII-5}$$

Table VII-1 shows the expansion of the reactions VII-4 and VII-5 and the contributions of the various subprocesses to the semi-inclusive channels of VII-2, 3. The assumption predicts that equal number of KOs and Λ will be produced, and that the total semi-inclusive rate will be,

$$(12/4)\left(\text{Number of } [\Phi K^\circ_s]\right) + (12/4)\left(\text{Number of } [\Phi\Lambda^\circ]\right)$$

The contribution of conjoint processes to the inclusive Φ production can then be estimated to be,

$N_{\Phi_{INC}}$ = Φ,s contributed to inclusive channel=$(12/8)N_{\Phi V^\circ}$

where

$$N_{\Phi V^\circ} = N_{\Phi\Lambda^\circ} \times W_{1\Lambda^\circ} \times W_{2\Lambda^\circ} + N_{\Phi K^\circ_s} \times W_{1K^\circ_s} \times W_{2K^\circ_s}$$

Here $W1K^\circ_s/\Lambda^\circ$ =(1.47/1.55)is the correction factor for neutral decay modes and $W2K^\circ_s/\Lambda^\circ$=(2.47/1.49) that for unobserved decays in the target and outside the streamer chamber.

Then, using $N_{\Phi\Lambda^\circ}$ =9 and $N_{\Phi K^\circ_s}$ =7, from Table VI-1, we calculate $N_{\Phi V^\circ}$ =46.2, the number of events in the entire run which produced a Φ-meson in association with a Λ° and a KOs. This number depends upon the analysis of the experimental data but not upon the assumption that the sub-processes in Table VII-1 are equally probable. Finally, we infer that the contribution of conjoint processes to the observed sample of inclusively produced Φ,s(VII-1) would be,

$$N_{\Phi_{INC}} = .08\,(12/8)\; N_{\Phi V^\circ} \sim 6 \text{ events}$$

where the factor 0.08 represents the fraction of the total data sample used in the present analysis of inclusive Φ production.

The observed spectrum of (K-K+) invariant mass for the inclusive data sample shows no statisticaly significant Φ signal above the background. Considering the number of events in the mass range of 1000<m(K-K+)<1060 MeV, and given the mass resolution estimated from the mass spectrum of VI-1 (17 MeV), a total of 72 background events is estimated to be in the Φ mass range. Using the statistical uncertainty in 72 events $\sim$ 8.5, an upper limit of 2σ =17 events, corresponding to a confidence level of 95 percent, is estimated for the number of Φ,s produced inclusively in the sample. The lower limit for the ratio $R=\sigma_{OZI}/\sigma_{Inclusive}$ would then be 6/17=.35 which means that at least 35 percent of the Φ,s are contributed by conjoint processes.(See Appendix D for a discussion on the effect of the K^+ contamination on conjoint production of Φ mesons.)

This result is also consistent with the recent results reported by ACCMOR collaboration on Φ production in $(\pi^-/P)P$ interactions at 63 and 93 GeV/c, which have set a lower limit of 40 percent for the contribution of conjoint processes to Φ production.

The substantial (35 percent from this work and 40 percent ACCMOR) contribution of conjoint processes to Φ production contradicts those theoretical models which predict that OZI violating processes such as gluon fusion and annihilation of light quarks(figs VII-2a, b) dominate the production of Φ-meson in hadronic interactions. It does however, rule in favor of quark fusion models which predict that the Φ-meson is produced as the result of fusion of s and $\bar{s}$ strange-quarks from the incident hadrons (Fig. VII-2c).

B-$\bar{K}^{*\circ}$ Production and Quark Fusion Models

Inclusive production of the $\bar{K}^{*\circ}(s\bar{d})$ has been studied. The transverse momentum distribution was fitted to an exponential function,

$$d\sigma/dPt = A\exp(-(3.3\pm.6)Pt^2)$$

The value of the exponential slope, $B=3.3\pm.6$ $(GeV/c)^{-2}$, is typical of other $\bar{K}^{*\circ}$ states produced in hadronic interactions[1,2]. Table VII-2 shows the value of B for several $\bar{K}^{*\circ}$ states from different experiments.

The longitudinal momentum distribution was studied in terms of the Feynmann variable Xf (Pl/Pmax). The spectrum covers the Xf range of Xf>.4, and declines sharply at high Xf(.8).

The spectrum is also compared with the predictions of a quark fusion model described in Chapter II (see Fig. VII-1). As can be seen in Fig. VII-1, the model has reproduced the shape of the experimentally observed distribution. A magnitude comparison of the spectrum with the prediction of the model also shows agreement consistent with experimental normalization uncertainty. The χ^2 for the fit is determined to be 5.8 for 6 degree of freedom.

The Xf distribution for K*+ production in $\pi^+ P$ interaction at 16 GeV/c shows a peak in the forward region (see Fig. II-4), which is clearly not the case in that of the $\overline{K}^{*\circ}$ observed from this present work. Considering that the production of K*+ involves also contributions from fusion of valence quarks in the proton (u) with sea quarks in pion($V^{\rho}\,S^{\pi}$) in addition to the terms involved in production of K* ($V^{\pi}P^{s}$+SS), the forward peak may be attributed mainly to the valence quarks of the proton.

C- Critique and Recomendation for Further Analysis

As was clearly demonstrated in previous sections the major difficulty in determination of the ratio ($R=\sigma OZI/\sigma$ inclusive) was the measurement of the inclusive cross-section for Φ production. Mass resolution comparable

to the natural resonance width ($\Gamma = 4$ MeV) was not possible because of the large uncertainties in hidden vertex determination. The results on $\bar{K}^{*\circ}$ production also involve large uncertainties reflecting the statistical errors and uncertainties in scanning, measuring, processing and vertex finding efficiencies. However, the continuation of the experimental analysis and the complete measurement of the remaining 90 percent of the inclusive data will provide a better determination of correction factors as well as a more significant (10 fold larger) data sample for the study of $\bar{K}^{*\circ}$ production. With the complete measurement of the data it may be also possible to reconstruct, using APACHE, the VO decays hidden in the target volume which were not detected in the V scan performed for the present analysis. This could yield an estimated 15 additional Φ,s produced in association with KOs or Λ°. Investigation of Φ production accompanied by charged kaons would also be possible using complete measurement of the film. It would then be possible to have a better determination of the Φ cross-sections in conjoint processes.

D- Critique of Experimental Procedure and Recomendation for Improvement

The analysis of the data for this experiment showed that the invisibility of the interaction vertices constituted the major difficulty in the analysis of photographed interactions in the streamer chamber. It was not found possible to resolve multiple interactions visually

in the scanning and measuring process. For a large portion of the data (~33 percent) the final result from the vertex reconstruction program, APACHE consisted of more than one solution (event vertex). Thus the task of selection of these events was based on rather arbitrary requirements imposed on APACHE fits and event charge balance. The uncertainty in determination of the primary vertex location resulted in a poor mass resolution which was not sufficient for an accurate study of inclusive production of the Φ meson. However a different arrangement of the experimental setup and operating conditions could have helped in resolving the multiple interactions. A lower beam rate($8\pi^+$/burst in this work) could reduce the fraction of the data containing multiple interactions. The information from beam PWC's could then have been used to determine the coordinates of the beam upstream of the streamer chamber and thus add an additional constraint to the vertex finding process in APACHE. The original plan of the experiment included two planes of spark chambers located behind the K+ Cerenkov counter and the recorded information from them were to be used later to identify (before scanning) those events which contained a forward positive particle hitting the chambers without producing light in the Cerenkov detector(Ck+). Such information would reduce the size of the data sample scanned for inclusive production of Φ-meson, requiring two forward kaon(K- and K+). The spark chambers were excluded from the experiment because of their inefficiency.

REFERENCES

1- K.Bockmann et al., CERN/EP 79-131

2- C.Evangelista et al., Phys. Lett., 70B(1977)373

3- C.Daum, et al, Phys. Lett. 98B. 313(1980)

4- See Reference 18, Chapter II.

TABLE VII-1

Contribution of Various Subprocesses to

Inclusive Channels ΦK_s^o and $\Phi \Lambda^o$

Conjoint Subprocess	Semi-Inclusive $\Phi \Lambda^o$	Semi-Inclusive ΦK_s^o
$\bar{K}^o \Phi K^o$	0	$\frac{1}{2}(\Phi K^o) + \frac{1}{2}(\Phi \bar{K}^o)$
$k^- \Phi K^o$	0	$\frac{1}{2}$
$k^+ \Phi \bar{K}^o$	0	$\frac{1}{2}$
$k^- \Phi K$	0	0
$k^+ \Phi \Lambda$	1	0
$k^+ \Phi \Sigma^+$	0	0
$k^+ \Phi \Sigma^-$	0	0
$k^+ \Phi \Sigma^o$	1	0
$k^o \Phi \Sigma^+$	0	$\frac{1}{2}$
$k^o \Phi \Sigma^-$	0	$\frac{1}{2}$
$k^o \Phi \Sigma^o$	1	$\frac{1}{2}$
$K^o \Phi \Lambda$	1	$\frac{1}{2}$
12	4	4

TABLE VII-2

Values of the Parameter B Obtained from the Fit to

$$\frac{d\sigma}{dP_t^2} = Ae^{-BPt^2}$$ to the K^* P_t^2 Distributions in Hadronic Interactions

Reaction	P_{Lab} (GeV/c)	P_t^2 Slope B $(GeV/c)^2$	Reference
$PP \rightarrow K^{*+} + X$	12	$3.6 \pm .4$	1
$PP \rightarrow K^{*+} + X$	24	$3.2 \pm .3$	1
$PP \rightarrow K^{*-} + X$	24	$3.3 \pm .5$	1
$\pi^+P \rightarrow K^{*+} + X$	16	$3.1 \pm .2$	1
$\pi^+P \rightarrow K^{*-} + X$	16	$3.8 \pm .5$	1
$\pi^-P \rightarrow \bar{K}^{*0} + X$	16	$2.82 \pm .17$	2
$\pi^+P \rightarrow \bar{K}^{*0} + X$	16	$3.3 \pm .6$	(This Work)

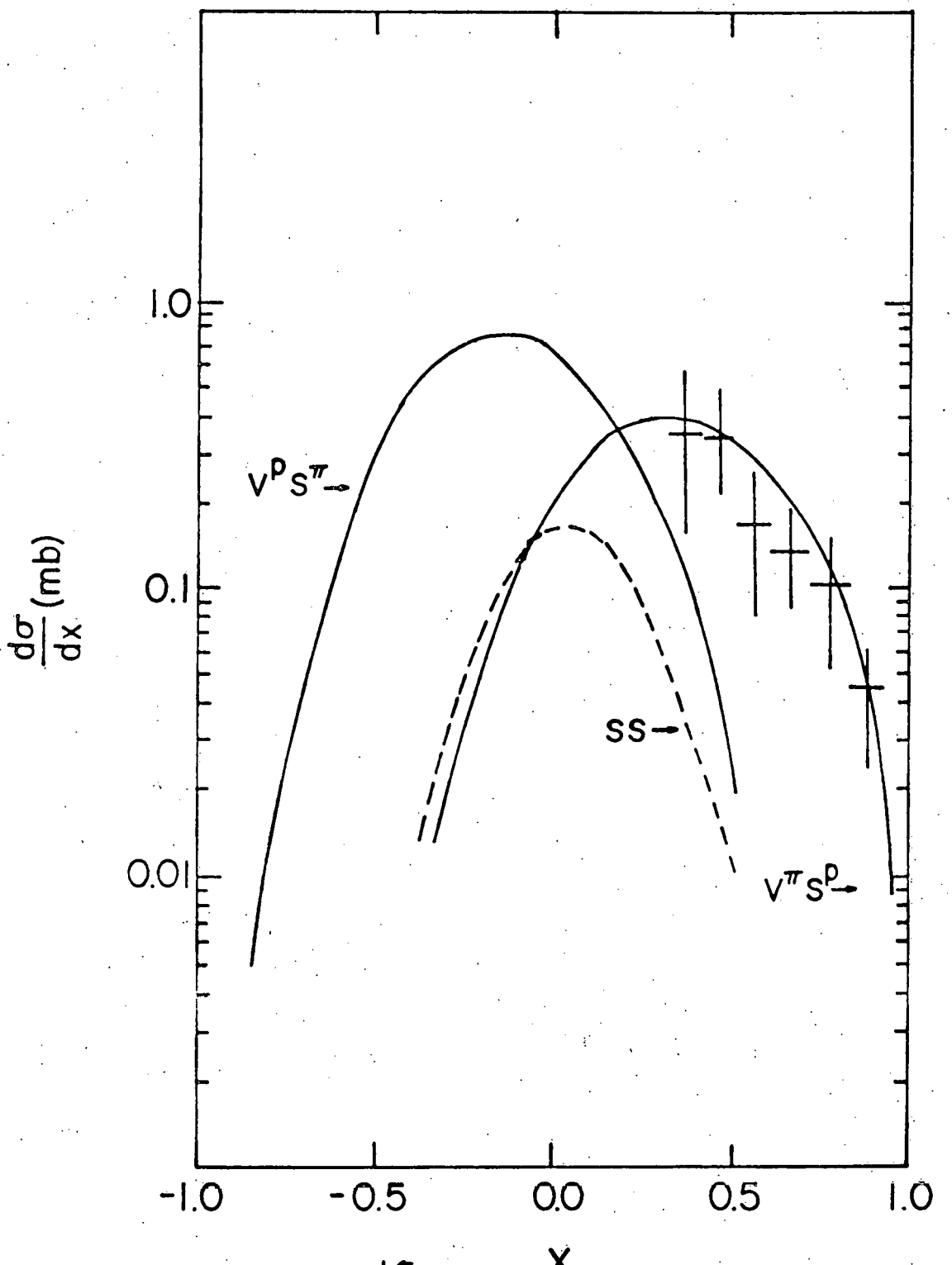

Fig. VII-1- $\frac{d\sigma}{dx_F}$ Distribution for $\bar{K}^{*\circ}$, compared with Predictions of Quark Fusion Models[4]

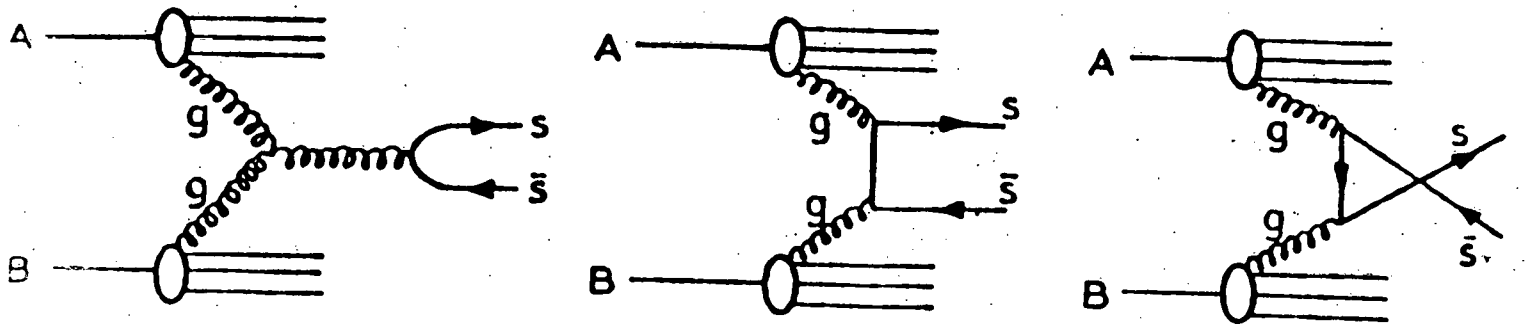

Fig. VII-2a
Gluon Fusion

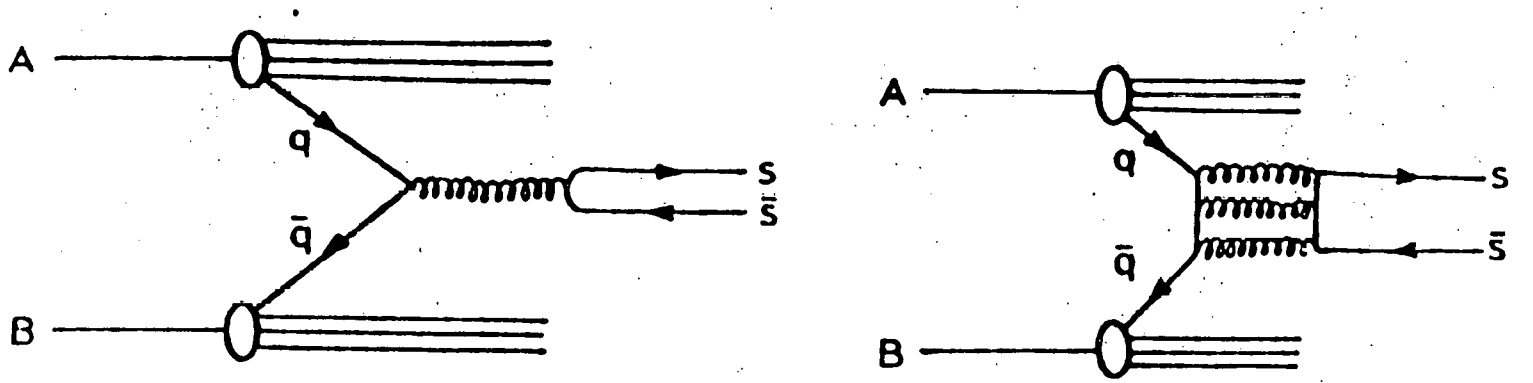

Fig. VII-2b
Light Quark annihilation

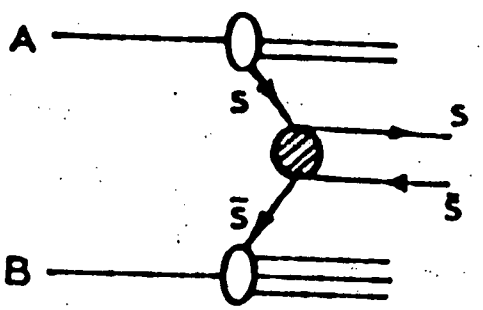

Fig. VII-2c
Strange Quark fusion

APPENDIX A- PERFORMANCE CHARACTERISTICS OF ČERENKOV COUNTERS

During a test run period, a 9 GeV/c π^- beam was used to measure the efficiency of each of the twenty Cerenkov cells with an atmospheric-pressure isobutane filling. At each of the four crossing points on an imaginary 3x3 grid that divided the useful area of a mirror surface into nine equal sectors, the probability that a Cerenkov signal from a beam particle traversing the Cerenkov counter was measured by the ratio,

$$\pi^-.C.S_6 \,/\, \pi^-.S_6 ,$$

where π^- was a logic signal for a 9 GeV/c π^- entering the streamer chamber. The counter S6 was a 1"x1" square scintillation counter of 1/4" thickness placed downstream from the Cerenkov counter. The signal ($\pi^-.S$), therefore, defined a π^- particle traversing the Cerenkov counter. This measurement was taken at a beam rate of less than one π^- per 1.5 μs beam spill. Even so account had to be taken of the long decay time of RCA 4522 Cerenkov phototube pulses in order to obtain the efficiency measurement to the high precision desired. Hence a veto circuit was used so as to ignore beam π^- occuring within 300 ns of another beam particle. The efficiency ranged from 98.8 percent to 100.0 percent for the eighty points measured. These results were combined for each mirror and are tabulated in Table A.1.

Averaged over the ten cells in each of the two Cerenkov counters, the overall efficiencies were 99.848 $\pm$.006 percent and 99.717 $\pm$.008 percent for the K- and K+ Cerenkov counters respectively.

TABLE A-1

Pion Rejection Efficiency

(9 GeV/c π^-)

Cell No.	K^- Čerenkov Counter	K^+ Čerenkov Counter
Upper 1	99.78 ± .02%	99.57 ± .03%
2	99.82 ± .02	99.62 ± .03
3	99.89 ± .02	99.75 ± .03
4	99.84 ± .02	99.42 ± .04
5	99.84 ± .02	99.83 ± .02
Lower 1	99.85 ± .02	99.74 ± .02
2	99.80 ± .02	99.78 ± .02
3	99.88 ± .01	99.87 ± .02
4	99.88 ± .02	99.89 ± .01
5	99.88 ± .02	99.78 ± .02
Average	99.848 ± .006%	99.717 ± .008%

APPENDIX B- APACHE VERTEX RECONSTRUCTION

1- The Vertex Finding :

The process of finding the best vertex of a given set of tracks for which track parameters (beginning coordinate, end coordinate, azimuth, dip, slope and error matrices) were known, was as follows:

a) Given the coordinates of the beginning point $\vec{X}k$ of tracks and those of a trial vertex, $\vec{X}v$, (initialy taken to be at the center of the target), then swim each track by the distance,

$$S=(\vec{X}v-\vec{X}k).\ (d\vec{X}k/ds),$$

where $d\vec{X}k/ds$ is the tangent to the track at the point $\vec{X}k$. This process is repeated until it converges to a track point which is the point of closest approach of that track to the trial vertex($\vec{X}v$). All other tracks are similarly extrapolated to find the point on them closest to $\vec{X}v$.

b) Form a χ^2 in terms of an adjustable point $\vec{X}$, as

$$\chi^2 = \sum_{i=1}^{n} (\vec{X}_i - \vec{X}_v)\, \Delta_i\, (\vec{X}_i - \vec{X}_v)$$

Where Δ_i is the inverse error matrix. Minimizing χ^2 gives a point $\vec{X}$ which is taken as an improved trial vertex, $\vec{X}v$.

c) Given this new trial vertex, steps (a) and (b) are repeated until the process converges. Convergence is defined by successive iterations in which no track changes in length by more than .1 mm in space. The χ^2 for this fit is then used as described in section B of the chapter V.

2- Correction of Track Parameters at the Vertex

Given the best fit vertex, a simple method is used to correct the track parameters to it. To simplify the calculation, it is assumed that the dip angle is uncorrelated with parameters in the X-Y plane. The basic mathematical procedure of the correction can be summarized in the following steps:

a) Coloumb Scattering

Track parameters are corrected for multiple Coloumb scattering in the target and target walls.

b) Dip angle

First the track is extrapolated from the beginning point to the vertex. It misses the vertex by Δz, then a correction of Δt is desired to correct the dip angle. Then a χ^2 defined as,

$$\chi^2 = \frac{(z-z_b)^2}{(\delta z)^2} + \frac{(\Delta t)^2}{(\delta t)^2} = \frac{(\Delta z - \Delta t\, s_1)^2}{(\delta z)^2} + \frac{(\Delta t)^2}{(\delta t)^2}$$

is minimized to determine the value of Δt. Here Zb is the normal to X-Y plane coordinate of the beginning point, t=tan(dip), δz and δt are uncorrelated errors for t and z corrected for coloumb scathering.

c) Azimuth and K(projected curvature) Correction

The recalculation of these TVGP parameters is done using a three point fit in the X-Y plane to a circle. The points used are the TVGP calculated beginning and end points and the APACHE fitted vertex.

The fit to the circle would be correct if the magnetic field was uniform. To account for the non-uniform magnetic field of the streamer chamber, the average TVGP calculated momentum of the track is used to extrapolate the track from the vertex to its beginnig and to its end point. The deflections in space from the TVGP points are found and subsequently are corrected for these deflections. Finally, the fit to the circle is made to the corrected beginning and end points and to the vertex.

APPENDIX C- DEPENDENCE OF APACHE χ^2 ON MEASUREMENT UNCERTAINTY (FRMS)

To study the dependence of the APACHE χ^2_ν on FRMS of the events, a sample of four prong events was selected from which were excluded events containing "halo" tracks(positive charge with momentum more than 10 GeV/c). All of these events were then processed through APACHE. Plots of χ^2_ν versus average total FRMS were made and a clear dependence of χ^2 upon FRMS was observed. χ^2_ν was then normalized to the actual measurement uncertainty for n tracks by a factor Fscale defined as

$$\text{Fscale}=\left(\sum(\text{FRMS})^2/16n\right)$$

Comparison of the histograms before and after normalization for different intervals of <(FRMS)> showed that the χ^2 distributions (figs. C-1a,d) before normalization tend broaden as <FRMS> increases. However, figs C-2a,d show that scaled χ^2 distributions after normalization are similar. This confirms that the scaled χ^2 can be used as a general variable to test the goodness of the APACHE vertex fits.

The Di-plot of Fig. C-3 shows the over-all dependence of χ^2 on $\langle(\text{FRMS})^2\rangle$. The superimposed line shows a linear dependence which is the basis of the definition of Fscale, above.

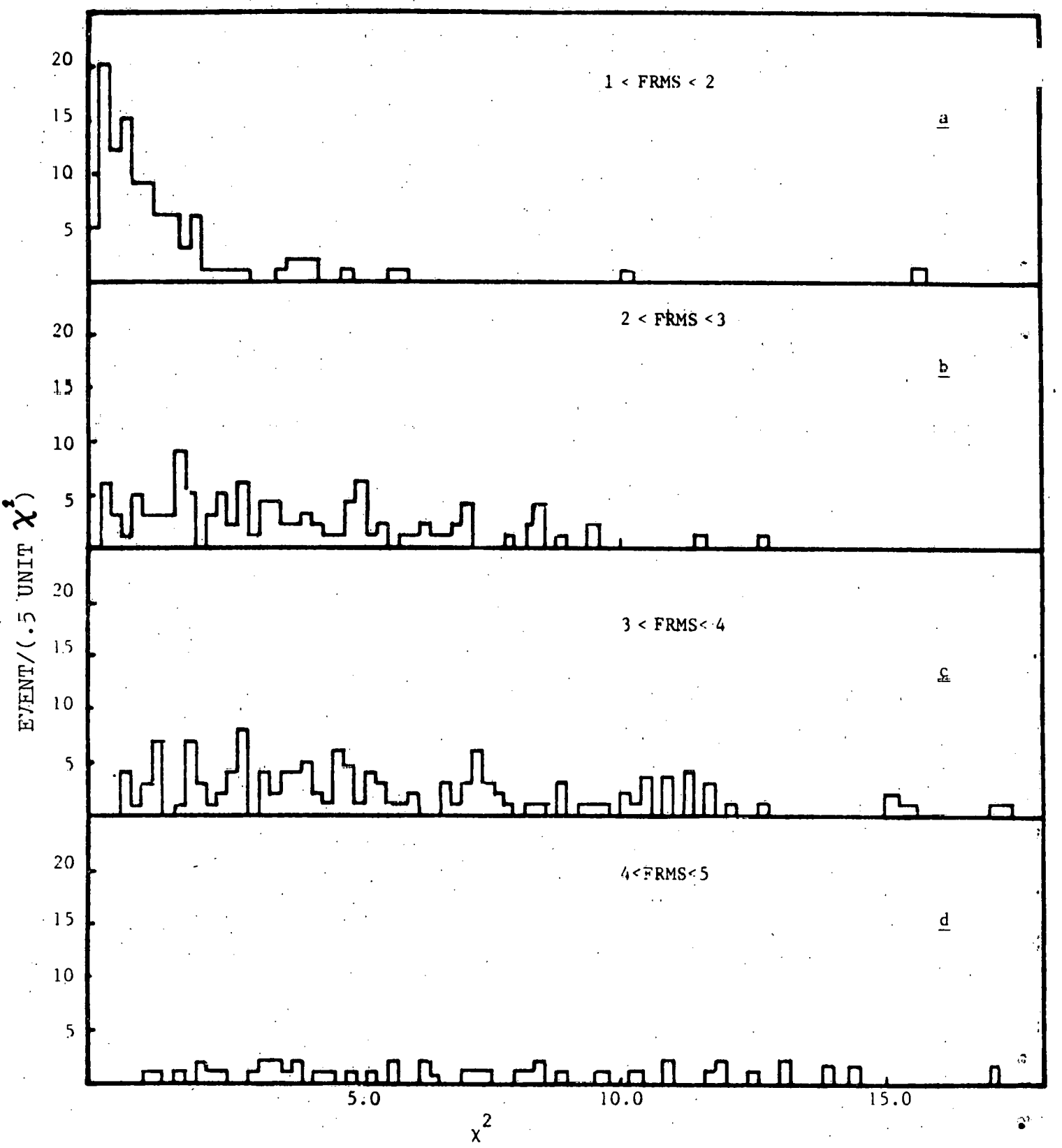

Fig. C-1- Distribution of APACHE X^2 for four ranges of average FRMS

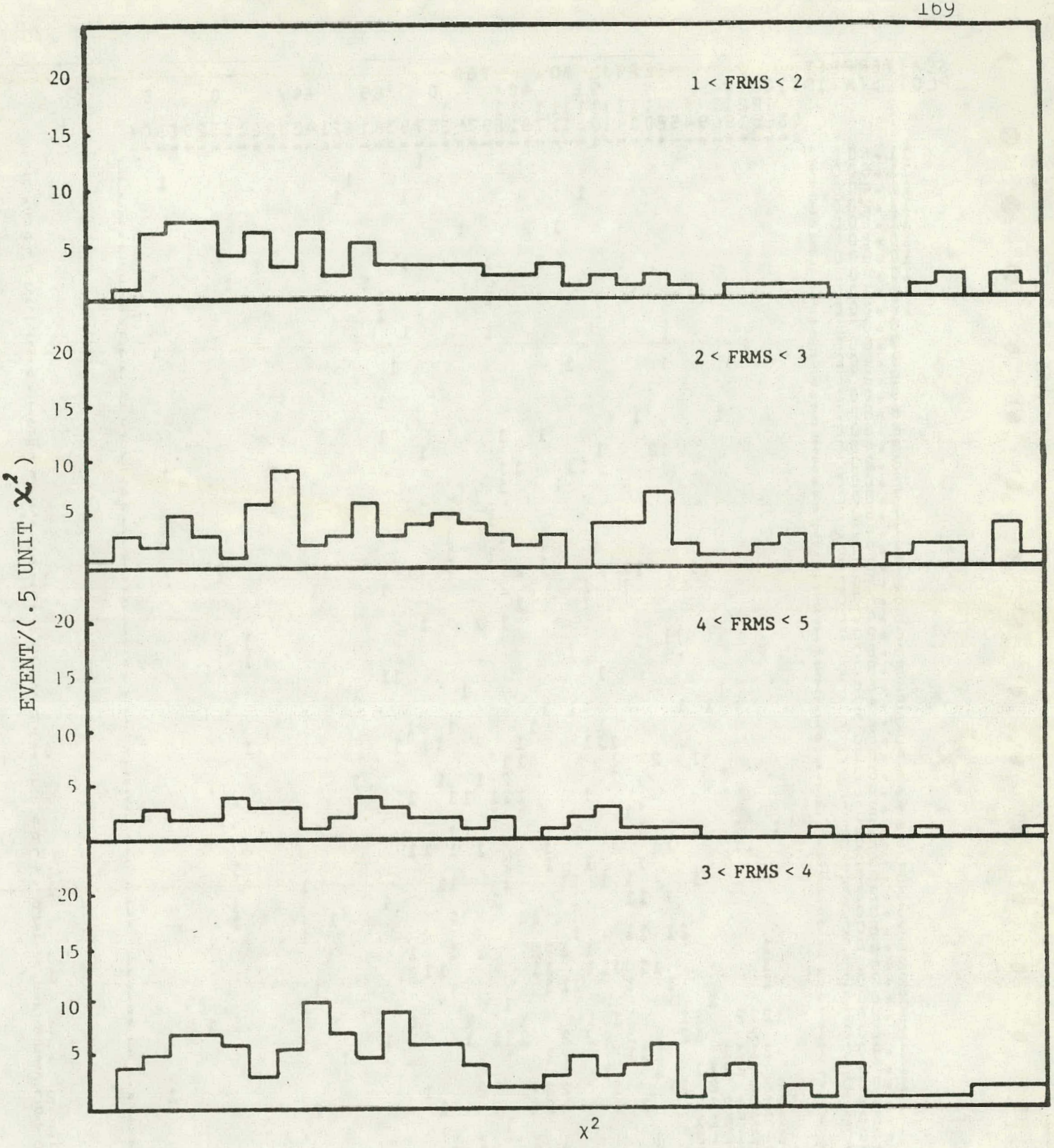

Fig. C-2- Distribution of APACHE χ^2 after scaling for four region of FRMS

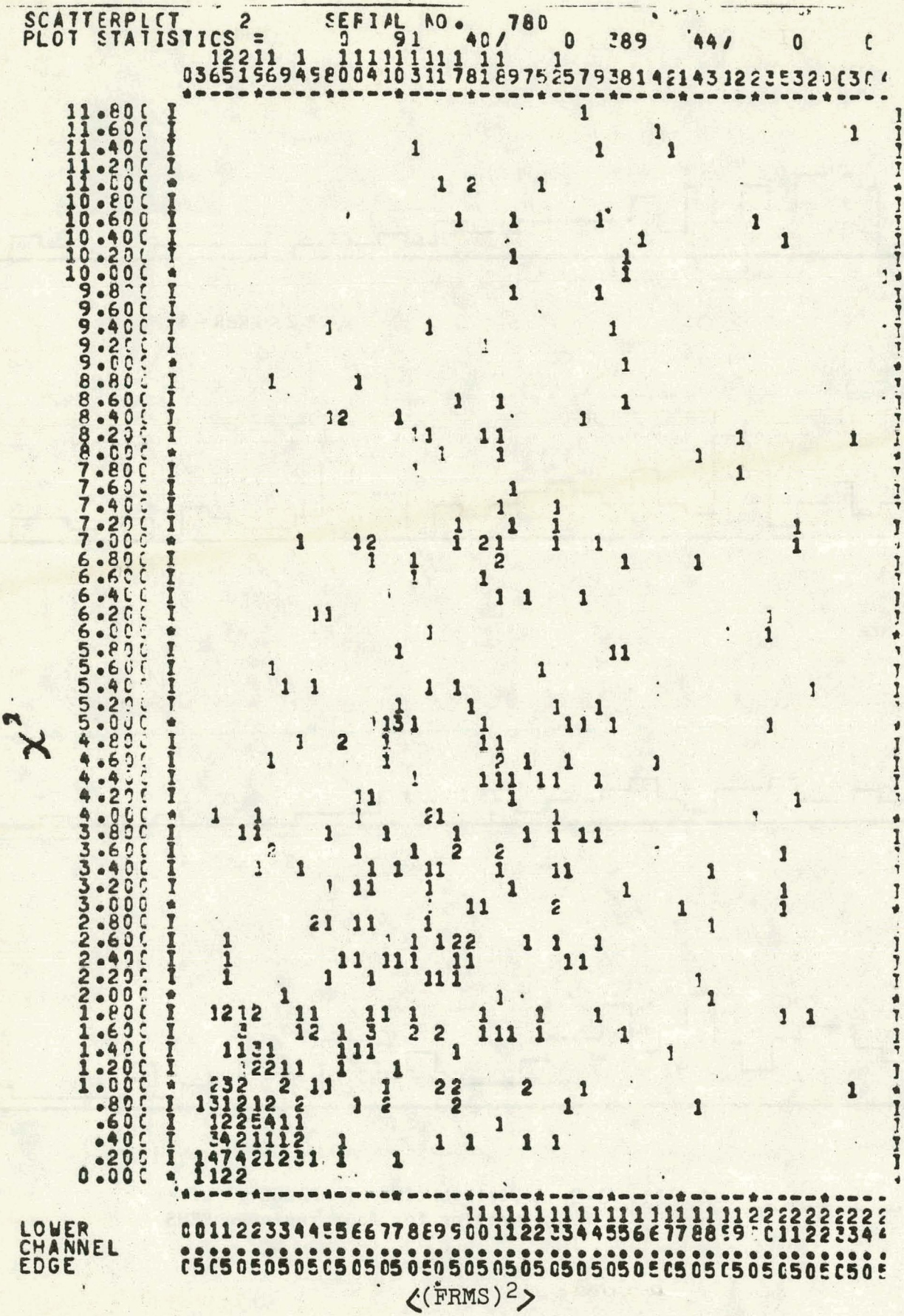

Fig. C-3 Scatter Plot of APACHE χ^2 versus $\langle(\dot{F}RMS)^2\rangle$

APPENDIX D- EFFECT OF K^+ CONTAMINATION IN THE INCIDENT BEAM ON THE RATIO R= $\sigma_{OZI}/\sigma_{\Phi INC}$

(See Section VII-A)

The lower-limit for R= $\sigma_{OZI}/\sigma_{\Phi INC}$ was estimated to be .35 using the measured cross-sections for reactions VII-1 and VII-2 and an upper-limit estimated for the inclusive cross-section. It can however, be argued that the contaminating K^+ mesons, which accounted for 1.1 percent of the incident beam particles, might have been responsible partly (or even entirely) for the production of (ΦK^0_S)'s.(It should be noted that strangeness conservation does not favor production of $\Phi\Lambda^0$ in K^+P interactions). Thus the cross-section for conjoint production of Φ in π^+P interactions would be reduced to .5 σ_{OZI}. From the existing experimental data on Φ production in K^+P and π^+P interactions[1] at 16 GeV/c, the ratio

$$\frac{\sigma(K^+P \rightarrow \Phi + X)}{\sigma(\pi^+P \rightarrow \Phi + X)} \simeq 8.5$$

for X_f .4 was found.

The contribution of K^+P interactions to the inclusive cross-section for Φ production is thus

$$\frac{1.1 \times 8.5\ \sigma_{\pi^+}}{98.9\ \sigma_{\pi^+} + 1.1 \times 8.5\ \sigma_{\pi^+}} \simeq .09$$

The ratio R for the OZI-allowed contribution to Φ production in π^+P interactions thus can be estimated as

$$R_{\pi^+} = \left.\frac{0.5\ \sigma_{OZI}}{0.91\ \sigma_{INC}}\right|_{meas} = \frac{.5}{.91} \times .35 = 0.19$$

It can be inferred however, that the contribution of K^+P interactions to the production of (φK^0_S)'s was not 100 percent because the experimental ratio $\left(\frac{\sigma(\pi^+p \to \varphi K^0_S + Y}{\sigma(\pi^+p \to \varphi \Lambda^0 + X} = \frac{1.4 \pm .08 \pm .82}{1.4 \pm .08 \pm .82} = 1 \pm \left(\frac{2.8}{.74}\right)\right)$ is in agreement with the predictions of a model based on equal probability of occurrence for conjoint processes. Significant contribution of a possible K^+ beam contamination to φK^0_S production would be expected to yield an excess of observed $\varphi' K^0_S$ over $\varphi \Lambda^0$. No such excess is apparent within the limited statistics of the present data. We conclude that in the worst case the ratio R could be reduced to as small as .19 by beam K^+ contamination.

REFERENCES:

1- D.R.O.Morrison, CERN/EP 79-102, 21 sept, 1979.